The Prediction of the Longitudinal Load Factors for a Simplified A-402M Transmission Line System using ANSYS

by

Andrew Gilarski

A Thesis submitted to the Faculty of Graduate Studies of

The University of Manitoba

in partial fulfilment of the requirement for the degree of

MASTER OF SCIENCE

Department of Civil Engineering

University of Manitoba

Winnipeg, Manitoba

Abstract

ASCE Manual No.74 (2010) and the Electric Power Research Institute (EPRI, 1997) provide methods for calculating the unbalanced longitudinal loads on a transmission line due to a wire breakage. The calculated loads from the two are different. In this study, a simplified transmission line was created using the equivalent geometric properties of a detailed transmission line. Non-linear dynamic analyses of the 10-span simplified transmission line due to cable breakage events in the first span were studied using ANSYS. The analyzed longitudinal loads were found to vary for different S/S, S/I, and K's as specified in the EPRI. An equation for the longitudinal load factor as a function of the S/S, S/I, and K was then formulated based on the analysis. The longitudinal load factors from the formulated equation were found to be almost double those given by the ASCE manual and comparable to those calculated using the EPRI formulation.

Acknowledgement

I would like to express my thanks and appreciation to my advisor, Dr. Nipon Rattanawangcharoen, P.Eng. for his help, advice, and guidance throughout the course of this study, Mr. Jon Kell, P.Eng, from Manitoba Hydro, for his help and advice, and the other members of the examining committee, Dr. Fariborz Hashemian, P.Eng, and Dr. Quan Wang, P.Eng.

I would also like to express my thanks and appreciation to Mr. Yang Liu, for his assistance and help with learning the program ANSYS, along with many of the problems that I had encountered during the course of this study. I would also like to thank Mr. Mohamed Mady for his help with learning the program ANSYS and helping to solve any problems encountered with the program.

Finally, I would also like express my deepest thanks to my family and friends for their continuous support throughout this study, without whom I would not have been able to complete this study.

This study is financially supported by NSERC.

Table of Contents

Abstract ..... **i**

Acknowledgement ..... **ii**

Table of Contents ..... **iii**

List of Figures ..... **vi**

List of Tables ..... **viii**

Chapter 1 Introduction **1**

1.1 General 1

1.2 Objectives 4

1.3 Outline of the Thesis 5

1.4 Scopes of the Research 5

Chapter 2 Literature review **7**

2.1 Applicable codes and guidelines 7

2.2 Broken wire analysis of an electric transmission line system 9

2.3 Transmission tower modelling in ANSYS 12

Chapter 3 Transmission line system modelling **14**

3.1 Simplified A-402M transmission tower line 16

3.2 Transmission tower elements 18

3.2.1 Straight latticed tower segment 18

3.2.2 Tapered latticed tower segment 20

3.3 Cable Elements 22

3.4 Validation of beam-column elements 23

3.5 Validation of cable elements 30

3.5.1 Static Analysis 31

3.5.2 Free vibration 35

3.6 Validation of simplified A-402M tower 37

3.6.1 Static Analysis 37

3.6.2 Free vibration 41

3.7 Validation of Cable Breakage 42

Chapter 4 Longitudinal Load Factors (LLF) 45

4.1 ANSYS Modelling 45

4.1.1 Cable Breakage Cases 46

4.1.2 Solution Controls 47

4.2 Results 50

Chapter 5 Conclusions and Recommendations 56

5.1 Conclusions 56

5.2 Recommendations for Future Work 58

References 59

Appendix - A 63

List of Figures

Figure 1.1: Latticed transmission tower 4

Figure 3.1: A-402M Tower 15

Figure 3.2: Simplified A-402M Tower 17

Figure 3.3: Latticed tower segment represented as a tapered beam-column element 17

Figure 3.4: Straight latticed tower segment 18

Figure 3.5: Torsion stiffness of a straight latticed tower segment 19

Figure 3.6: Tapered latticed tower segment 21

Figure 3.7: Parabolic cable profile 22

Figure 3.8: A cantilevered beam with point load at free end 23

Figure 3.9: A cantilevered beam subjected to an end moment 24

Figure 3.10: Curved Cantilever bend with a concentrated load 25

Figure 3.11: A simply support beam with a step force with finite rising time loading 27

Figure 3.12: The vertical displacement history under loading point 28

Figure 3.13: A cantilevered beam with sinusoidal load at free end 29

Figure 3.14: The free end of vertical displacement history 30

Figure 3.15: Point load on a cable 32

Figure 3.16: Uniformly distributed load on a cable 32

Figure 3.17: Out of plane conductor frequencies 36

Figure 3.18: In plane conductor frequencies 36

Figure 3.19: Detailed tower compared to simplified tower 37

Figure 3.20: Load case forces and nodes on which they act 38

Figure 3.21: Detailed and simplified tower nodes 38

Figure 3.22: Five span transmission line in Peyrot's full scale test (Peyrot, 1980).....43

Figure 3.23: Tension at point B of the insulator string AB [Dash line – full scale case 1 test (Peyrot *et al.* 1980), Solid line – ANSYS simulation] 44

Figure 4.1: A ten-span tower model.....45

Figure 4.2: LLF at the conductor location for the tower next to the broken wire event 51

Figure 4.3: LLFs from ANSYS simulation and EPRI calculation 53

Figure 4.4: The effect of K on the LLFs 54

Figure 4.5: LLFs comparison between 4.13 and EPRI report 55

List of Tables

Table 3.1: A comparison of the results for a large deformation cantilevered beam 24

Table 3.2: The maximum deflection of the beam and the result comparison 25

Table 3.3: The tip location (in) of the cantilevered 45-degree bend.....26

Table 3.4: The undamped displacement under loading point.....28

Table 3.5: The damped displacement under loading point 29

Table 3.6: Properties of the conductors, ground wires, and guyed cables 31

Table 3.7: Maximum deflection and stress for a point load on a conductor cable mid-span.....33

Table 3.8: Maximum deflection and stress for a uniformly distributed load on a conductor cable 34

Table 3.9: Transmission Tower Load Cases 39

Table 3.10: Detailed and Simple Tower Deflections for Load Case 1 (unit mm).....40

Table 3.11: Detailed and Simple Tower Deflections for Load Case 2 (unit mm).....40

Table 3.12: Detailed and Simplified Tower Mode Frequencies.....41

Table 3.13: Five span transmission line material properties 43

Table 3.14: Comparison of ANSYS results to Peyrot *et al.* results for five span cable break.....44

Table 4.1: Cable breakage cases.....46

Table 4.2: First mode shape natural frequencies and damping coefficients 49

Table 4.3: Longitudinal Load Factors.....50

Table 4.4: Effect of S/I on LLF 52

Table 4.5: Effect of the K on the LLFs 53

Chapter 1 Introduction

1.1 General

Electrical transmission line systems are a key role in today's society that has become reliant on a constant supply of energy. Any type of failure in the transmission line system that causes a disruption in the energy supply will consequently result in economic losses. In order to maintain the reliability of the transmission line system, as well as be economical, great care needs to be taken to ensure that they are designed well.

With the advent of finite element software, the behaviour of transmission towers has been analyzed vigorously. One area that has not been sufficiently analyzed is the unbalanced longitudinal load that transmission towers are subjected to. The unbalanced longitudinal load is a dynamic load in the direction of transmission line, and can be caused by unbalanced ice and wind load, breakage of a conductor, collapse of a tower, etc. ASCE Manual No.74 (ASCE, 2010) provides guidelines for calculating the approximate unbalanced longitudinal load using the span/sag ratio and the span/insulator ratio. Since the towers in a transmission line system are connected to one another, when one tower in the system fails or suffers a conductor breakage, it will produce an unbalanced longitudinal load on the adjacent towers, which may exert a larger force on the adjacent towers than they would experience in the balanced condition. This may create a domino effect that results in a cascading failure of the transmission line system if the towers are unable to resist the additional forces created by the unbalanced longitudinal load.

On September 5th, 1996, 19 A-402 Manitoba Hydro transmission towers collapsed as a result of a high-intensity downburst wind event. The first tower to fail caused the unbalanced longitudinal loads on the adjacent towers to be greater than the towers could resist, which resulted in a successive, cascading failure. The overall damage to the towers along with the economic damages resulting from power disruption totalled to over 10 Million USD. Other examples include 289 transmission towers collapsed in Wisconsin in 1975, and 406 supporting structures collapsed in Nebraska in 1993. These are just a select few of the many similar cases that have happened around the globe.

ASCE Manual No.74 (ASCE, 2010) section 3.3.2 provides three methods of failure containment to prevent a large scale cascade failure, these methods are as follows:

1. Design all structures for longitudinal loads. The manual provides a figure used to calculate the residual static load (RSL) factor corresponding to the broken wire condition in the longitudinal direction as a function of the span/insulator ratio (S/I) and the span/sag ratio (S/S). The manual also provides longitudinal load factors (LLF's) as a function of the S/S ratio, the S/I ratio, and the stiffness (K) of the supporting towers. The LLF includes dynamic effects, structural stiffness, and insulator lengths. It is assumed that all structures are expected to resist cascading but the localized structure loss of one or two structures adjacent to the origin of the failure is acceptable.
2. Install failure containment structures at specified intervals. These structures have little ability to withstand the longitudinal loads. To strengthen each structure to resist cascading would be costly and undesirable. Failure containment structures, often being ordinary suspension structures with extra longitudinal guys, are placed at the desired interval.

3. Install released mechanisms. The released mechanisms are slip and suspension clamps that will limit the longitudinal loads applied to the wires when wires are broken. The technique, however, is not recommended in the areas of heavy ice loadings due to the unbalanced ice load.

A common practice done in Manitoba is to install stop-structures at regular intervals to prevent a cascade failure. These structures have an increased structural resistance. In practice, stop structures are placed at an interval of about every ten structures, as it is assumed in analysis that ten spans are affected by the cascading failure.

Many transmission towers are designed as steel lattices guyed cables. Figure 1.1 shows a common type of latticed steel transmission tower. Since transmission towers are very tall and slender, wind load is what normally governs the design. Moreover the tower has a low natural frequency, a dynamic analysis is important to determine design loads. A dynamic analysis of the entire transmission line system is needed because the properties of the system as a whole, including the conductors, insulators, and ground wires, needs to be taken into account to accurately predict the loads.

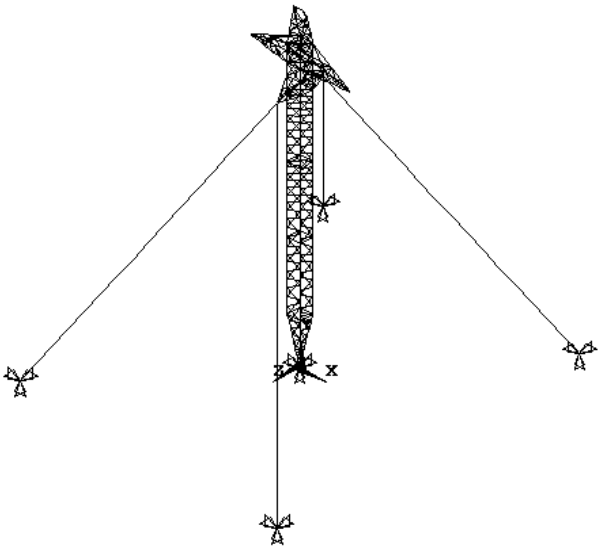

Figure 1.1: Latticed transmission tower

1.2 Objectives

Up until now, sufficient attention has not been given to finite element analysis of the dynamic effects of unbalanced longitudinal loads as a result of wire breakage. The effects of the conductors in a transmission line system have a significant impact on the loads experienced by the adjacent towers. As a result, finite element analysis of a full transmission line needs to be undertaken to determine an accurate prediction of the entire system. Since the number of elements in a latticed steel transmission tower is very large, a simplified transmission tower of beam elements is needed in order to reduce computing time. The objectives of this study are:

- To develop an equivalent beam element in ANSYS that can accurately represent a latticed tower segment both statically and dynamically.

- To develop a simplified transmission model in ANSYS that can accurately represent a detailed transmission tower model both statically and dynamically.

- To perform a broken wire analysis of a 10-span simplified transmission tower line in ANSYS

- To determine the LLF obtained from the broken wire analysis and compare them to the ones provided by ASCE Manual No. 74 as well as those by the EPRI report.

1.3 Outline of the Thesis

This thesis consists of five chapters. Chapter 2 is a literature of the applicable codes and guidelines of transmission tower design, broken wire analysis of a transmission line, and modelling of a transmission tower in ANSYS.

Chapter 3 is the formulation of a simplified beam element to represent a latticed tower segment, validation of ANSYS ability to accurately represent beam and cable elements, both statically and dynamically, the validation of the simplified transmission tower being able to accurately represent the detailed transmission tower, and the validation of ANSYS to accurately predict the unbalanced longitudinal loads as a result of a broken wire.

Chapter 4 is the modelling of the system in ANSYS, the parametrical study of the effects of the S/S ratio, the S/I ratio and the K of the supporting towers on the LLFs, as well as the analysis of the results against the ASCE manual and the EPRI report.

Finally, Chapter 5 is the conclusion and recommendations of this thesis.

1.4 Scopes of the Research

The scopes of this thesis are:

- The simplified tower consists of equivalent beam elements in ANSYS
- A nonlinear dynamic analysis is performed on a 10-span simplified transmission tower line
- All broken cables are taken to be from the left-most span of the transmission line
- Torsional mass of the transmission line is not considered
- Buckling of a tower leg is not taken into account
- All supporting towers do not fail from the resulting unbalanced load
- All cables are modelled as three dimensional truss elements in ANSYS
- A consistent mass matrix is used in dynamic analysis
- Rayleigh damping is used for all dynamic analyses.
- All end restraints of the transmission line are pin supports.

Chapter 2 Literature review

The objective of this work is to study and develop a simplified electrical transmission line system in the finite element program ANSYS, and perform a dynamic analysis to determine the unbalanced longitudinal loads on the system. The presentation of the literature review will begin with the applicable codes and guidelines for transmission tower design and analysis, followed by the broken wire analysis of a transmission line system, the development of a simplified beam-column element with equivalent properties of a latticed tower section, and closed with computer modelling of transmission towers in the program ANSYS.

2.1 Applicable codes and guidelines

The applicable codes and guidelines for the design of an electrical transmission line are: the ASCE Manual on the Design of Steel Transmission Towers No.52 (ASCE, 1988), the ASCE Manual on Electrical Transmission Line Structural Loading No.74 (ASCE, 2010), and the ASCE Manual on the Design of Latticed Steel Transmission Structures No.10 (ASCE, 1997).

ASCE Manual No.52 provides guidelines for the design of self-supporting and guyed steel transmission towers subject to multiple types of loadings, such as: oblique wind loads, transverse wind loads, overhead ground wire loads, maximum and minimum transverse and longitudinal loads, etc.

ASCE Manual No.74 provides detailed guidelines for determining the structural loading on electrical transmission lines. The manual provides methods for determining wind, ice,

longitudinal, construction, maintenance, and various other loads. Section 3.3 of this manual provides information on the calculation of the unbalanced longitudinal load due to broken wires. This method requires the determination of the residual static load (RSL) which is the static longitudinal load on a wire support point under a broken wire condition. To calculate the RSL, the manual provides RSL factors as a function S/S ratio and S/I ratio. These RSL factors are then multiplied by the initial wire tension to give an approximate RSL. The RSL provides the minimum static load that must be resisted by the attached structures. The RSL does not take into account any dynamic effects resulting from the wire break. To consider dynamic effects, the manual provides a method to determine the (LLF) as a function of S/S ratio and the K of the support structures. The initial wire tension multiplied by the LLF gives an approximate design load that takes into account dynamic effects, which must be resisted by the attached structures.

The Electric Power Research Institute (EPRI, 1997) developed formulas to determine the LLF's of a transmission line. These formulas were the basis for the figures that were developed by ASCE Manual No. 74. The EPRI formulas contain correction factors for the tower stiffness and the S/I ratio.

ASCE Manual No.10 provides requirements for the design of self-supporting and guyed latticed steel electrical transmission structures subjected to loading that is determined from ASCE Manual No.74. It also provides information on the design requirements for individual structural elements with respect to size, shape, length, applied loads, etc.; as well as design requirements for connections with respect to connection type, applied loads, etc.

2.2 Broken wire analysis of an electric transmission line system

Electric transmission line systems subjected to unbalanced longitudinal loads have been studied by many researchers. Three approaches have been used: the full-scale test, the model-scale test, and numerical simulation. In the full-scale test and model-scale test approaches, the behaviors of the electric transmission line system with a broken wire are obtained from experimental testing. In numerical simulation, the finite element program is used to investigate this phenomenon.

Peyrot *et al.* (1980) performed a full-scale broken conductor test. The test was carried out on an existing electric transmission line system with latticed steel towers designed for a cascading failure. In their work, the conductor tension-time history was investigated. They also developed a theoretical method called the energy method to calculate the Dynamic Impact Factor (DIF). This factor was used to multiply a residual static tension determined from a 2D static finite element program called CABLE5 to predict the peak dynamic tension in the conductor. They reported 0.4% difference between the predicted peak tension and the measured one. The study was the only study of a full-scale broken conductor test available in the literature. This is because the full-scale test is expensive and difficult to conduct. Following this study, a few model-scale tests were reported. In 1981, Mozer *et al.* carried out a 1/30 model-scale experimental study of the broken conductor. In their test, the electric transmission line system consists of steel pole tangent structures, suspension insulators, conductors, and shield wires. They also developed a theoretical method to calculate the structural response factors which they used to predict maximum responses of the structure. They reported that difference between the predicted responses and the measured responses was within 2%. Kempner (1997) developed a containment failure philosophy from a scale test of an electrical transmission line system. The system was modeled

with pin bases tabular aluminum shafts attached with masses and springs. A single conductor was used in the study. The properties of the aluminum shafts were selected to provide a representation of real tower's stiffness and natural frequencies. Longitudinal displacements were used as criteria of tower failure. He reported that the unbalanced longitudinal load in the system reduced to half in the fifth tower away from the broken conductor span.

Even though the scale-model tests were relatively cheaper than the full-scale tests, they are still uncommon. Most of the past researchers selected to study the behavior of an electrical transmission line system subjected to an unbalanced longitudinal load using a numerical simulation. Campbell (1970) was the first one who developed a nonlinear static analysis procedure to analyze an unbalanced longitudinal load in an electric transmission line system. He formulated the conductor and the insulator string stiffness incorporating their geometric nonlinearity. He concluded that the Newton's type iterative method provided better results than a linear increment method. In 1978, Fleming *et al.* also developed a nonlinear static finite element program considering the geometric nonlinearity of the conductor and the insulator string. In their study, the stiffness of a supporting tower was expressed by a longitudinal force and the associating degree-of-freedom of the insulator string. In 1984, Siddiqui and Fleming modified the program originally written by Fleming et al. (Fleming *et al.*, 1978) to study a dynamic response of an electric transmission line system subjected to an unbalanced longitudinal load. A time history of wire tension arm loads and the tower support moment or the ground line moment due to a conductor loss were computed. The accuracy of this program was verified by comparing their results with the small scale experimental results (Mozer *et al.*, 1977) which they reported 10% and 20% errors in the arm loads and the ground line moment calculations, respectively.

In order to appropriately describe the dynamic behavior, with the advancement of the computing facilities, researchers moved towards the dynamic numerical simulations of an electrical transmission line system. Thomas and Peyrot (1982) developed a 2D dynamic finite element program, CABLE7, to study a broken wire phenomenon. They modeled an insulator string and a conductor using the same type of cable element. The tower stiffness was represented by an elastic spring with an equivalent horizontal stiffness along the line in their analysis. They compared the peak insulator tension due to a broken wire event from their analysis with a full scale and model-scale experimental test results and reported that tension history were within 30% difference. McClure and Tinawi (1987) used ADINA, a commercial finite element program, to create the 2D and 3D finite element models of an electric transmission line system and to perform a nonlinear dynamic analysis of the system subjected to an unbalanced longitudinal load due to a broken wire phenomenon. Their numerical results were compared with Mozer's experimental results (Mozer *et al.*, 1981). They reported that the 3D model was considered a more realistic model for an electric transmission line system. Later, Lapointe (2002) and McClure and Lapointe (2003) used a tower torsional moment-time history from the analysis of a similar model to explain the two tower failures during an ice storm on a 120 kV electric transmission line system in Quebec.

Recently, Shen *et al.* (2011) developed a general finite element analysis procedure in ABAQUS to study the various electric transmission line systems' responses after the conductor breakage, and to determine the broken wire load for the design. In their model, they simulated that the broken conductor fell down to the ground and moved along the ground. The accuracy of this procedure was verified by comparing their result with the Peyrot (1980) experimental result. They concluded that their model can be used to predict the time history of loading accurately.

As can be seen from the literature review, the study of the behavior of an electrical transmission line system subjected to unbalanced longitudinal broken conductor loading shifted from a full-scale test to a model-scale test, then to a numerical simulation of a static system, follow by a numerical simulation of a dynamic system using commercial program, and finally to a numerical simulation of the dynamic system using their own formulation. The main drawback of commercial programs is the versatility of the program which can be cumbersome for a very specific study.

2.3 Transmission tower modelling in ANSYS

ANSYS is a 3D finite element analysis (FEM) program that is very useful for conducting both static and dynamic simulations of a system. ANSYS has been used by many different researchers and companies as a very useful way to simulate the effects of an electrical transmission tower and an electrical transmission tower line under broken wire, wind, downburst, tornado, seismic, unbalanced, and various other types of loads.

Horr *et al.* (2004) performed a dynamic simulation of an A-402 guyed suspension tower and tower line subjected to extreme wind conditions in ANSYS and CDSET. The elements modelled in ANSYS were done with the built in beam and cable functions, while the elements modelled in CDSET were done with an alternative spectral approach. A modal analysis of a single guyed tower was conducted using ANSYS and CDSET. The frequencies for the first six modes of the tower were shown to be in good agreement when compared. A non-linear perturbed full dynamic time history collapse analysis was simulated for series of three guyed towers with all attached cables. The time history results from the finite element method with ANSYS and the spectral

element method with CDSET were compared and found to be in good agreement when compared.

Disney and Parke (2004) conducted an analysis of a single A-402 guyed suspension tower subjected to Manitoba Hydro's seven static design load cases, as well as extreme wind downburst loading. Analysis of the models was done using ANSYS built in static, transient-dynamic, modal, and buckling analysis sections. For the seven design load cases and for the extreme wind downburst it was found that the main form of collapse was the buckling failure of the cross arms of the tower. They suggested that by reviewing the mode shapes of the tower, additional members could be added to the guyed arms to enhance the survivability of the tower.

Chapter 3 Transmission line system modelling

The electrical transmission-line system for this study is modelled after the A-402M guyed suspension tower shown in Figure 3.1. The transmission-line system consists of structural beam-columns, truss elements, conductor cables, guyed cables, ground wire cables, and insulator strings. The conductor cables are attached to the insulator strings at the top cross-arm of the tower, while the guyed cables are attached to the bottom cross-arm of the tower. The ground wire cables are attached the top of tower. The conductor, guyed, and ground wire cables are all pre-stressed and take the form of a parabolic curve when installed. The insulator strings consist of a vertical cable that is attached to the top cross-arm of the tower at one end, and attached to the two joining conductor cables at the other end. The beam-column and truss elements of the tower consist of steel angles that are connected to one another with structural bolts.

Since the transmission tower contains a large number of elements, it is very complex and time consuming when running a simulation for several spans. As a result, a simplified tower is used.

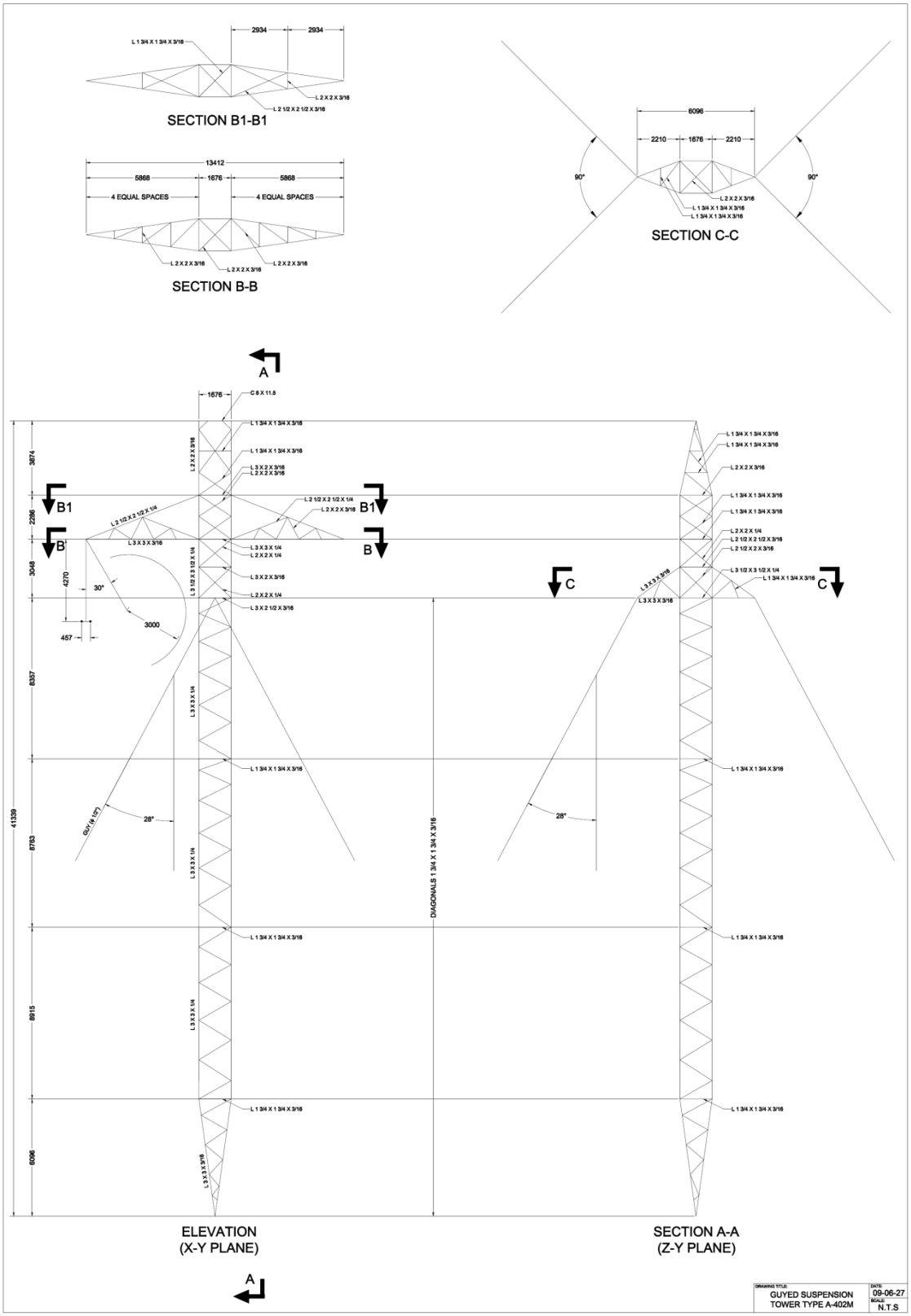

Figure 3.1: A-402M Tower

3.1 Simplified A-402M transmission tower line

Computer analysis of an electrical transmission line takes a sizable amount of processing power and is very time consuming. To save on processing power and analysis time, Tabet (2009) developed a simplified transmission tower using equivalent properties of the latticed tower segments. A latticed tower modelled with segments of tapered and prismatic beam-column elements has much less number of degrees of freedom than a tower modelled in detail and hence reduce time consumed in the analysis as well as increase the capacity to analyse a system with more number of spans. The cables modelled were assumed to be parabolic and have a modified Dischinger's modulus of elasticity. He analyzed the transmission tower line with a developed finite element program called Static and Dynamic Analysis Program. The results of the simplified and detailed transmission tower line, for static and free vibration analysis, were found to be within 7%; therefore the simplified beam-column element with equivalent properties was an adequate representation of a latticed tower segment.

The simplified tower, shown in Figure 3.2, is developed in this analysis to save on the computing time that each different load case will take to run. The simplified tower is modelled to represent the detailed A-402M tower. The simplified tower was created by taking the geometric properties of the detailed A-402M tower at the latticed segments and converting them into beam-column elements with equivalent properties to that of the detailed section. These equivalent properties include the cross-sectional area, moments of inertia, torsion constant, and mass of the original detailed section. An example representation a simplified latticed tower segment is shown in Figure 3.3. Since the latticed segments of the tower have been simplified into beam-columns, the

number of elements and degrees of freedom of the system has been greatly reduced, resulting in a less complex model that takes less time to simulate in ANSYS.

The equations for calculating the equivalent properties of the beam-column elements are presented in Section 3.2 (Tabet, 2009) formulation of tower elements for the A-402M tower.

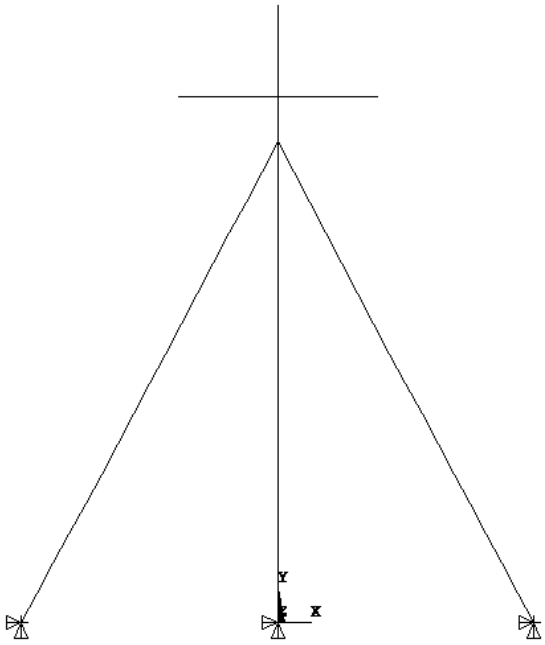

Figure 3.2: Simplified A-402M Tower

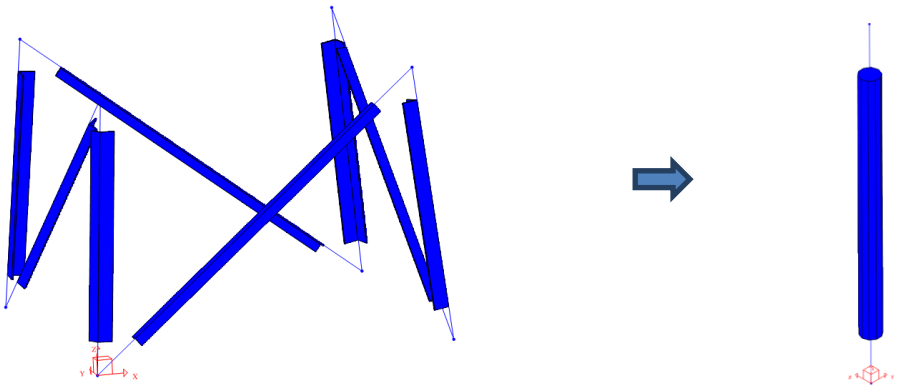

Figure 3.3: Latticed tower segment represented as a tapered beam-column element

3.2 Transmission tower elements

3.2.1 Straight latticed tower segment

The tower segment shown in Figure 3.4 represents a straight segment of a latticed transmission tower that will be modelled as a straight beam-column element with equivalent geometric properties in ANSYS.

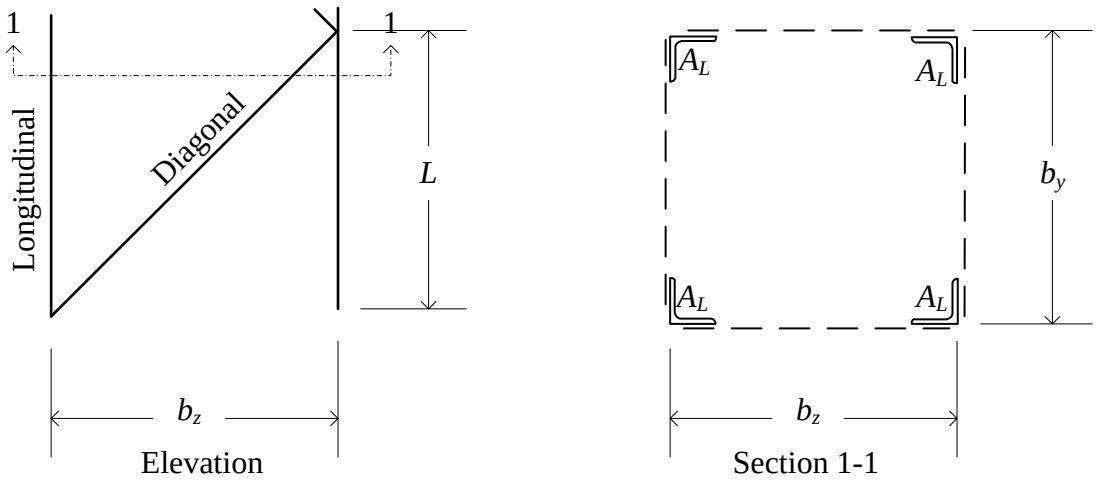

Figure 3.4: Straight latticed tower segment

The torsion stiffness of the segment is considered to be provided by the diagonal bars only. Figure 3.5 shows the torsion of a straight latticed tower segment. The formula for the torsion stiffness is shown in Equation 3.1 where k_T is the torsion stiffness, A_D of the area of one diagonal bar, F_D is the force in the diagonal bar, and T is the torsional moment.

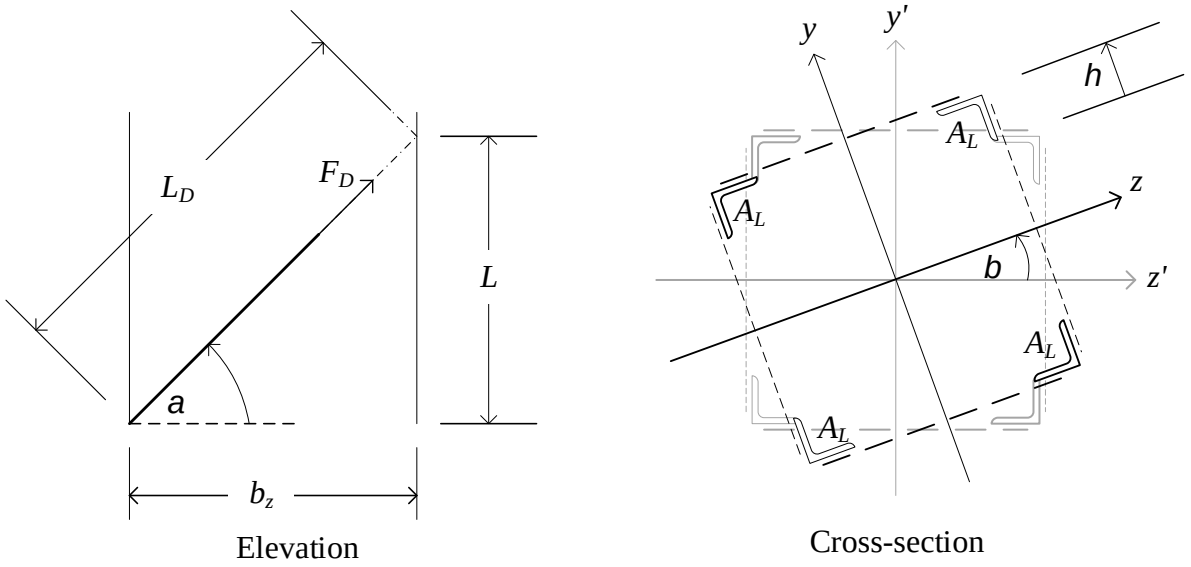

Figure 3.5: Torsion stiffness of a straight latticed tower segment

$$\mathrm{h} = \sin(\mathrm{b})\frac{\sqrt{b_y{}^2 + b_z{}^2}}{2} \approx \mathrm{b}\frac{\sqrt{b_y{}^2 + b_z{}^2}}{2}$$

$$F_D = \frac{EA_D}{L_D}\mathrm{h}\cos(\mathrm{a})$$

$$F_{D,y} = \frac{EA_D}{L_{D_y}}\mathrm{h}\cos^2(\mathrm{a}_y)$$

$$F_{D,z} = \frac{EA_D}{L_{D_z}}\mathrm{h}\cos^2(\mathrm{a}_z)$$

$$T = F_{D,z}b_y + F_{D,y}b_z$$

$$T = EA_D\mathrm{b}\frac{\sqrt{b_y{}^2 + b_z{}^2}}{2}\left(\frac{b_y\cos^2(\mathrm{a}_z)}{L_{D_z}} + \frac{b_z\cos^2(\mathrm{a}_y)}{L_{D_y}}\right)$$

$$k_T = \frac{T}{\mathrm{b}} = EA_D\frac{\sqrt{b_y{}^2 + b_z{}^2}}{2}\left(\frac{b_z{}^2 b_y}{\left(\sqrt{b_z{}^2 + L^2}\right)^3} + \frac{b_y{}^2 b_z}{\left(\sqrt{b_y{}^2 + L^2}\right)^3}\right) \qquad (3.1)$$

The formula for the moment of inertia is given in Equation 3.2, A is the cross sectional area of the segment, A_L is the area of one of the longitudinal bars, and I_y and I_z are the moments of inertia about the local y and z axes, respectively.

$$
\begin{aligned}
A &= 4A_L \\
I_y &= A_L b_z^{\,2} \\
I_z &= A_L b_y^{\,2} \\
k_T &= EA_D \frac{\sqrt{b_y^{\,2} + b_z^{\,2}}}{2} \left(\frac{b_z^{\,2} b_y}{\left(\sqrt{b_z^{\,2} + L^2}\right)^3} + \frac{b_y^{\,2} b_z}{\left(\sqrt{b_y^{\,2} + L^2}\right)^3} \right)
\end{aligned}
\tag{3.2}
$$

The formula for the mass of the segment is shown in Equation 3.3, where M is the mass of the segment, L_D is the length of the diagonal bar, ρ is the density of steel, assumed to be 7860 $\frac{kg}{m^3}$, and L is the longitudinal length of the segment.

$$
\begin{aligned}
M &= 4A_L L\rho + 4A_D L_D \rho \\
L_D &= \frac{\sqrt{b_z^{\,2} + L^2} + \sqrt{b_y^{\,2} + L^2}}{2}
\end{aligned}
\tag{3.3}
$$

3.2.2 Tapered latticed tower segment

The tower segment shown in Figure 3.6 represents a tapered segment of a latticed transmission tower that will be modelled as a straight beam-column element with equivalent geometric properties in ANSYS. The tapered section causes the moment of inertia change with length. Since ANSYS does not allow the input of tapered properties for an arbitrary beam-column element, an average moment of inertia of the top and bottom section is used, and will be verified for accuracy later. The diagonal bars are once again assumed to only resist torsion. The formulas for calculating the equivalent beam properties are given in Equation 3.4.

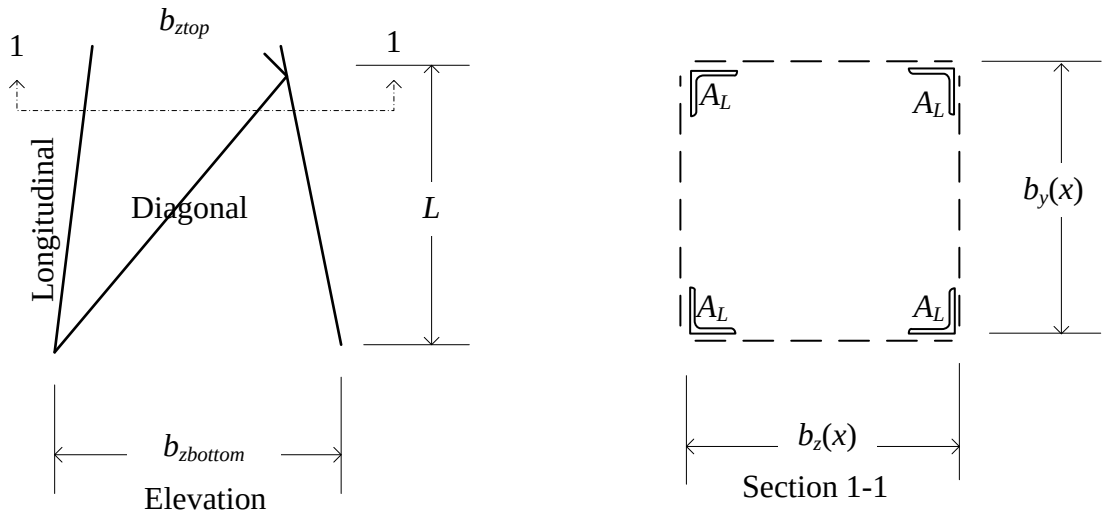

Figure 3.6: Tapered latticed tower segment

$$
\begin{aligned}
A &= 4A_L \\
I_{ybottom} &= A_L b^2{}_{zbottom} \\
I_{ytop} &= A_L b^2{}_{ztop} \\
I_{zbottom} &= A_L b^2{}_{ybottom} \\
I_{ztop} &= A_L b^2{}_{ytop} \\
I_{yave} &= \frac{I_{ybottom} + I_{ytop}}{2} \\
I_{zave} &= \frac{I_{zbottom} + I_{ztop}}{2} \\
k_T &= EA_D \frac{\sqrt{b^2{}_{yaver} + b^2{}_{zaver}}}{2} \left[\frac{b^2{}_{zaver} b_{yaver}}{\left(\sqrt{L^2 + b^2{}_{zaver}}\right)^3} + \frac{b^2{}_{yaver} b_{zaver}}{\left(\sqrt{L^2 + b^2{}_{yaver}}\right)^3} \right]
\end{aligned}
\tag{3.4}
$$

The formula for the mass of the segment is shown in Equation 3.5, where L_{Dz} is the diagonal length in the local z direction, and L_{Dy} is the diagonal length in the local y direction.

$$
\begin{aligned}
M &= 4A_L L\rho + 4A_D L_D \rho \\
L_{Dz} &= \sqrt{\left(\frac{b_{ybottom} + b_{ytop}}{2}\right)^2 + L^2 + \left(\frac{b_{zbottom} - b_{ztop}}{2}\right)^2} \\
L_{Dy} &= \sqrt{\left(\frac{b_{zbottom} + b_{ztop}}{2}\right)^2 + L^2 + \left(\frac{b_{ybottom} - b_{ytop}}{2}\right)^2} \\
L_D &= \frac{L_{Dy} + L_{Dz}}{2}
\end{aligned}
\tag{3.5}
$$

3.3 Cable Elements

The conductor, ground wire, and guyed cables form a parabolic shape as a result of the uniformly distributed load from self-weight and pre-stressing force. The parabolic shape was calculated according to the formulas presented in *Cable Structures* by Max Irvine (1981). The profile for a parabolic cable is presented in Figure 3.7. The formulas for the determination of the cable profile are presented in Equation 3.6, where *z* is the dip of the profile below the chord, *m* is mass per unit length, *g* is gravity, *l* is the horizontal length of the cable, and *H* is the horizontal component of the pre-stressing force. The cables were inputted into ANSYS with the predetermined parabolic profile to accurately represent the sagging cables.

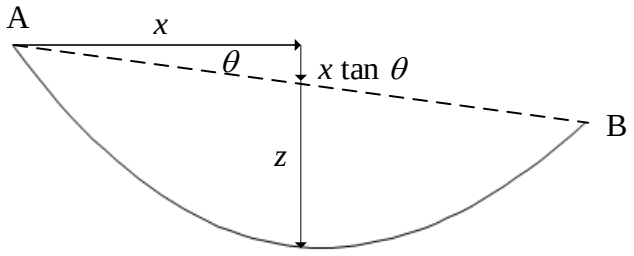

Figure 3.7: Parabolic cable profile

$$z = \left(\frac{mg \sec\theta l^2}{H} \right) \frac{1}{2} \frac{x}{l} \left(1 - \frac{x}{l} \right) \left[1 + \frac{mgl \sin\theta}{6H} (1 - 2\frac{x}{l}) \right] \tag{3.6}$$

3.4 Validation of beam-column elements

The beam-column elements were validated using 3D beam-column elements in ANSYS set to have a cubic shape function, and were compared to the theoretical results for displacement, rotation and natural frequencies. The following examples are presented to validate the accuracy of the beam-column element used in ANSYS.

Example 1: A cantilevered beam subjected to a free end loading

A cantilevered beam subjected to a free end loading shown in Figure 3.8 is considered in this example. The problem is a 2D large deformation problem. The beam geometrical properties are $L = 5$ m, $A = 4.8 \times 10^{-3}$ m^2, $I_2 = I_3 = 4.45 \times 10^{-5}$ m^4 and the material properties are $E = 210$ GPa and $G = 80.775$ GPa. The applied force has a magnitude of $F_2 = -600$ kN.

Figure 3.8: A cantilevered beam with point load at free end

Table 3.1 shows the free end displacement and rotation compared with Crivelli's results (1990). The percent difference (P.D) in table 1 is calculated using Crivelli's results for 16 elements, as they are the most accurate for each of Crivelli's cases. The ANSYS results were found to be accurate by using only one element.

Table 3.1: A comparison of the results for a large deformation cantilevered beam

Number of elements	Displacement (m)		Rotation (rad)		P.D. (%)	
	ANSYS	Crivelli (1990)	ANSYS	Crivelli (1990)	Displacement	Rotation
1	2.157	1.833	0.672	0.747	0.00	0.00
2	2.158	2.078	0.672	0.688	0.05	0.00
4	2.158	2.139	0.672	0.676	0.05	0.00
8	2.158	2.154	0.672	0.676	0.05	0.00
16	2.158	2.157	0.672	0.672	0.05	0.00

Example 2: A cantilevered beam subjected to end moments

A 2D cantilevered beam of length $L = 1\text{ m}$ with a cross-sectional area $A = 1\times10^{-4}\text{ m}^2$, the moments of inertia $I_2 = I_3 = 5\times10^{-8}\text{ m}^4$, the Poisson's ratio of $\nu = 0.3$ and the elastic modulus $E = 210\text{ GPa}$ is considered in this example. This cantilever beam is subjected to an end moment of $M_3 = 10000\text{ N-m}$ as shown in Figure 3.9. The problem is a 2D large displacement and large rotation problem.

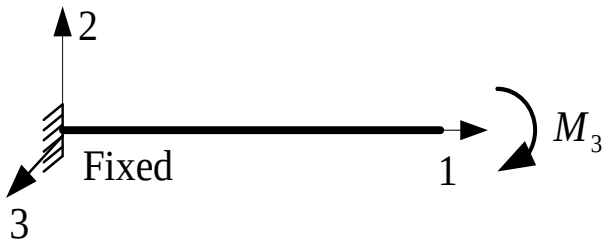

Figure 3.9: A cantilevered beam subjected to an end moment

The maximum values of the beam deformation are compared with the results from Wang *et al.* (2008), shown in Table 3.2. In this example, ten loading steps with ten elements were used. Wang et al. (2008) used 10 loading steps and 20 elements. It should be noted that the results from ANSYS remain the same, regardless of the number of elements used.

Table 3.2: The maximum deflection of the beam and the result comparison

Deformation (mm)	ANSYS	Wang et al. (2008)	P.D. (%)
u_x	144.46	147.0	1.73
u_y	441.27	471.9	6.49

Example 3: A 45^o bend subjected to an out-of-plane loading

In this example, a 3D response of a cantilevered 45^o bend in a horizontal plane subjected to a vertical load at free end, shown in Figure 3.10, is presented. The problem was studied by Simo and Vu-Quoc (1986), Cardona and Geradin (1988), Crisfield (1990) and Li (2007). The problem is considered to be a 3D large displacement and large rotation.

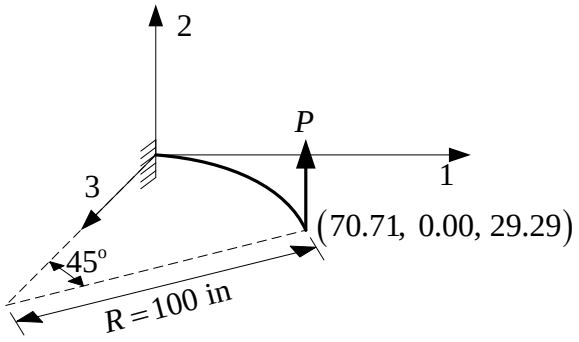

Figure 3.10: Curved Cantilever bend with a concentrated load

Table 3.3: The tip location (in) of the cantilevered 45-degree bend

	Tip location (in)		
	$P = 300$ lb	$P = 450$ lb	$P = 600$ lb
ANSYS	58.84, 40.09, 22.33	52.31, 48.41, 18.61	47.22, 53.39, 15.80
Simo and Vu-Quoc (1986)	58.84, 40.08, 22.33	52.32, 48.39, 18.62	47.23, 53.37, 15.79
Cardona and Geradin (1988)	58.64, 40.35, 22.14	52.11, 48.59, 18.38	47.04, 53.50, 15.55
Crisfield (1990)	58.53, 40.53, 22.16	51.93, 48.79, 18.43	46.84, 53.71, 15.61
Li (2007)	58.78, 40.15, 22.28	52.24, 48.46, 18.56	47.15, 53.43, 15.74

The bend has a unit cross-section with elastic modulus $E = 10^7$ psi and zero Poisson's ratio. The ANSYS analysis uses eight straight beam elements as used in all other studies. The maximum load is $P = 600$ lb. The tip locations at loads $P = 300,\ 450$ and 600 lb are shown in Table 3.3. It can be seen that the results from ANSYS are in good agreement with the results from the other studies.

Example 4: A simply supported beam subjected to a step force with finite rising time loading

In this example, a simply supported beam subjected to a step force with finite rising time loading shown in Figure 3.11 is considered. The beam geometrical properties are $L = 12$ m,

$A = 8.06 \times 10^{-3}$ m^2, the moments of inertia $I_2 = I_3 = 1.858 \times 10^{-4}$ m^4 and the material properties are $E = 210$ GPa, $G = 80.775$ GPa and $\rho = 7850$ kg/m^3.

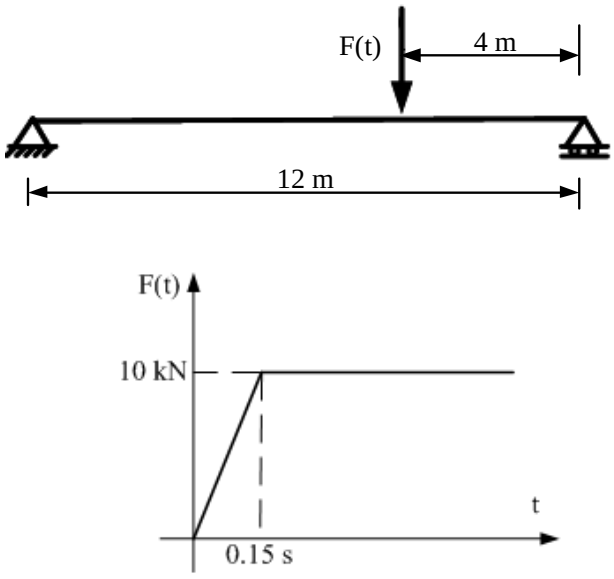

Figure 3.11: A simply support beam with a step force with finite rising time loading

a) Without Damping

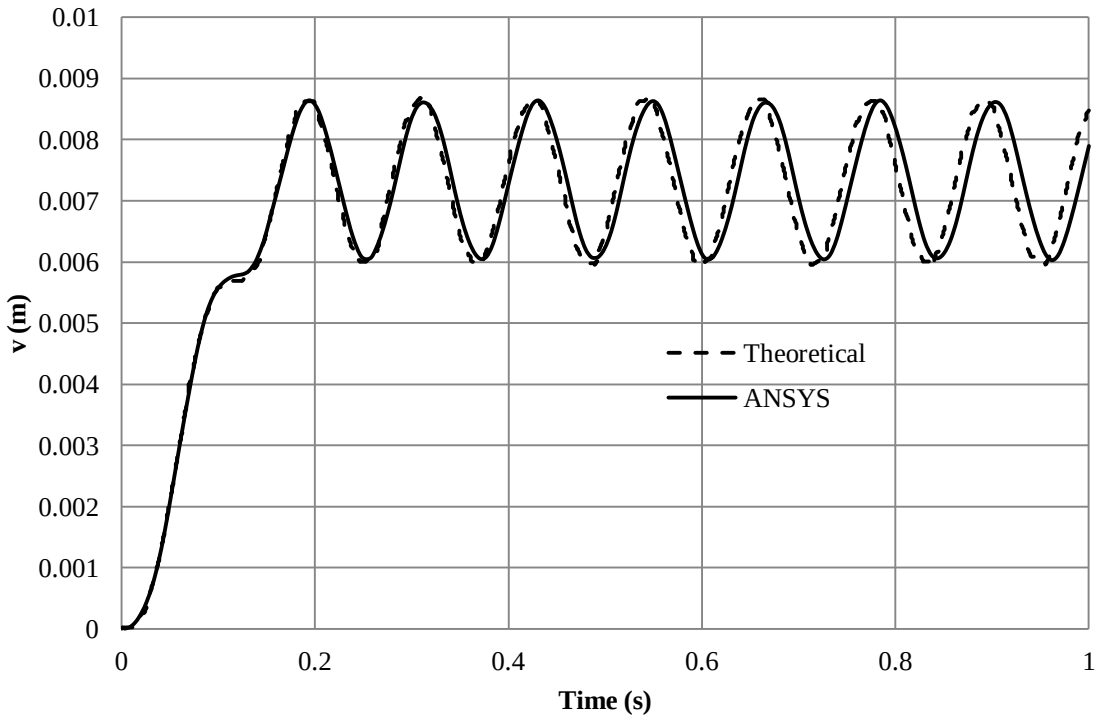

Figure 3.12: The vertical displacement history under loading point

Figure 3.12 shows the displacement under the loading point compared with theoretical results. The maximum displacement and the displacement at 0.15s under the loading point are shown in Table 3.4, where they are compared to the theoretical results.

Table 3.4: The undamped displacement under loading point

Deformation (mm)	ANSYS	Theoretical result	P.D. (%)
$u_y(0.15\ \mathrm{s})$	6.501	6.456	0.69
$u_{y\ \mathrm{Maximum}}$	8.637	8.617	0.23

b) With Damping, $\xi = 0.01$.

The results from ANSYS for the damped analysis are compared to the solution presented by Tabet (2009) in Table 3.5.

Table 3.5: The damped displacement under loading point

Deformation (mm)	ANSYS	Tabet (2009)	P.D. (%)
$u_y(0.15\text{ s})$	6.53	6.43	1.56
$u_{y\text{ Maximum}}$	8.48	8.49	0.12

Example 5: A cantilever beam support to a sinusoidal force

A cantilever beam shown in Figure 3.13 has a rectangular cross section $h = 0.25\text{ m}$ and $b = 0.5\text{ m}$, where *h* and *b* denote the depth and the width, respectively. This cantilever beam has a length $L = 10\text{ m}$, elastic modulus $E = 210\text{ GPa}$, the Poisson's ratio $\nu = 0.3$ and mass density $\rho = 7850\text{ kg/m}^3$. A sinusoidal force $P = 10\sin 50t\text{ MN}$ is applied at the free end of the beam. This problem is a large displacement and large rotation problem.

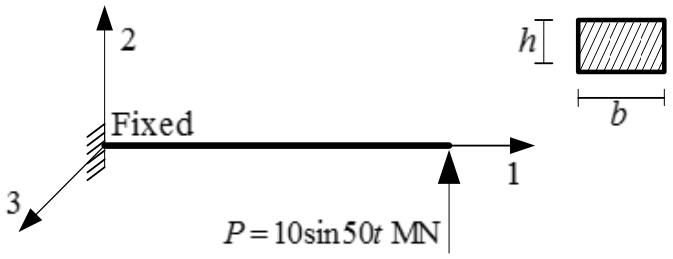

Figure 3.13: A cantilevered beam with sinusoidal load at free end

Le *et al.* (2011) used the Co-rotational finite element to solve the problem. In his analysis, he used 3 elements with the CR mass matrix to solve this problem while 10 elements with lumped mass were used in ANSYS for comparison. Both of the free end displacement-time histories are shown in Figure 3.14.

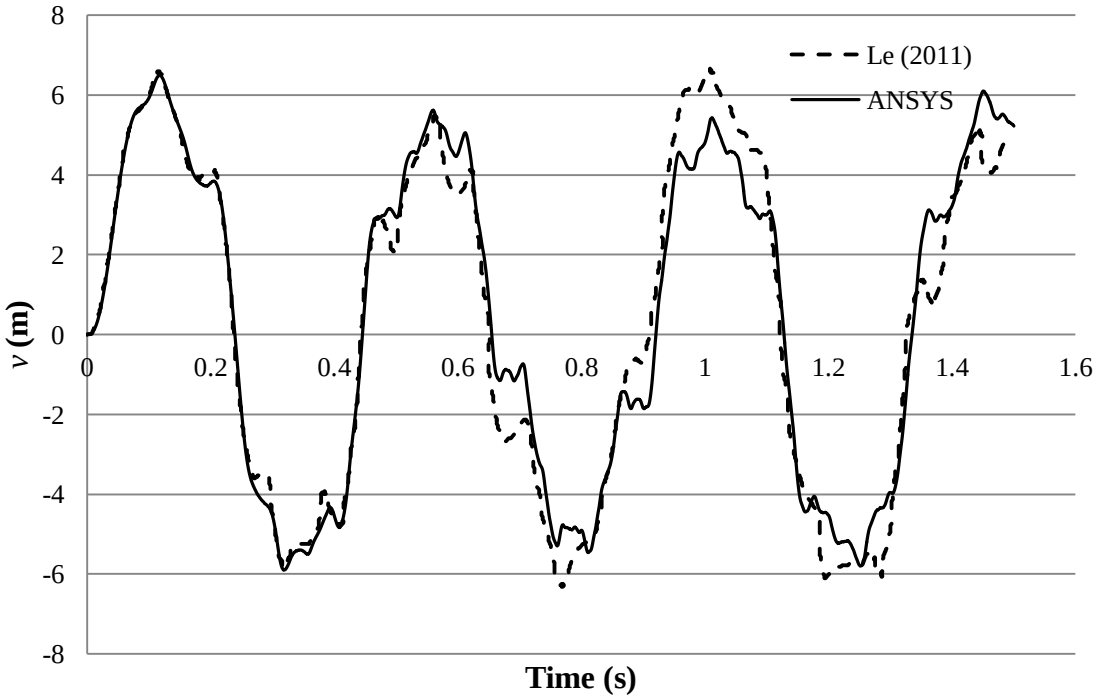

Figure 3.14: The free end of vertical displacement history

3.5 Validation of cable elements

The cable elements were modelled using truss members set to tension only. For both static and dynamic check of the cable, the results obtained from using a varying number of truss elements in ANSYS were compared to the theoretical results by Irvine (1981). The conductor cable, ground wire, and a guyed cable of a transmission tower system were chosen for the verification purpose. Since the ground wires and guyed cables are modelled similarly to the conductor cables, only the verification results of the conductor cables are shown here. Table 3.6 shows the properties used for the analysis of the cables considered in this analysis.

Table 3.6: Properties of the conductors, ground wires, and guyed cables

	Conductor	**Ground Wire**	**Guyed Cable**
Horizontal Span (m)	480	480	24.16
Effective Diameter (mm)	57.47	9.00	11.10
Effective Area (m^2)	2.5944E-03	6.3617E-05	1.9355E-04
Density (ton/m^3)	2.2765	6.25	7.86
Weight(N/m)	57.94	3.90	14.92
Modulus of Elasticity (kN/m^2)	6.23E+07	1.86E+08	1.86E+08
Sag (m)	20.00	13.54	0.113
Pretension per cable (kN)	83.44	8.30	26.68

3.5.1 Static Analysis

To validate the use of truss elements to represent a conductor cable in the static analysis, the cable was inputted into ANSYS with the parabolic profile for this analysis. Two load cases were considered, i.e. a point load applied at the mid-span and a uniformly distributed load applied between two points on the cable. Figure 3.15 shows the deflection resulting from a point load on a cable, where L is the length between supports, P is the point load, x_1 is the distance to the point load from the left support, x is the distance from the left support to the point of interest, z is the sag as the point of interest, and w is the deflection at the point of interest. Table 3.7 shows a comparison of the resulting deflection at mid-span along with the maximum stress in each cable obtained due to a point load applied at the mid-span of the conductor cable.

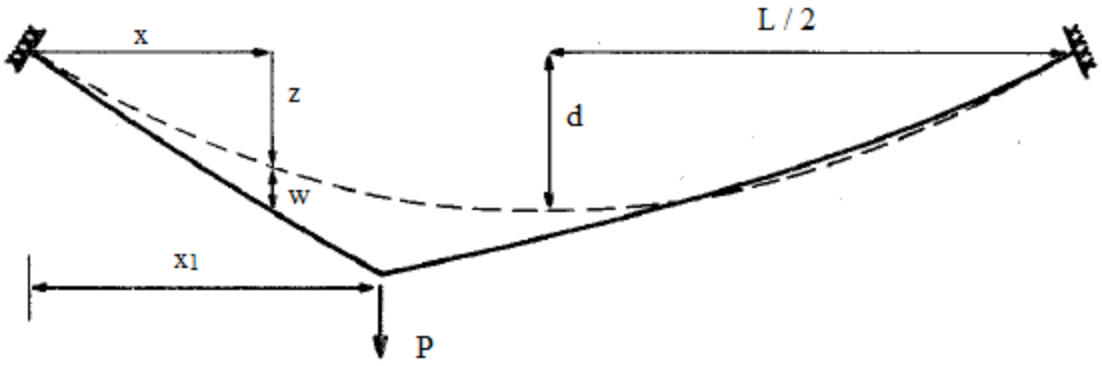

Figure 3.15: Point load on a cable

Figure 3.16 shows the deflection resulting from a uniformly distributed load applied partially on a cable, where p is the load per unit length, where x_2 is the distance from the left support to the beginning of the uniformly distributed load, and x_3 is the distance from the left support to the end of the uniformly distributed load.

Table 3.8 shows a comparison of the resulting deflection at mid-span along with the maximum stress in each cable obtained due to a uniformly distributed load applied between two points on the conductor cable.

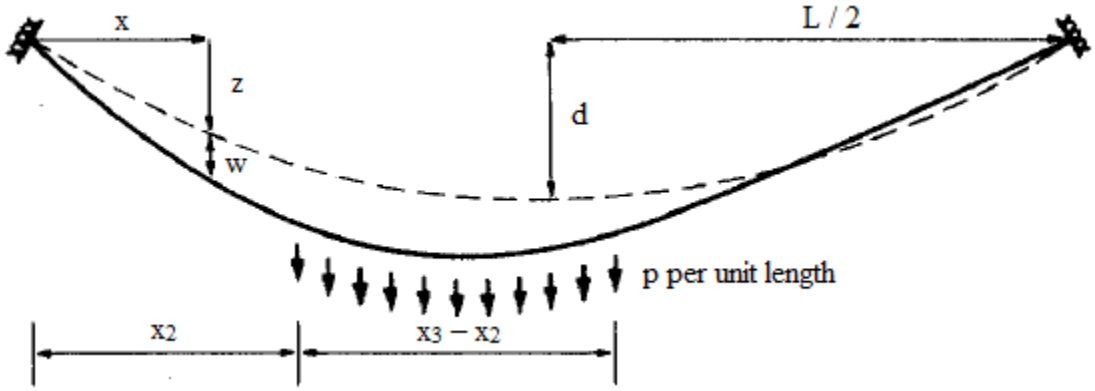

Figure 3.16: Uniformly distributed load on a cable

Table 3.7: Maximum deflection and stress for a point load on a conductor cable mid-span

	Maximum Deflection (m)					Maximum Stress (MPa)				
	ANSYS		Irvine	P.D. (%)		ANSYS		Irvine	P.D. (%)	
Load (N)	8 elements	16 elements		8 elements	16 elements	8 elements	16 elements		8 elements	16 elements
25000	4.1102	4.2020	4.2333	2.9	0.7	75.41	75.17	74.96	0.6	0.3
50000	5.8722	5.9678	5.9922	2.0	0.4	115.43	115.05	114.71	0.6	0.3
75000	7.2578	7.3501	7.3626	1.4	0.2	152.51	152.05	151.60	0.6	0.3
100000	8.4610	8.5494	8.5483	1.0	0.0	187.28	186.75	186.19	0.6	0.3

Table 3.8: Maximum deflection and stress for a uniformly distributed load on a conductor cable

			Maximum Deflection (m)					Maximum Stress (MPa)				
			ANSYS		Irvine	P.D. (%)		ANSYS		Irvine	P.D. (%)	
p (N/m)	x_2 (m)	x_3 (m)	8 elements	16 elements		8 elements	16 elements	8 elements	16 elements		8 elements	16 elements
500	120	360	6.2378	6.2019	6.1433	1.5	1.0	186.33	186.63	186.04	0.2	0.3
1000	120	360	9.7711	9.7089	9.5751	2.0	1.4	308.32	309.00	307.64	0.2	0.4
1500	120	360	12.5411	12.4611	12.2488	2.4	1.7	415.26	416.30	414.03	0.3	0.5
2000	120	360	14.8764	14.7828	14.4898	2.7	2.0	512.84	514.23	510.93	0.4	0.6

The maximum percent difference for the static analysis from Table 3.7 and Table 3.8, was 2.7% for 8 elements, and 2.0% for 16 elements, respectively. Using 8 elements gives a fairly accurate representation of the conductor cable while using 16 elements gives a more accurate representation of the cable, therefore, 16 elements was found to be sufficiently accurate for static analysis.

3.5.2 Free vibration

Free vibration of a conductor cable was validated for the first five modes in ANSYS with the frequencies arrived from Irvine's (Irvine, 1981) theoretical results. Here the conductor cable had to be modelled without sag in order to achieve the first mode. As in section 3.5.1, only the conductor cable's results will be presented here. Figure 3.17 and Figure 3.18 show the convergence of the results obtained from ANSYS compared to the results obtained from Irvine's formulas for both the Out-of-Plane and In-Plane natural frequencies for an increasing number of elements, respectively. The solid lines in Figure 3.17: Out of plane conductor frequencies and Figure 3.18 represent the theoretical values obtained using Irvine's formulas.

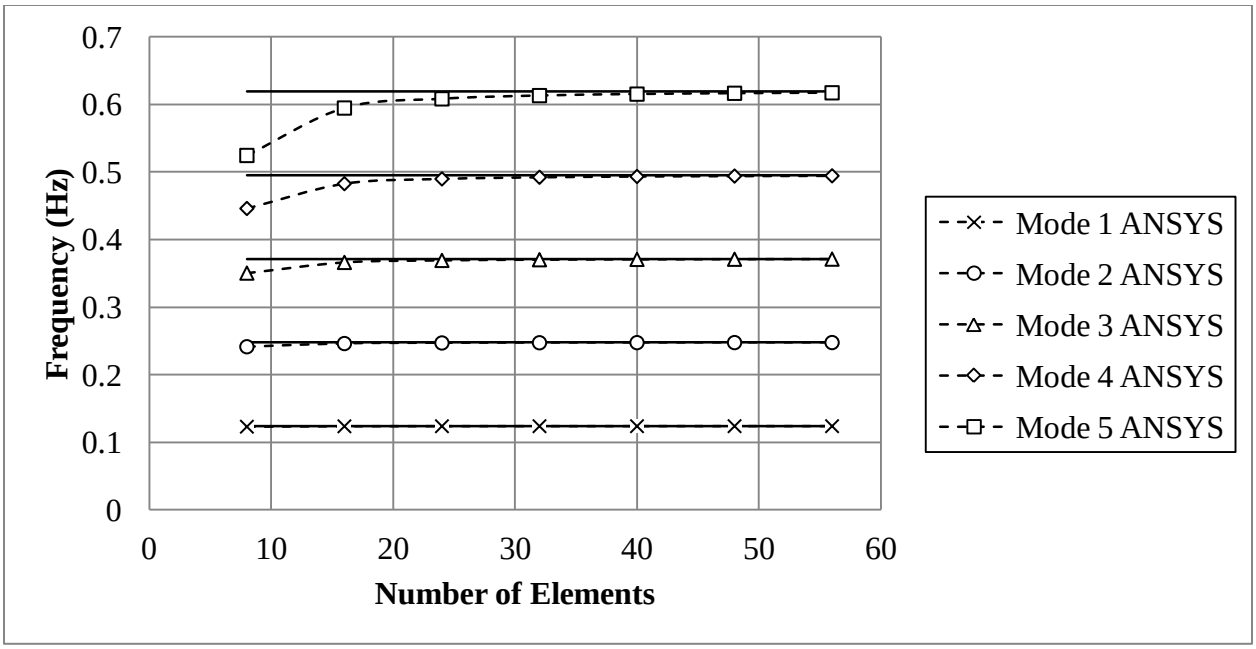

Figure 3.17: Out of plane conductor frequencies

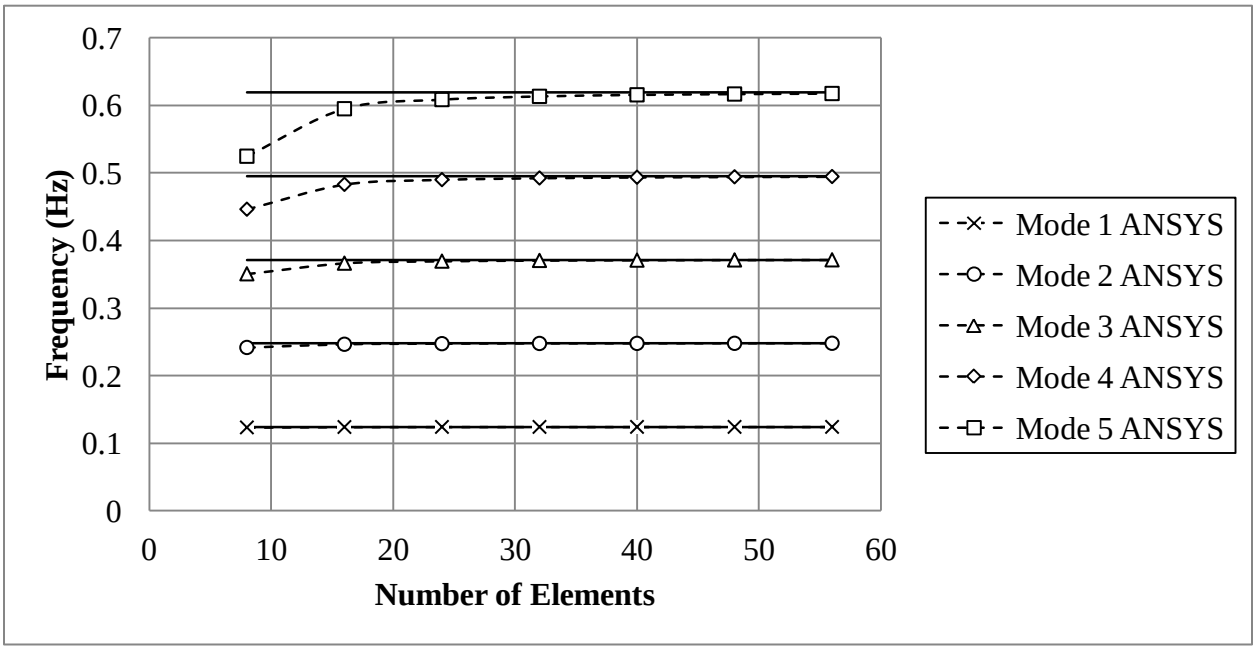

Figure 3.18: In plane conductor frequencies

From the figures, using 16 elements does not give achieve a good representation of the dynamic analysis for higher modes, although it provides an accurate representation of the static analysis.

Using 32 elements was found to accurately predict the frequencies for higher modes, therefore, 32 truss elements will be used to represent each sagging cable in ANSYS.

3.6 Validation of simplified A-402M tower

3.6.1 Static Analysis

The validation of a simplified tower to accurately represent a detailed tower was carried out using several load cases with only two will be presented here. Figure 3.19 shows an isometric view of the detailed tower and the simplified tower. Table 3.9 shows two of the load cases used for this verification. Figure 3.20 shows the locations and axis on which each force acts for the tower. Figure 3.21 shows the corresponding node numbers at which the loads act for the detailed and simplified towers top section and cross arms.

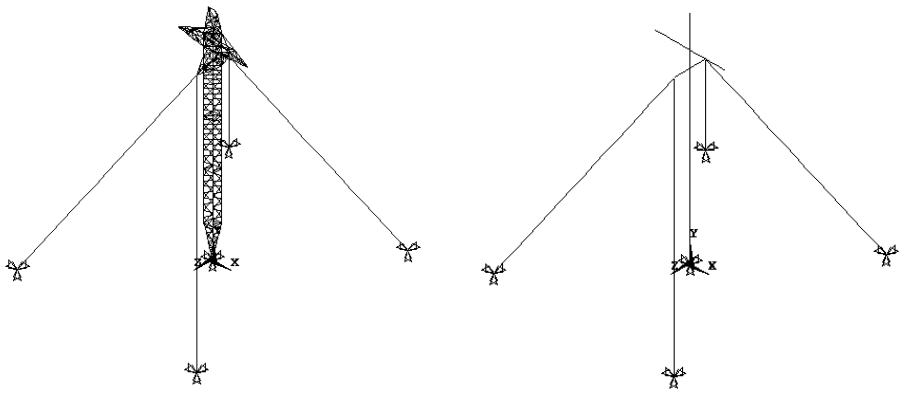

Figure 3.19: Detailed tower compared to simplified tower

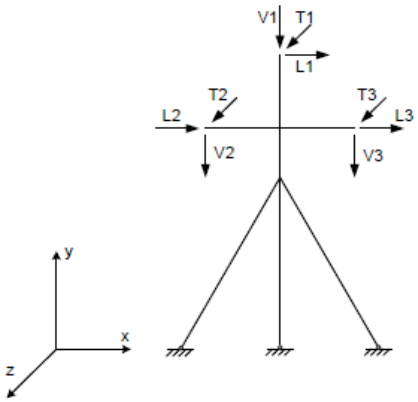

Figure 3.20: Load case forces and nodes on which they act

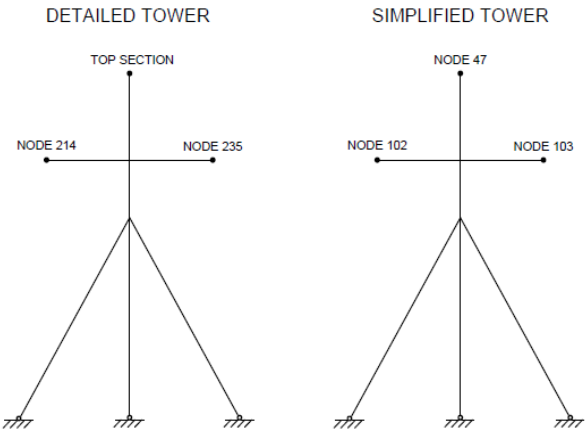

Figure 3.21: Detailed and simplified tower nodes

Table 3.9: Transmission Tower Load Cases

Load Case 1						
		kN		kN		kN
Ground Wire	V1	-8.3800	L1	8.4960	T1	0.0000
Conductor1	V2	-70.4780	L2	32.4360	T2	0.0000
Conductor2	V3	-70.4780	L3	32.4360	T3	0.0000
Load Case 2						
		kN		kN		kN
Ground Wire	V1	2.8470	L1	1.9570	T1	2.1260
Conductor1	V2	-43.4010	L2	18.7710	T2	9.2660
Conductor2	V3	-43.4010	L3	18.7710	T3	9.2660

Table 3.10 and Table 3.11 present the results of load cases one and two for the deflection of the detailed and simplified tower top section and cross arms, respectively.

Table 3.10: Detailed and Simple Tower Deflections for Load Case 1 (unit mm)

Detailed tower				Simplified tower				P.D. (%)		
Node	UX	UY	UZ	Node	UX	UY	UZ	UX	UY	UZ
214	274.52	56.502	0.23765	102	269.34	54.714	1.74E-10	1.9	3.3	NA
235	264.84	-131.75	-0.09306	103	267.83	-135.53	-8.57E-11	1.1	2.8	NA
Top Section	358.92	-17.765	0.0153	47	357.91	-16.618	5.59E-11	0.3	6.9	NA

Table 3.11: Detailed and Simple Tower Deflections for Load Case 2 (unit mm)

Detailed tower				Simplified tower				P.D. (%)		
Node	UX	UY	UZ	Node	UX	UY	UZ	UX	UY	UZ
214	144.99	22.459	190.76	102	142.01	21.536	190.88	2.1	4.3	0.1
235	137.86	-69.347	-21.523	103	139.93	-71.881	-21.402	1.5	3.5	0.6
Top Section	184.66	-10.534	88.879	47	184.31	-10.112	90.713	0.2	4.2	2.0

From the results presented in Table 3.10 and Table 3.11, it can be seen that the simplified tower model gives an accurate representation of the detailed tower model.

3.6.2 Free vibration

A free vibration analysis of the detailed and simplified towers was conducted to validate that the simplified tower can accurately represent the dynamics of the detailed tower. The frequencies of the first 50 mode shapes of the detailed and simplified tower are compared in Table 3.12.

Table 3.12: Detailed and Simplified Tower Mode Frequencies

	Detailed Tower		Simplified Tower	
Mode	Freq (Hz)	Mode	Freq (Hz)	P.D. (%)
1	1.49327	1	1.49311	0.01
2	1.49519	2	1.49468	0.03
3	1.49763	3	1.49647	0.08
4	1.50428	4	1.50359	0.05
5	1.51117	5	1.51092	0.02
6	1.51405	6	1.51358	0.03
7	1.51561	7	1.51547	0.01
8	1.52534	8	1.52478	0.04
9	2.29582	9	2.27249	1.03
10	2.41437	10	2.48061	2.67
11	2.97219	11	2.94659	0.87
12	3.00466	12	3.00327	0.05
13	3.00471	13	3.00337	0.04
14	3.00492	14	3.00353	0.05
15	3.00493	15	3.00353	0.05
16	3.00494	16	3.00355	0.05
17	3.01817	17	3.01538	0.09
18	3.01878	18	3.02047	0.06
19	3.43632	19	3.22646	6.50
20	3.53811	20	3.45077	2.53
21	4.41072	21	4.44386	0.75
22	4.49832	22	4.49627	0.05
23	4.49850	23	4.49650	0.04
24	4.49911	24	4.49702	0.05
25	4.49915	25	4.49705	0.05
26	4.50116	26	4.49908	0.05
27	4.50153	27	4.49979	0.04

28	4.50877	28	4.50405	0.10
29	4.51759	29	4.53110	0.30
30	5.98052	30	5.97785	0.04
31	5.98075	31	5.97809	0.04
32	5.98094	32	5.97817	0.05
33	5.98095	33	5.97817	0.05
34	5.98095	34	5.97817	0.05
35	5.98275	35	5.98036	0.04
36	5.98334	36	5.98102	0.04
37	5.98664	37	5.98289	0.06
38	7.44799	38	7.44515	0.04
39	7.44850	39	7.44520	0.04
40	7.44911	40	7.44566	0.05
41	7.44924	41	7.44579	0.05
42	7.44927	42	7.44580	0.05
43	7.44949	43	7.44638	0.04
44	7.45011	44	7.44684	0.04
45	7.45158	45	7.44801	0.05
46	8.89656	46	8.89384	0.03
47	8.89702	47	8.89397	0.03
48	8.89728	49	8.89521	0.02
49	8.89869	48	8.89472	0.04
50	8.89934	50	8.89523	0.05

3.7 Validation of Cable Breakage

The validation of the cable breakage simulator was done by comparing results obtained from ANSYS to results obtained by Peyrot *et al.* (1980). Peyrot *et al.* performed a full scale transmission line test in Wisconsin on a 138 kV segment. The segment used for the conductor breakage consisted of five spans on one side of the conductor cable breakage shown in Figure 3.22. Peyrot *et al.* determined that a minimum of three spans was needed in order to prevent reduction of the broken wire forces. Five different cases were compared to the results obtained by Peyrot *et al.* Each of the five cases have different properties that are presented in Table 3.13. The first tower at the location of the cable break was modelled as a spring element with a stiffness of 392400 N/m. A lumped mass of 100 kg was added to the arm of the first tower to represent the tower mass for dynamic analysis.

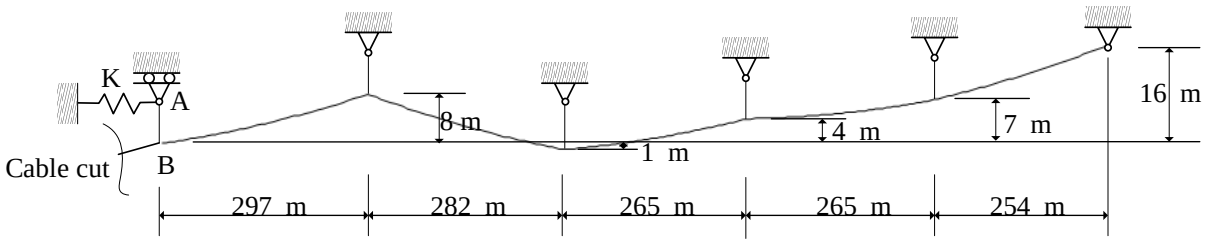

Figure 3.22: Five span transmission line in Peyrot's full scale test (Peyrot, 1980)

Table 3.13: Five span transmission line material properties

Case	Conductor Area ($\times 10^{-4}$ m^2)	Conductor Modulus (GPa)	Conductor Mass (kg/m)	Pretension Force (N)	Insulator Length (m)	Insulator Area ($\times 10^{-4}$ m^2)	Insulator Modulus (GPa)	Insulator Mass (kg/m)
1	1.438	102.97	1.296	18639	2.2	7.9173	200	18.18
2	1.438	102.97	1.296	19130	2.2	7.9173	200	18.18
3	2.342	65.651	0.814	12459	2.2	7.9173	200	18.18
4	2.342	65.651	0.814	17756	2.2	7.9173	200	18.18
5	2.342	65.651	0.814	21288	2.2	7.9173	200	18.18

In the analysis, the "ekill" command was used in ANSYS to simulate the conductor cable break. Each conductor span was modelled using 50 elements with a catenary profile that follows Equation 3.7. A damping ratio of 2% was used for all five cases. A time step of 0.001 seconds was used and the "ekill" command was issued at 0.001 seconds. The analysis was run up until 2 seconds in order to determine the force of the first two peaks in the insulator string at point B. The results obtained from ANSYS were compared to the results presented by Peyrot *et al.* in Table 3.14. The results that were compared were the final residual static force of the insulator string, and the first and second peak forces. Figure 3.23 shows a comparison of the tensile forces obtained from ANSYS and those presented by Peyrot *et al.* in the insulator string at point B.

Table 3.14: Comparison of ANSYS results to Peyrot *et al*. results for five span cable break

Case	ANSYS			Peyrot *et al.*			Percent Difference (%)		
	Final Tension (N)	First Peak (N)	Second Peak (N)	Final Tension (N)	First Peak (N)	Second Peak (N)	Final Tension (N)	First Peak (N)	Second Peak (N)
1	11103	24121	37196	10987	24623	31883	1.06	2.04	16.66
2	11287	24362	37725	10987	24623	34727	2.73	1.06	8.63
3	7050	18787	25651	7063	15009	20307	0.18	25.17	26.32
4	8459	22393	28966	8731	20307	24623	3.12	10.27	17.64
5	9345	24720	28951	9320	24623	21778	0.27	0.39	32.94

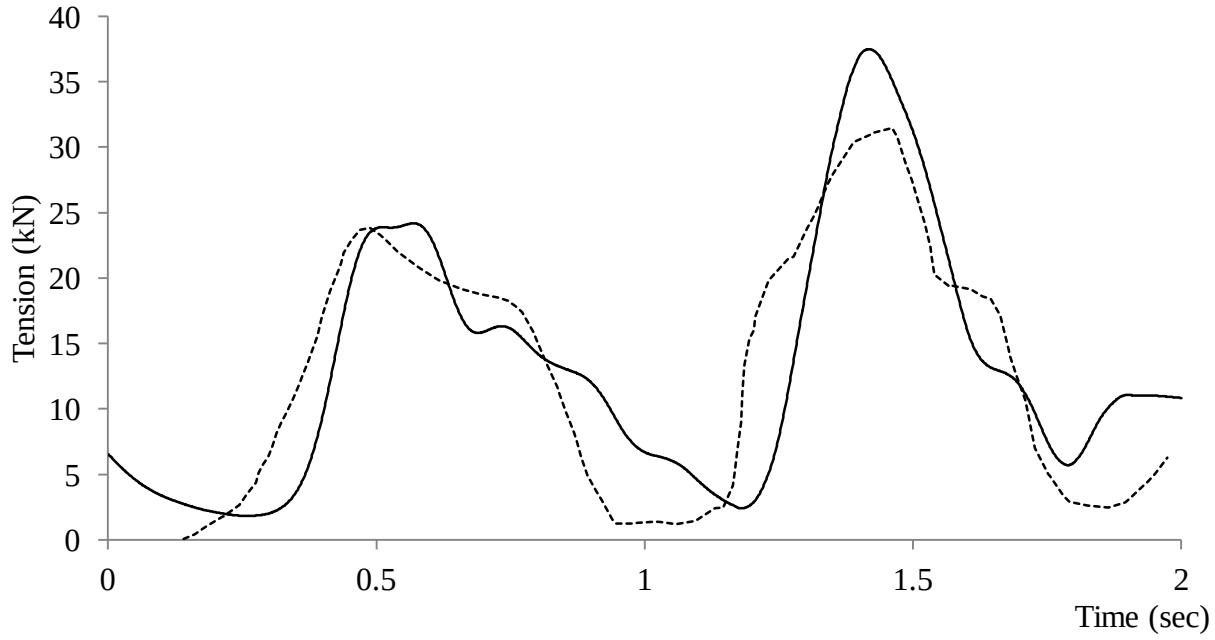

Figure 3.23: Tension at point B of the insulator string AB [Dash line – full scale case 1 test (Peyrot *et al.* 1980), Solid line – ANSYS simulation (Smoothed with RLOESS 0.15%)

Chapter 4 Longitudinal Load Factors (LLF)

The main objective of this paper is to investigate the LLF's as a result of cable breakages in the A-402M transmission line system. A ten-span transmission line system that consisted of nine simplified towers and two dead end towers was modelled in ANSYS to investigate this objective. It should be noted that the conductors and the ground wire were considered to break simultaneously for all cases that were considered. The properties of the conductor, ground wire, and guyed cable are the same as those that were presented in Table 3.6. As stated earlier, section 3.3.2 of ASCE Manual No.74 provides figures to calculate the approximate LLFs of a transmission line system as a function of the S/S ratio, the S/I ratio and the stiffness of the supporting tower. The results obtained from ANSYS were then compared to the results obtained from using ASCE Manual No.74 and the EPRI equations.

4.1 ANSYS Modelling

A ten-span transmission line was created in ANSYS using nine simplified towers and two-dead end models that are shown in Figure 4.1 in order to simulate the different cable breakage cases. The two-dead end models are modelled using pin supports in ANSYS to resist movement in all directions. The conductors and ground wire cable were all broken simultaneously in the left-most span of the developed model.

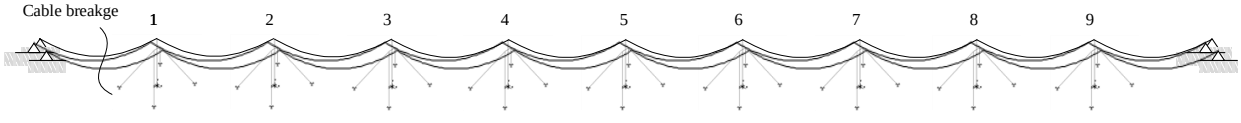

Figure 4.1: A ten-span tower model

4.1.1 Cable Breakage Cases

Several cases were needed to accurately compare the results from ANSYS to those obtained with the ASCE and the EPRI methods. Therefore, ten different cases were considered and simulated in ANSYS to obtain accurate results by varying the S/S ratios, the S/I ratios, and the stiffness K of the towers. The stiffness of both the detailed and simplified A-402M towers was calculated to be 296 kN/m at the conductor location. The properties used for each case are presented in Table 4.1. It should be noted that the span length for all cases is 480 metres.

Table 4.1: Cable breakage cases

Case	Sag (m)	Insulator Length (m)	K (kN/m)	S/S	S/I
1	8	4.27	296.0	60	112.4
2	10	4.27	296.0	48	112.4
3	15	4.27	296.0	32	112.4
4	20	4.27	296.0	24	112.4
5	20	3.27	296.0	24	146.8
6	20	5.27	296.0	24	91.1
7	20	6.27	296.0	24	76.6
8	20	4.27	274.9	24	112.4
9	20	4.27	243.9	24	112.4
10	20	4.27	212.7	24	112.4

4.1.2 Solution Controls

4.1.2.1 Time Step Size

In order to obtain an accurate solution with ANSYS, a small enough time must be used. The time step used for all cases was 0.001 seconds. This time step was found to provide an accurate solution for all cases, while also maintaining a relatively quick analysis time. All cases were run for a 16 second analysis, with the cable breakages occurring at 1 second.

4.1.2.2 Damping Coefficients

Damping is a key part of dynamic as it takes into account the structures ability to dissipate energy. There are several different methods that can be used to determine the damping of a structure. In this analysis, Rayleigh damping was used for all cases.

Damping of a structure can be determined by experimental results. Battista *et al*. recommends a damping ratio of 2% for steel bolted structures when no experimental results are given (Battista *et al*. 2003). Since no experimental results are given in this analysis, a damping ratio of 2% was assumed for all cases. Rayleigh damping assumes that the damping matrix [**C**] is proportional to both the mass [**M**] and the stiffness [**K**] of the structure. If the structure has natural frequencies lower than 1 Hz, damping can be assumed to be proportional to the mass matrix only, and when the natural frequencies are much higher than 1 Hz the damping matrix can be assumed to be proportional to the stiffness matrix only (Tabet, 2009). Since the tower in this study has natural frequencies that range from 1.49 Hz to 1.52 Hz for the first eight mode shapes, the damping matrix was assumed to be proportional to both the mass and stiffness of the structure. The formula for the damping takes the form of

$$[\mathbf{C}] = \alpha[\mathbf{M}] + \beta[\mathbf{K}] \tag{4.1}$$

Where the coefficients α and β are a function of the i^{th} frequencies ω_i and the i^{th} modal damping ratios ξ_i, and is shown in Equation 4.2.

$$\xi_i = \frac{\alpha}{2\omega_i} + \frac{\beta\omega_i}{2} \tag{4.2}$$

The equation can then be rearranged in term of α and β, and takes the form:

$$\begin{aligned} \alpha &= 2\xi_i\omega_i - \beta\omega_i^2 \\ \beta &= \frac{2\xi_j}{\omega_j} - \frac{\alpha}{\omega_j^2} = \frac{2(\xi_j\omega_j - \xi_i\omega_i)}{\omega_j^2 - \omega_i^2} \end{aligned} \tag{4.3}$$

When the damping ratio of the system is assumed to be constant, Equation 4.3 can be simplified into the following:

$$\begin{aligned} \alpha &= 2\xi\frac{\omega_i\omega_j}{\omega_i + \omega_j} \\ \beta &= \frac{2\xi}{\omega_i + \omega_j} \end{aligned} \tag{4.4}$$

Where ω_i and ω_j are chosen from the extremes of the design frequency range (Oliveira, 2006). For this study, the values of ω_i were taken to be the frequency of the first mode shape, and the value of ω_j was taken to be 18.97 Hz for all cases. This value of ω_j was chosen because all models have that frequency within the specified range and a change in value has a negligible effect on the damping matrix (Tabet, 2009). The frequency of the first mode shape for all ten cases and the resulting damping coefficients that were used for analysis in ANSYS are presented in Table 4.2.

Table 4.2: First mode shape natural frequencies and damping coefficients

Case	ω_i (Hz)	α	β
1	0.15039	0.037499	0.000333
2	0.14494	0.036151	0.000333
3	0.12536	0.031299	0.000333
4	0.11198	0.027979	0.000334
5	0.11443	0.028587	0.000334
6	0.10966	0.027402	0.000334
7	0.10745	0.026853	0.000334
8	0.11195	0.027971	0.000334
9	0.11190	0.027959	0.000334
10	0.11185	0.027946	0.000334

4.1.2.3 Element Death

In order to model the cable breakage in ANSYS, the command "*ekill*" must be issued to all elements that are required to be killed. To ensure that the program converges properly, the "*ekill*" command was issued for every conductor and ground wire element in the far left span. Since ANSYS has no command to kill nodes, every node in the far left span was constrained from moving. It was found that if this was not done, the elements would be free to move about the model as they have no stiffness matrix, and would result in ANSYS giving displacements that are larger than the program can handle for the analysis. As a result, these conditions had to be met to ensure proper convergence.

4.2 Results

The resulting LLF's for all ten cases are presented in Table 4.3. The LLF's are the maximum tension at the conductor location (obtained from the dynamic analysis mentioned in section 4.1) divided by the initial conductor tension.

Table 4.3: Longitudinal Load Factors

Case	K (kN/m)	S/S	S/I	LLF
1	296.0	60	112.4	1.3277
2	296.0	48	112.4	1.5403
3	296.0	32	112.4	2.0630
4	296.0	24	112.4	2.5432
5	296.0	24	146.8	2.3649
6	296.0	24	91.1	2.4470
7	296.0	24	76.6	2.3196
8	274.9	24	112.4	2.5212
9	243.9	24	112.4	2.4545
10	212.7	24	112.4	2.3211

Figure 4.2 shows the plot of normalized LLF's for cases 1 to 4, which is used to investigate the effect of S/S on the LLF values when both S/I and K are fixed. The normalized value of LLF at each point is equal to the LLF at the considered point divided by the maximum value of LLF among the data points. The normalized values of LLF in Figure 4.2 are for the first tower adjacent to the cable breakage, i.e. tower 1 in Figure 4.1. Here the S/I and the K values of the tower are fixed at 112.4 and 296 kN/m, respectively.

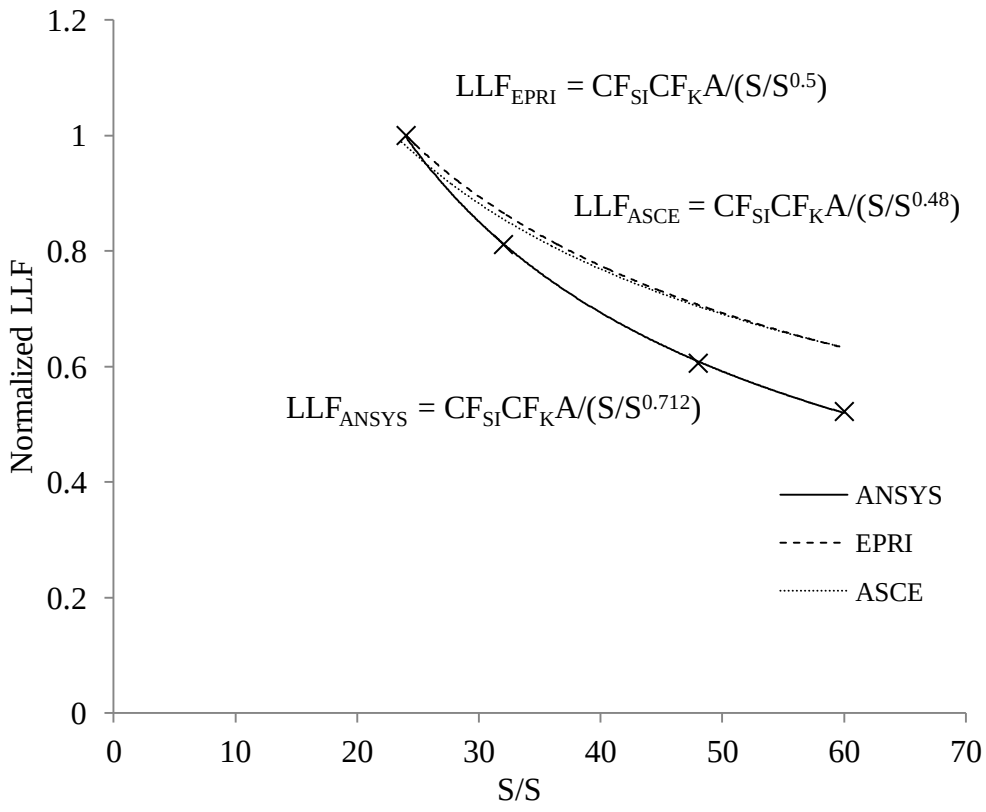

Figure 4.2: Normalized LLF at the conductor location for the first tower

The LLF's based on the EPRI report is given by the equation:

$$LLF = CF_{S/I} CF_K \frac{\mathrm{A}}{(S/S)^{0.5}} \tag{4.5}$$

Where $CF_{S/I}$ is the S/I Correction Factor, CF_K is the K Correction Factor, and A is the response coefficient of the structure. It is therefore assumed that the values of LLF obtained from ANSYS will follow the same format. A trend line was then added to the ANSYS simulation to determine the equation of LLF, which is found to be:

$$LLF = CF_{S/I} CF_K \frac{\text{constant}}{(S/S)^{0.712}} \tag{4.6}$$

Where $CF_{S/I}$ is the S/I Correction Factor, and CF_K is the K Correction Factor. The plot of the LLF's based on the EPRI report includes the Span/Insulator and Stiffness Correction Factors for the first tower.

The LLF's calculated by ANSYS contain the correction factors from for S/I and K that are shown in Equation 4.6. The correction factor for S/I must first be determined by varying the length of the insulator string. Table 4.4 lists the LLF's for the tower adjacent to the cable breakage obtained from ANSYS. The S/S and K values are fixed at 24 and 296 kN/m, respectively. The correction factor of S/I based on the EPRI report is given by the equation:

$$CF_{S/I} = 1 - \frac{S/I}{2000} \tag{4.7}$$

The plot of the LLF vs. S/I for ANSYS in Figure 4.3 (cases 4 to 7), which are obtained from the analysis, shows polynomial dependency. It is therefore assumed that the relationship of the correction factor will be a second order polynomial as:

$$CF_{S/I} = \frac{1}{\text{constant}}\left[1 + a\left(S/I\right) + b\left(S/I\right)^2\right] \le 1.0 \tag{4.8}$$

Using the information in Table 4.4 with Equation 4.8, the correction factor is found to be:

$$CF_{S/I} = 0.10006 + 1.56985\times10^{-2}\left(S/I\right) - 6.84333\times10^{-5}\left(S/I\right)^2 \tag{4.9}$$

Table 4.4: Effect of S/I on LLF

S/I	76.6	91.1	112.4	146.8
LLF	2.3196	2.4470	2.5432	2.3649

The effect of the tower stiffness, K, is determined by fixing the values of S/S and S/I. Here these values are set at 24 and 112.4, respectively. The results of cases 4, 8, 9, and 10 are presented in Table 4.5 and Figure 4.4, which show the effect of K on the LLF's.

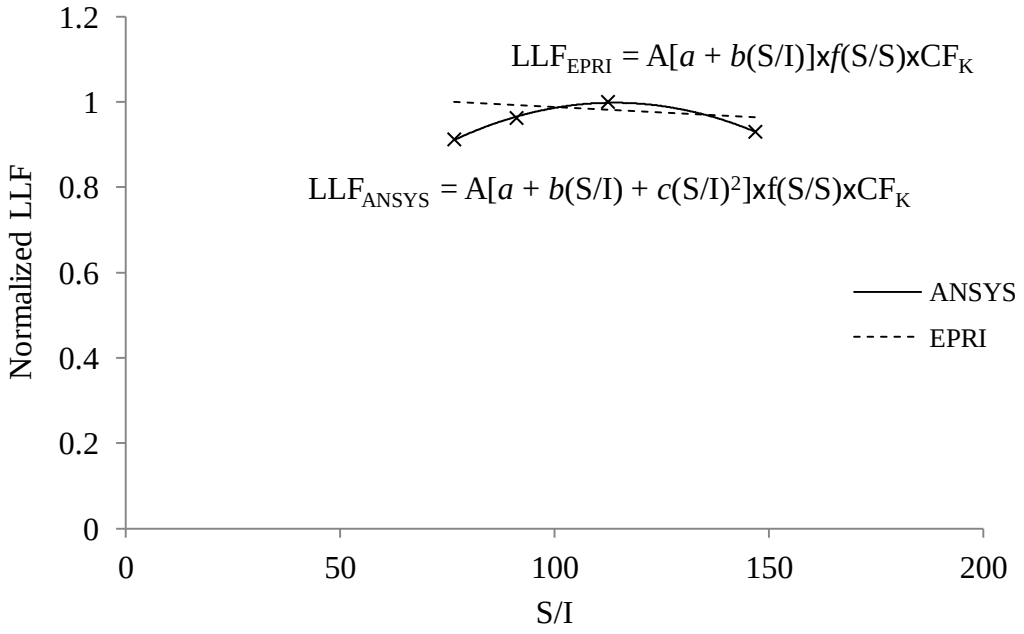

Figure 4.3: Normalized LLFs from ANSYS simulation and EPRI calculation

Table 4.5: Effect of the K on the LLFs

K (kN/m)	296.0	274.9	243.9	212.7
LLF	2.5432	2.5212	2.4545	2.3211

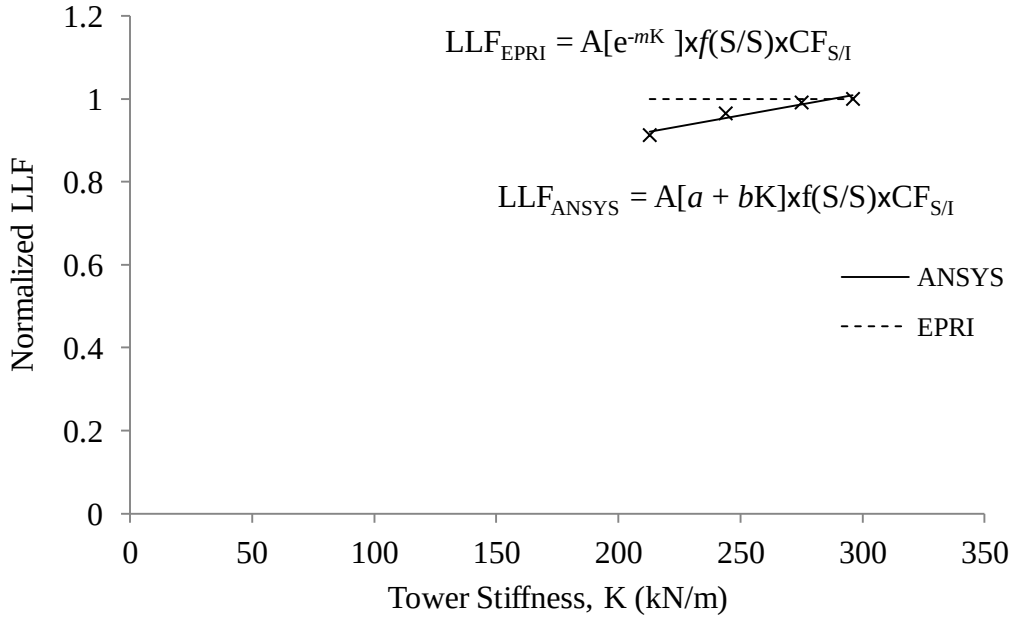

Figure 4.4: The effect of K on the normalized LLFs

The equation for the correction factor due to the stiffness of the supporting tower given by the EPRI report is:

$$CF_{1/K} = e^{-\frac{1/K}{200}} \tag{4.10}$$

Where, K is in kip/in. The plot from the ANSYS simulation indicates that the relationship between LLF and K is linear. The correction factor therefore assumed to be in the form:

$$CF_K = \frac{1}{\text{constant}}(a + bK) \leq 1.0 \tag{4.11}$$

Using equation 4.11 and Table 4.5, this correction factor was found to be:

$$CF_K = 0.87824 + 4.1134\text{x}10^{-4} K \tag{4.12}$$

From Equations 4.6, 4.9, and 4.12, along with the results from the ANSYS simulations, the LLF can be expressed as:

$$LLF = CF_{S/I} CF_K \frac{24.305}{(S/S)^{0.712}} \tag{4.13}$$

The above equation is valid for $20 \leq S/S \leq 90$; $70 \leq S/I \leq 130$. It should be noted that the stiffness of the supporting structure has a prominent effect on the resulting value of LLF. This reason for this is that when the tower stiffness increases, the unbalanced force will be larger. The ASCE manual shows that the LLF for rigid support structures is almost 1.4 times that of a flexible supporting structure. The plots of the LLF's that were calculated based on Equation 4.13 and those obtained by the EPRI equation by varying S/I from 70 to 105 with a fixed K value of 275 kN/m are shown in Figure 4.5. The figure shows that the LLF values calculated using both Equation 4.13 developed from ANSYS and equation 4.5 from the EPRI report are in very good accordance. At an S/S value of 20, the difference is 14%, and at an S/S value of 90, the difference is 3%. Increasing K from 275 to 300 kN/m, will result in difference of 15% at an S/S value of 20, and a difference of 2% at an S/S value of 90.

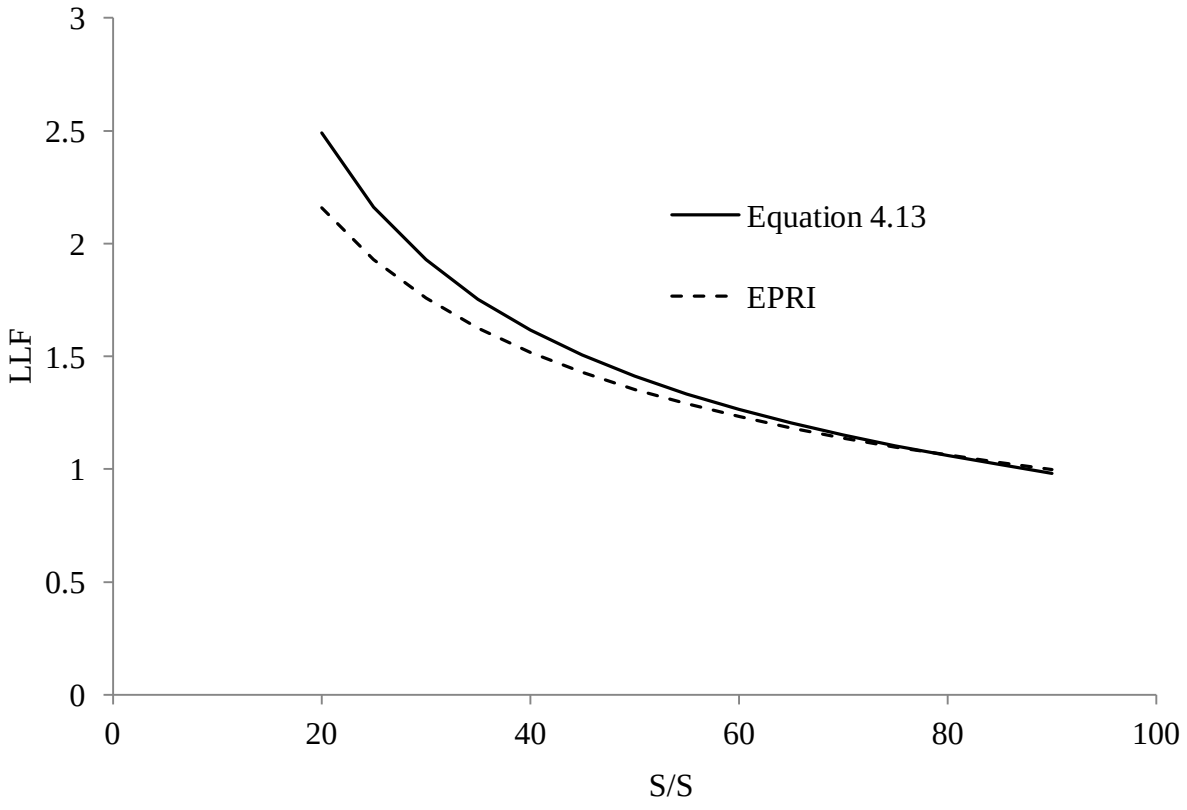

Figure 4.5: LLFs comparison between 4.13 and EPRI report

Chapter 5 Conclusions and Recommendations

5.1 Conclusions

The finite element program ANSYS was used to analyse a 10-span guyed transmission line system. In the analysis, the towers were modelled with the simplified towers. These simplified towers used equivalent geometric properties developed to represent the detailed towers. Non-linear transient dynamic analyses of this 10-span transmission line system subject to conductor and ground wire cable breakages in the first span was simulated using the dynamic solver in ANSYS for ten different cases. The results from these ten cases were then used to formulate an equation that can be used to predict the LLF for this guyed transmission line having different S/S, S/I, and K values.

In summary, the program ANSYS was used to:

a) Model both the detailed and simplified version of the A-402M transmission tower using beam and three-dimensional truss elements.
b) Verify the non-linear static and dynamic solver.
c) Verify the accuracy of the number of beam and three-dimensional truss elements needed to represent the transmission line.
d) Verify that the simplified tower can accurately represent the detailed tower in both non-linear static and dynamic analysis.
e) Verify that the dynamic solver could accurately simulate a cable breakage.
f) Simulate conductor and ground wire cable breakages in the first span of a ten-span transmission line for ten different cases.

This study showed that:

a) The simplified tower that was developed from using equivalent geometric properties could accurately represent the detailed tower both statically and dynamically to within a 7% margin of error.

b) A minimum of 32 three-dimensional truss elements are needed to accurately model a sagging cable in a transmission line both statically and dynamically.

c) The LLF depends on the S/S ratio, the S/I ratio, and the K of the supporting tower.

d) The LLF for an A402-M guyed transmission line can be obtained using the equation:

$$LLF = CF_{S/I} CF_K \frac{24.305}{(S/S)^{0.712}}$$

where the correction factors due to the S/I ratio and the K of the supporting structures are, respectively:

$$CF_{S/I} = 0.10006 + 1.56985 \times 10^{-2} (S/I) - 6.84333 \times 10^{-5} (S/I)^2$$

$$CF_K = 0.87824 + 4.1134\text{x}10^{-4} K$$

e) The predicted LLFs using the equation are comparable with the LLFs calculated using the EPRI report and almost doubled the values suggested in the ASCE manual.

f) The effect of the K of the supporting structures is found to be more pronounced than what is suggested by the EPRI report.

5.2 Recommendations for Future Work

The author recommends the following for future research:

a) Perform a non-linear dynamic cable breakage analysis for values of S/S, S/I, and K that are outside the spectrum of this study.

b) Perform a non-linear dynamic analysis under other types of unbalanced longitudinal loadings (i.e. wind and ice load).

c) Consider the buckling of one or more tower members and their effect on the longitudinal loads.

d) Perform a non-linear dynamic cable breakage analysis under different combinations of cable breakages (e.g. Conductor cable breakages in different spans).

References

ASCE. (2010). *Manual of Practice No. 74, Guidelines for Electrical Transmission Line Structural Loading. 3rd Edition.* Reston: American Society of Civil Engineers.

ASCE. (1997). *Manual of Practice No.10, Design of Latticed Steel Transmission Structures.* Reston: American Society of Civil Engineers.

ASCE. (1988). *Manual of Practice No.52, Guide for Design of Steel Transmission Towers. 2nd Edition.* New York: American Society of Civil Engineers.

Battista, R. C., Rodrigues, R. S., & Pfeil, M. S. (2003). Dynamic Behaviour and Stability of Transmission Line Towers Under Wind Forces. *Wind Engineering* , 1051-1067.

Campbell. (1970). Unbalanced Tension in Transmission Lines. *ASCE: Journal of the Structural Division , 96* (10), 2189-2207.

Cardona, A., & Geradin, M. (1988). A Beam Finite Element Non-Linear Theory with Finite Rotations. *International Journal for Numerical Methods in Engineering* , 26: 2403-2438.

Crisfield, M. A. (1990). A Consistent Co-rotational Formualtion for Non-linear, Three-dimensional, Beam-elements. *Computer Methods in Applied Mechanics and Engineering* , 81: 131-150.

Crivelli, L. A. (1990). *A Total-Lagrangian Beam Element for Analysis of Nonlinear Space Structures.* University of Colorado.

Disney, P., & Parke, G. (2004). *The Appraisal of Manitoba Hydro A-402 Guyed Suspension Towers Under High Intensity Winds.* University of Surrey.

EPRI. (1998). *Longitudinal Load and Cascading Failure Risk Assessment.* Portland: Electronic Power Research Institute.

Fleming, J. F., Atkins, R. S., & Mozer, J. D. (1978). A Program for Longitudinal Load Analysis of Electric Transmission Lines. *Computers and Structures , 9* (3), 237-253.

Horr, A. M., Yibulayin, A., & Disney, P. (2004). Nonlinear Spectral Dynamic Analysis of Guyed Towers. Part II: Manitoba Towers Case Study. *Canadian Journel of Civil Engineering* , 1061-1076.

Irvine, M. (1981). *Cable Structures.* Toronto: Massachusetts Institute of Technology.

Kempner, L. (1997). *Longitudinal Impact Loading on Electrical Transmission Line Towers - A Scale Model Study.*

Lapointe, M. (2002). *Dynamic Analysis of a Power Line Subjected to Longitudinal Loads.* Montreal: McGill University.

Le, T. N., Battini, J. M., & Hjiaj, M. (2011). Efficient Formulation for Dynamics of Corotational 2D Beams. *Computational Dynamics* , 1-9.

Li, Z. X. (2007). A Co-Rotational Formulation for 3D Beam Elements Using Vectorial Rotational Variables. *Computer Mechanics* , 39: 309-322.

McClure, G., & Lapointe, M. (2003). Modelling the Structural Dynamic Response of Overhead Transmission Lines. *Computers and Structures , 81*, 825-834.

McClure, G., & Tinawi, R. (1982). Mathematical Modelling of the Transient Response of Electric Transmission Lines due to Conductor Breakage. *Computers and Structures , 26* (1/2), 41-56.

Mozer, J. D., Pohlman, J. C., & Fleming, J. F. (1977). Longitudinal Load Analysis of Transmission Line Systems. *IEEE Transactions on Power Apparatus and Systems , PAS-96* (5), 1657-1665.

Mozer, J. D., Wood, W. A., & Hribar, J. A. (1981). Broken Wire Tests on a Model Transmission Line System. *IEEE Transactions on Power Apparatus and Systems , PAS-100* (3), 938-947.

Oliveira, M. R. (2006). *Structural Analysis of Energy Transmission Towers Subjected to Dynamic Effects Induced by Wind.* University of the State of Rio de Janeiro.

Peyrot, A. H., Kluge, R. O., & Lee, J. W. (1980). Longitudinal Loads from Broken Conductors and Broken Insulators and their Effect on Transmission Lines. *IEEE Transactions on Power Apparatus and Systems , PAS-99* (1), 222-234.

Shen, G. H., Cai, C. S., Sun, B. N., & Lou, W. J. (2011). Study of Dynamic Impacts on Transmission-Line Systems Attributable to Condcutor Breakage Using the Finite-Element Method. *Journal of Performance of Constructed Facilities , 25* (2), 130-137.

Siddiqui, F. M., & Fleming, J. F. (1984). Broken Wire Analysis of Transmission Line Systems. *Computers and Structures , 18* (6), 130-137.

Simo, J. C., & Vu-Quoc, L. (1986). A Three-Dimensional Finite-Strain Rod Model Part II: Computation Aspects. *Computer Methods in Applied Mechanics and Engineering* , 58: 79-116.

Tabet, F. (2009). *Static and Dynamic Analyses of a Transmission Tower-Line System Using a Simplified Model.* Winnipeg: University of Manitoba.

Thomas, M. B., & Peyrot, A. H. (1982). Dynamic Repsonse of Ruptured Conductors in Transmission Lines. *IEEE Transaction on Power Apparatus and System , PAS-101* (9), 3022-3027.

Wang, Z. Q., & Rattanawangcharoen, N. (2008). *The Analysis of a Transmission Guyed Tower Line System Subjected to Downburst Wind.* Winnipeg: Manitoba Hydro.

Appendix - A

The mode shapes of the detailed and simplified transmission towers

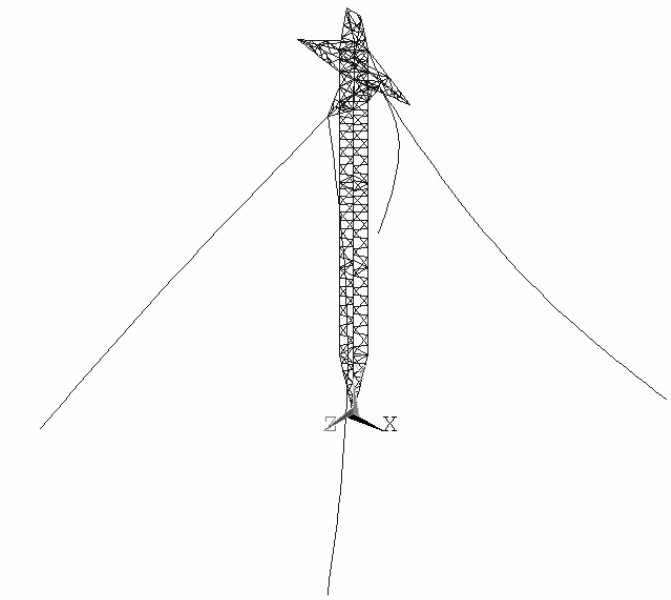

Isometric view

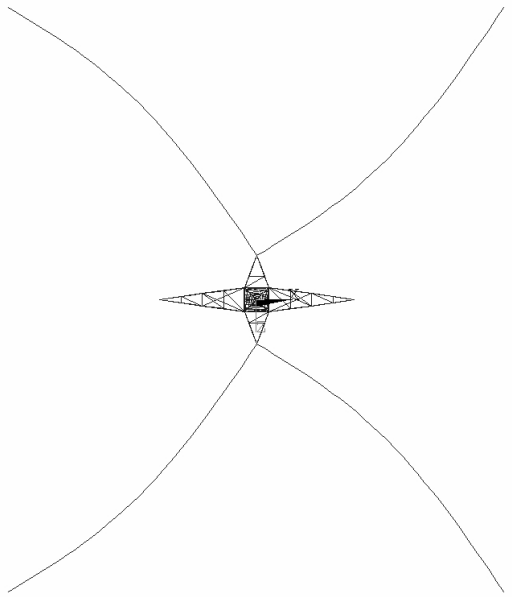

Top view

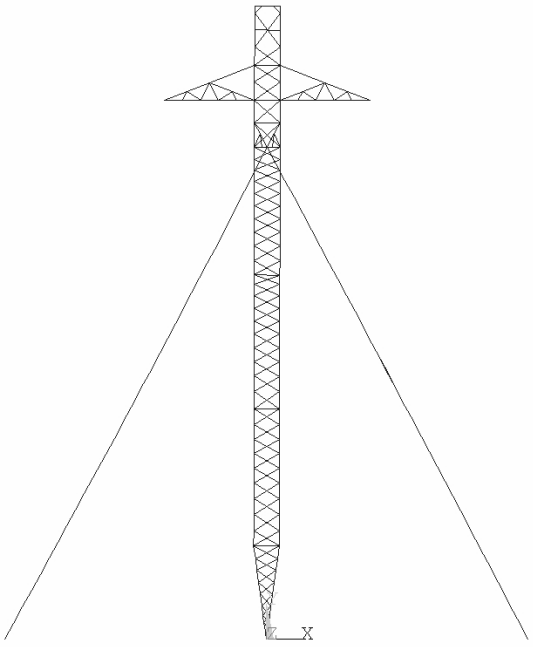

Longitudinal view

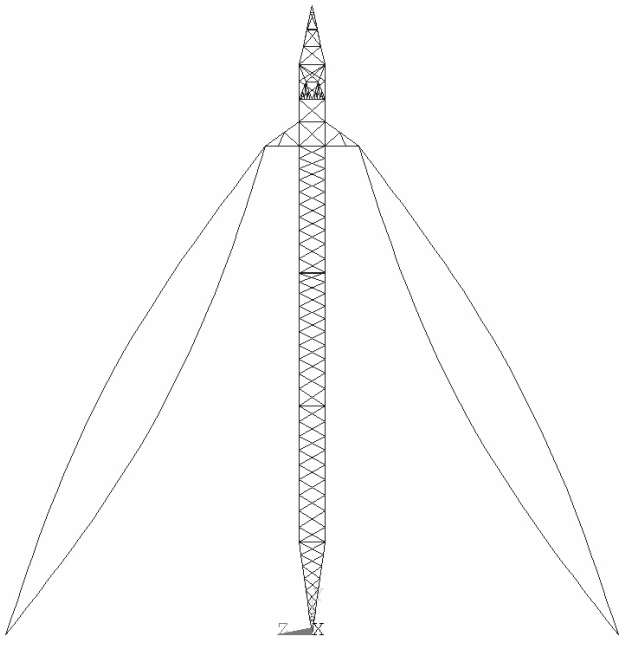

Transverse view

Figure A.1: 1st mode shape of the detailed tower (Frequency = 1.49 Hz)

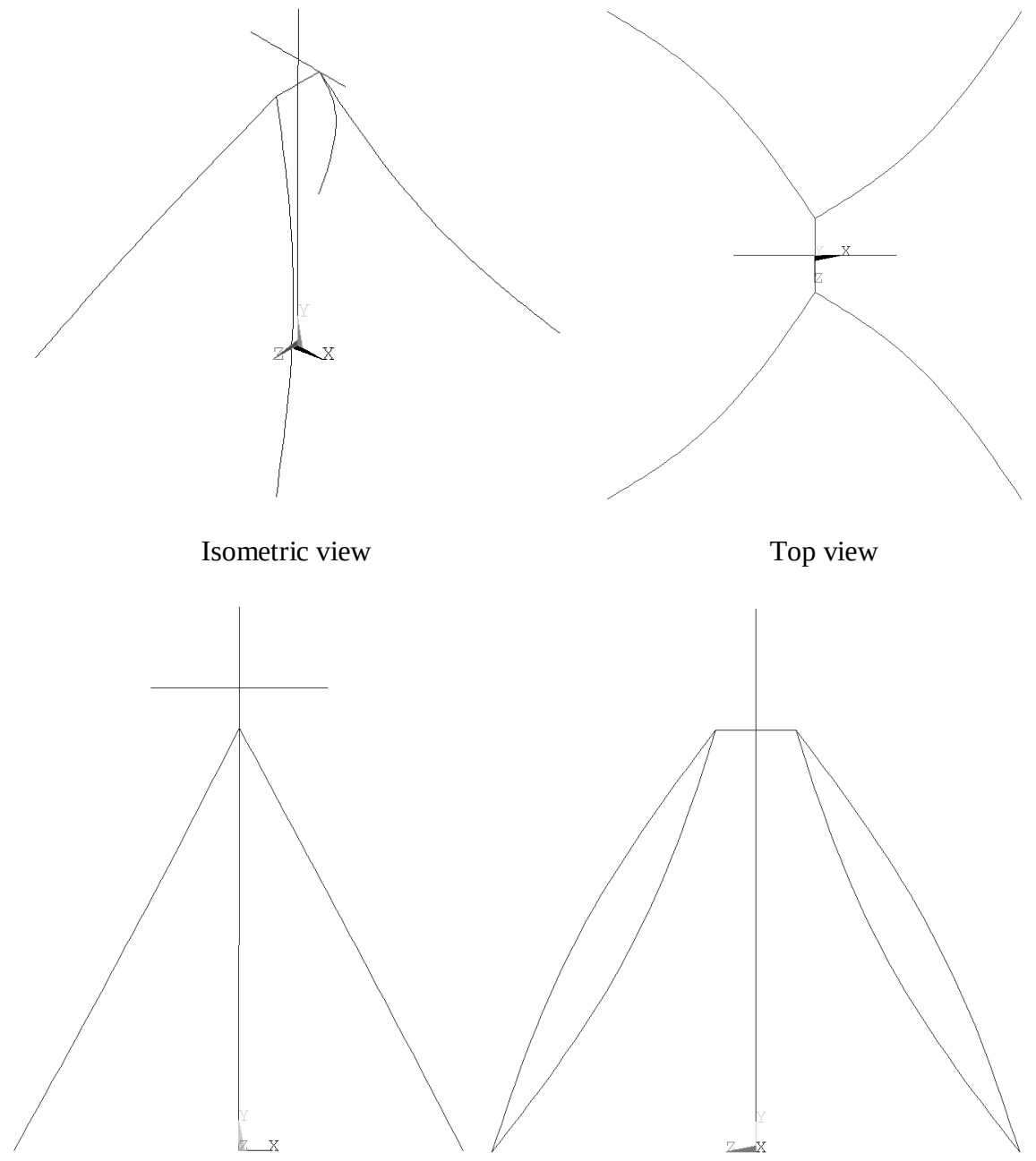

Figure A.2: 1st mode shape of the simplified tower (Frequency = 1.49 Hz)

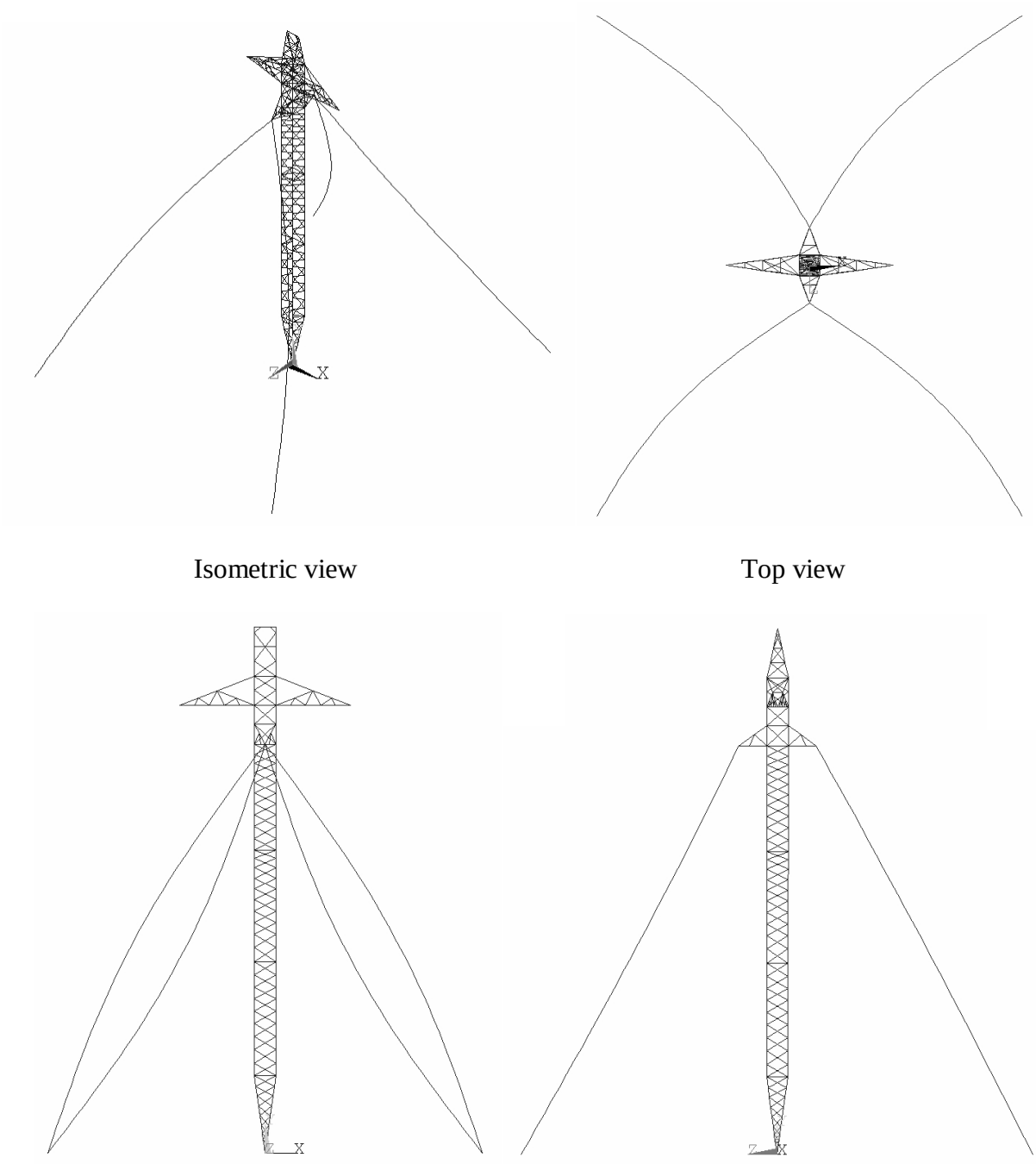

Figure A.3: 2nd mode shape of the detailed tower (Frequency = 1.50 Hz)

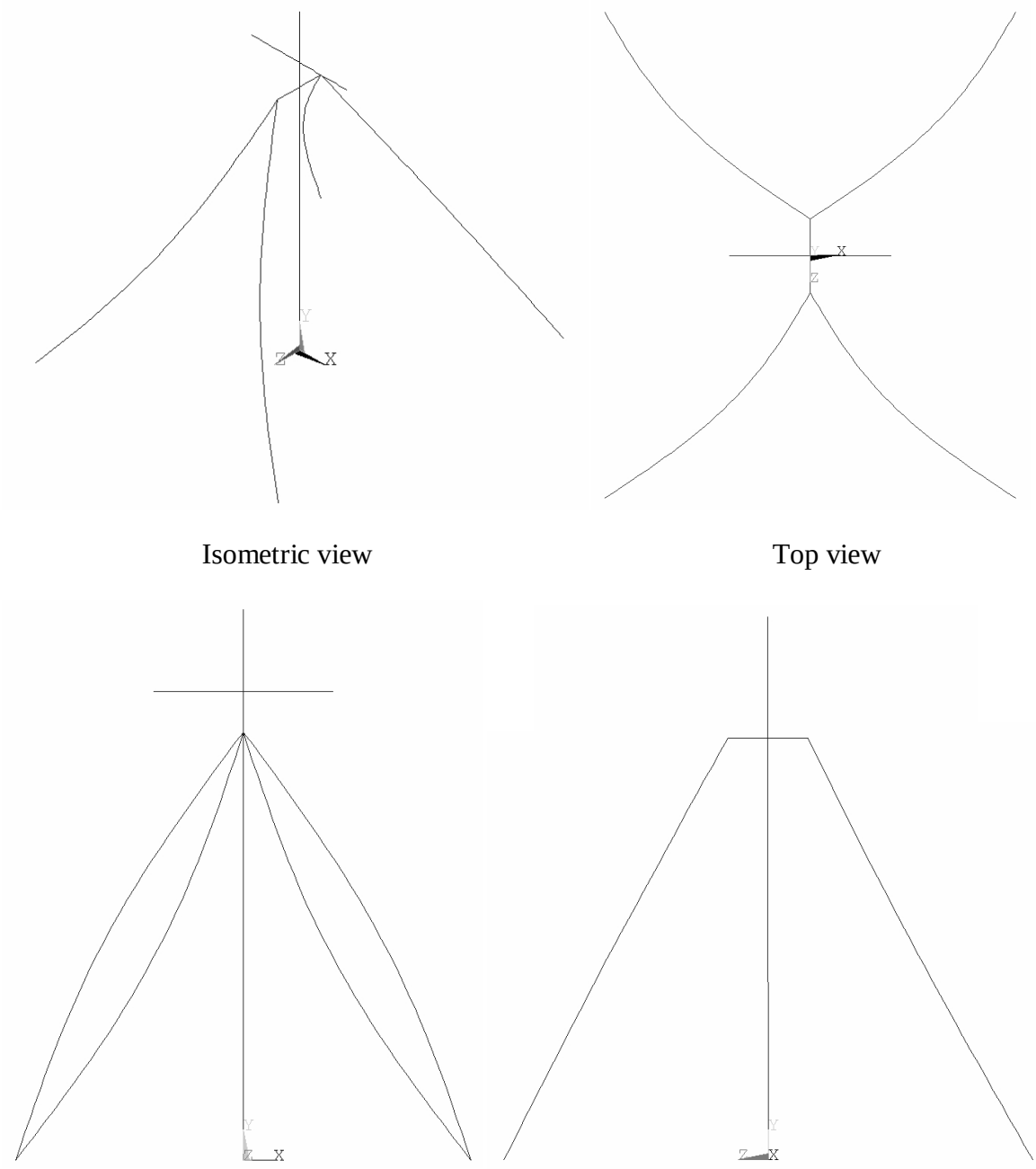

Figure A.4: 2nd mode shape of the simplified tower (Frequency = 1.49 Hz)

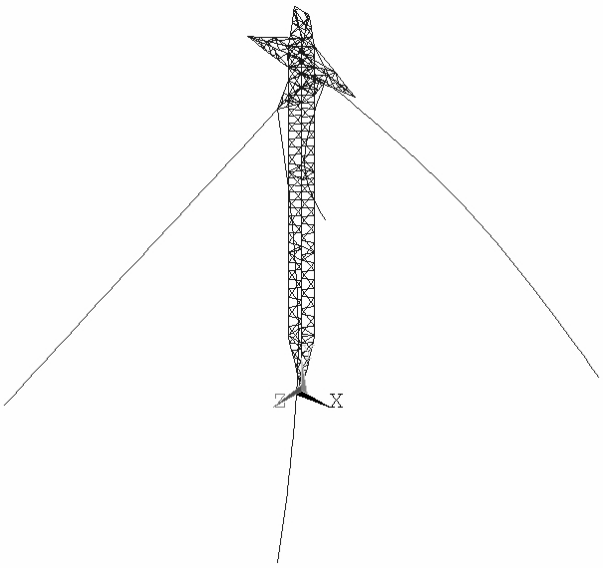

Isometric view

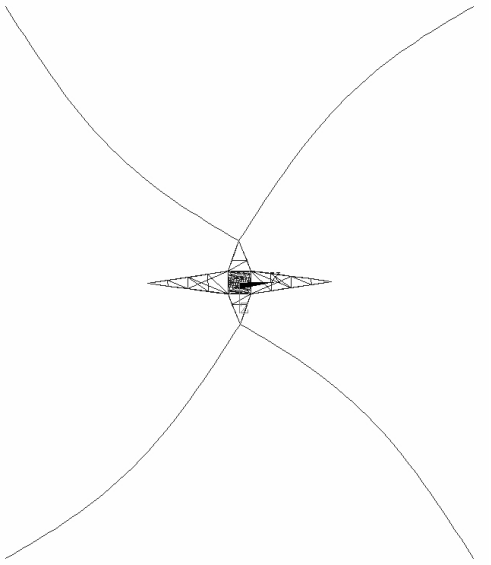

Top view

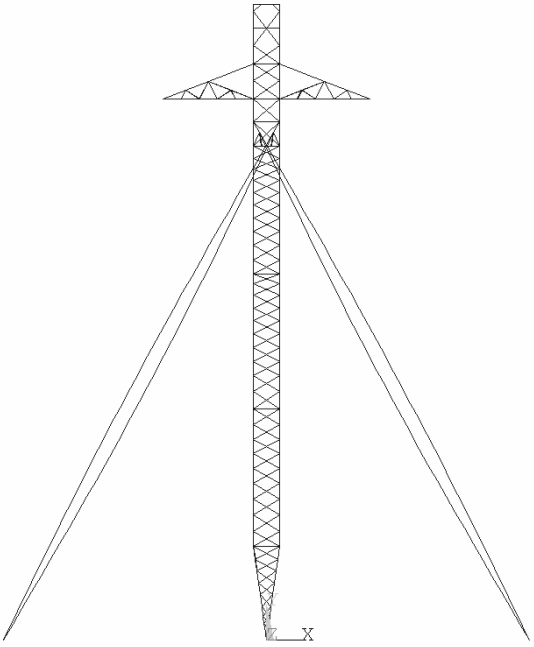

Longitudinal view

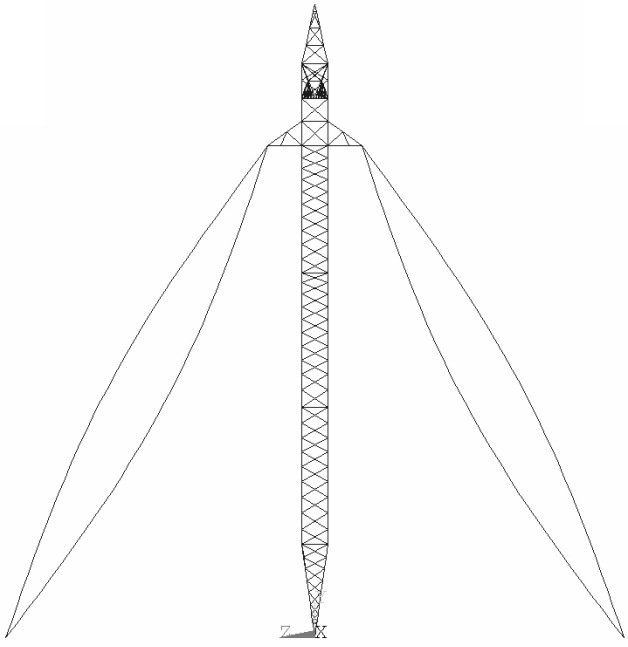

Transverse view

Figure A.5: 3rd mode shape of the detailed tower (Frequency = 1.49 Hz)

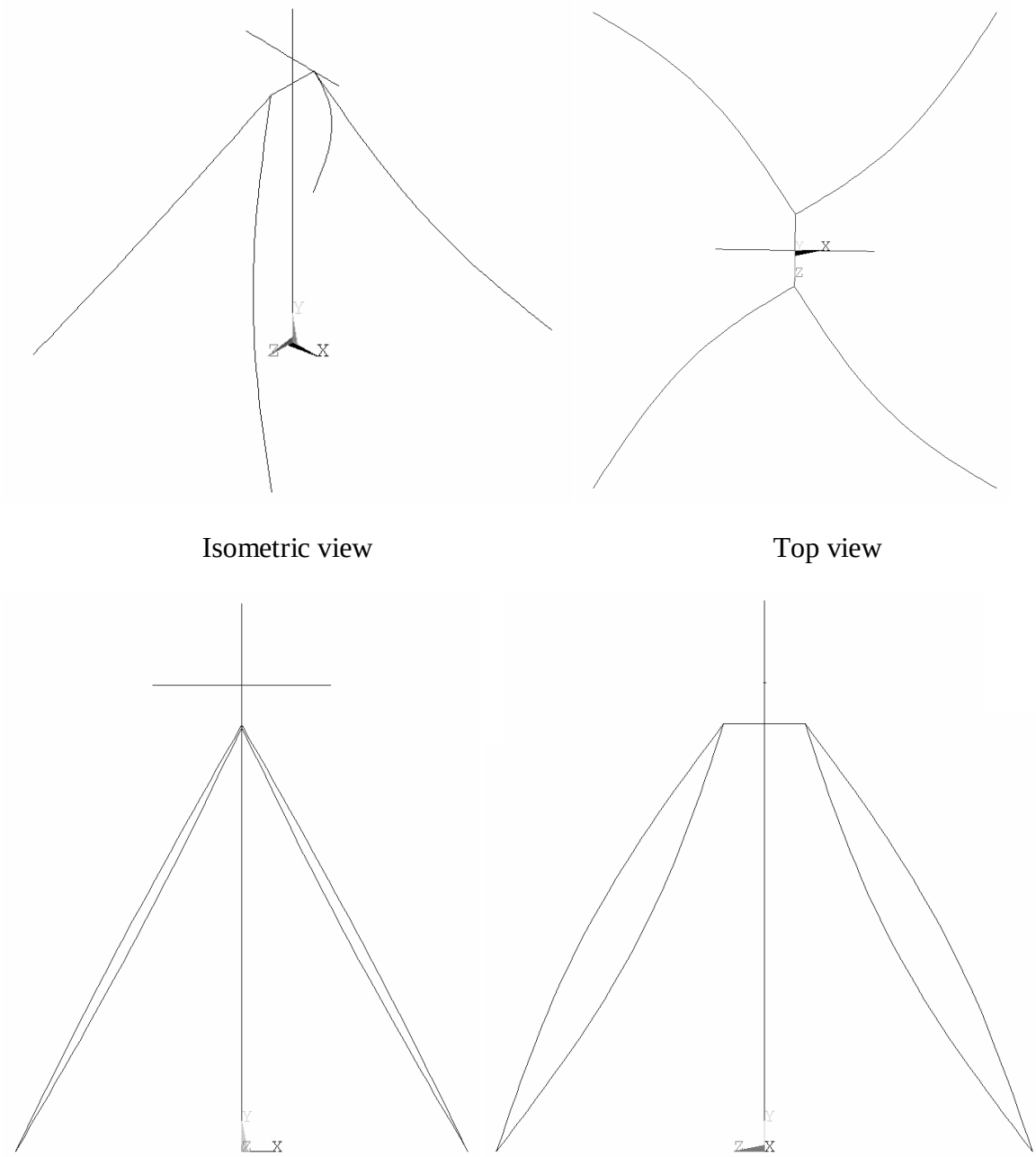

Figure A.6: 3rd mode shape of the simplified tower (Frequency = 1.50 Hz)

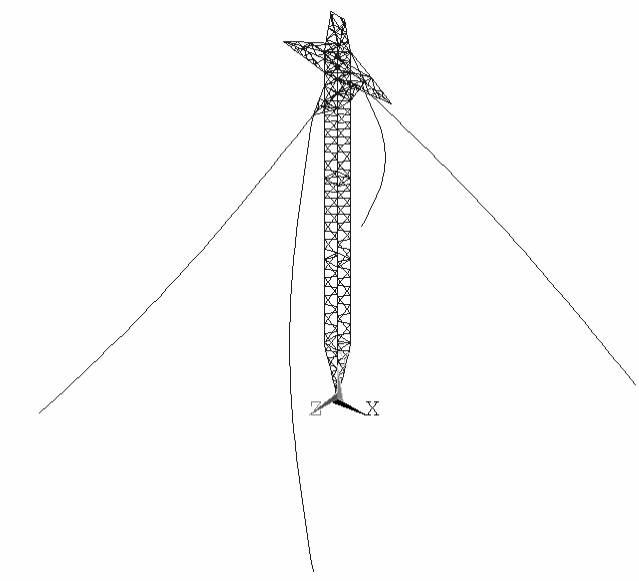

Isometric view

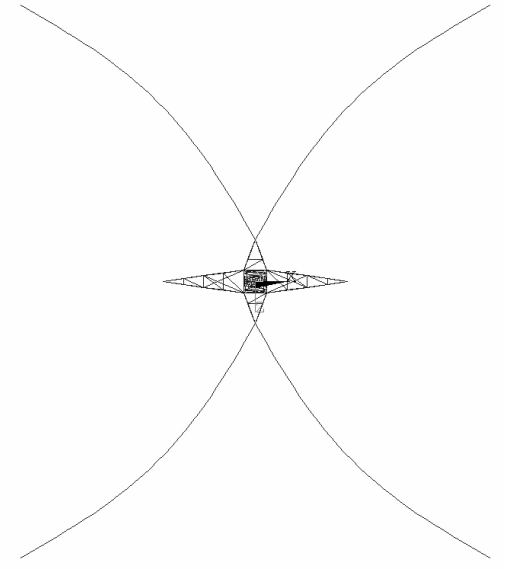

Top view

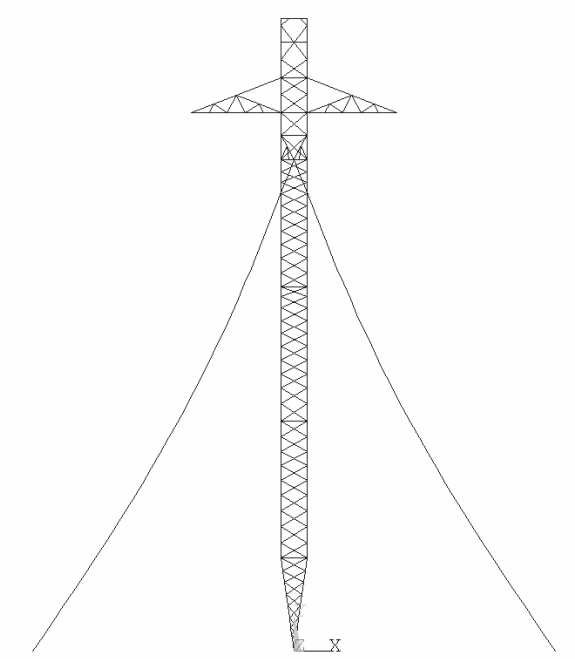

Longitudinal view

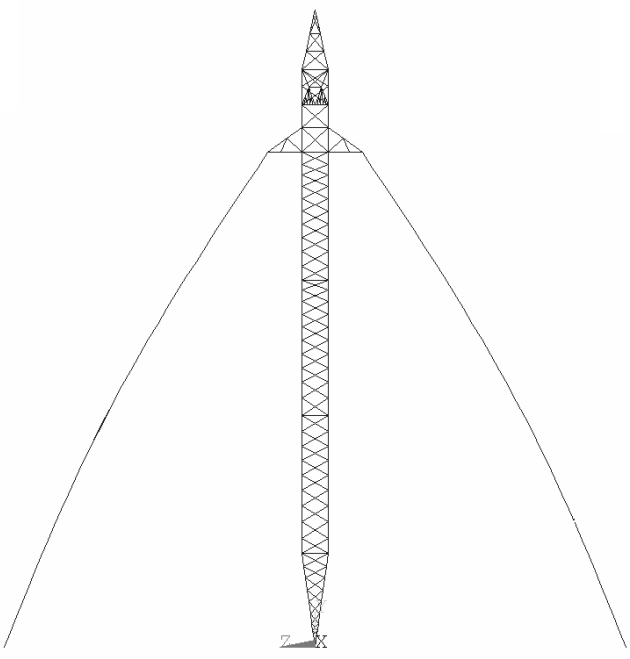

Transverse view

Figure A.7: 4th mode shape of the detailed tower (Frequency = 1.50 Hz)

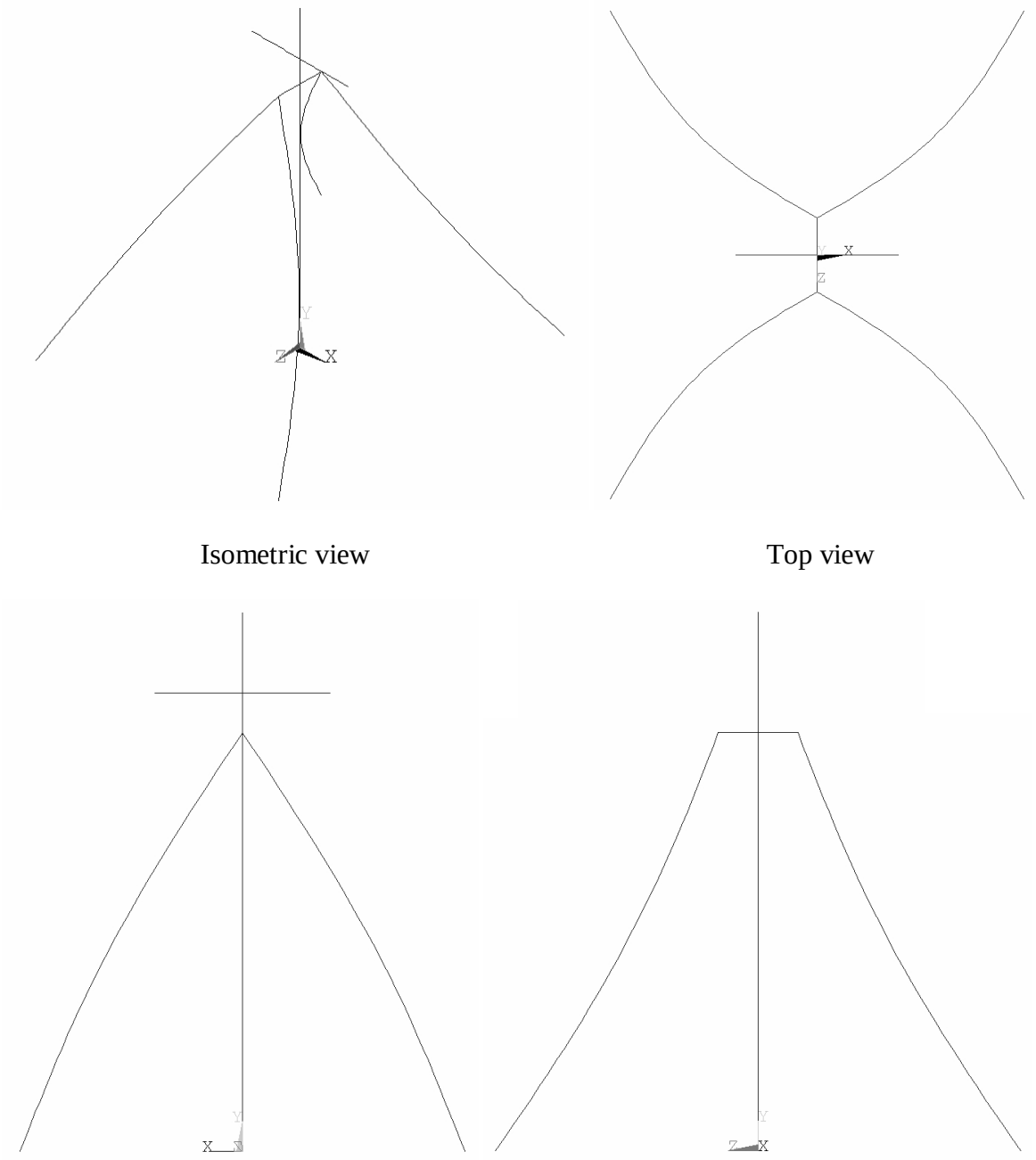

Figure A.8: 4th mode shape of the simplified tower (Frequency = 1.50 Hz)

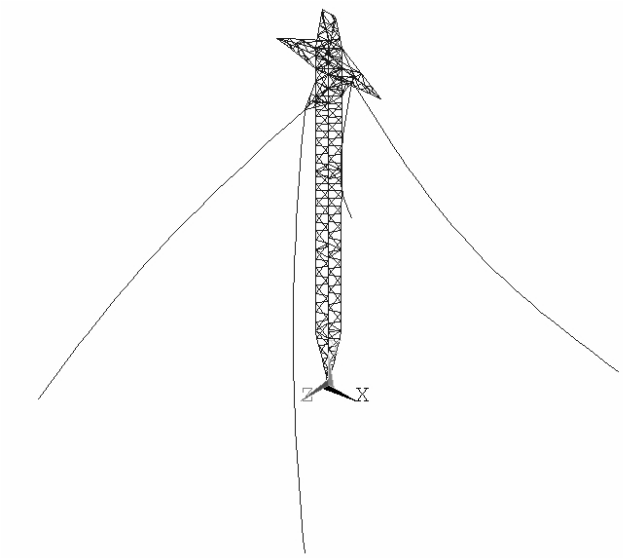

Isometric view

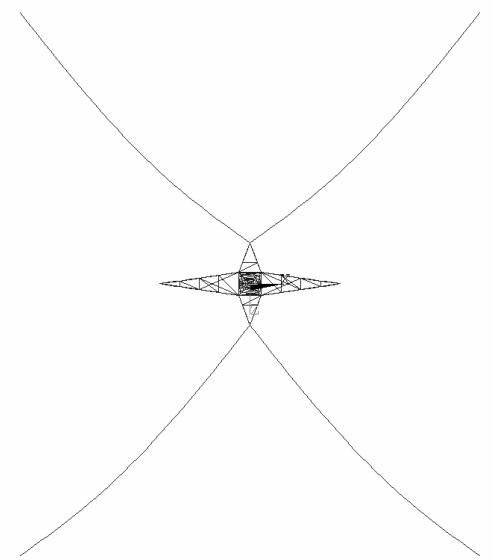

Top view

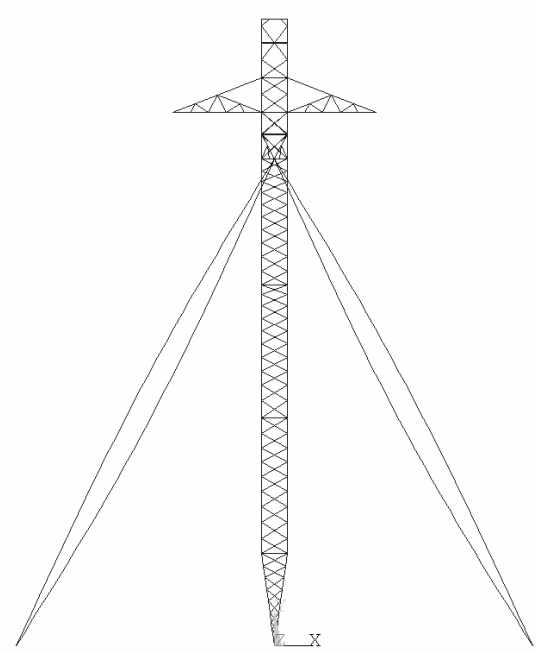

Longitudinal view

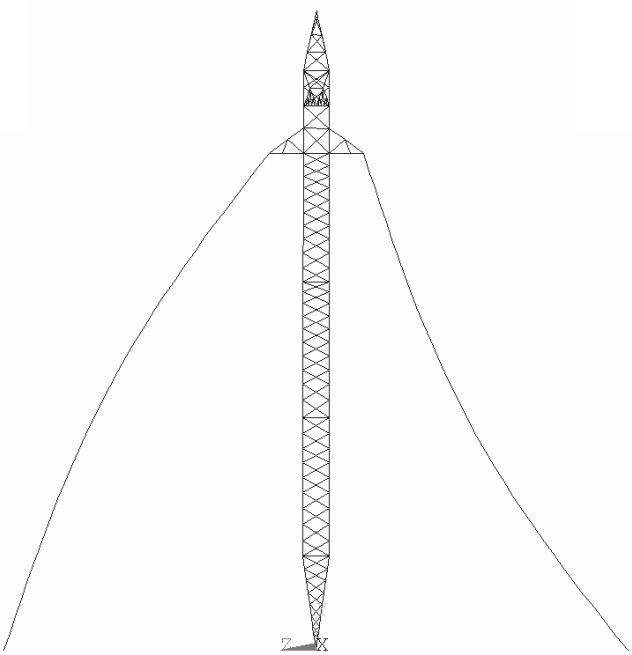

Transverse view

Figure A.9: 5th mode shape of the detailed tower (Frequency = 1.51 Hz)

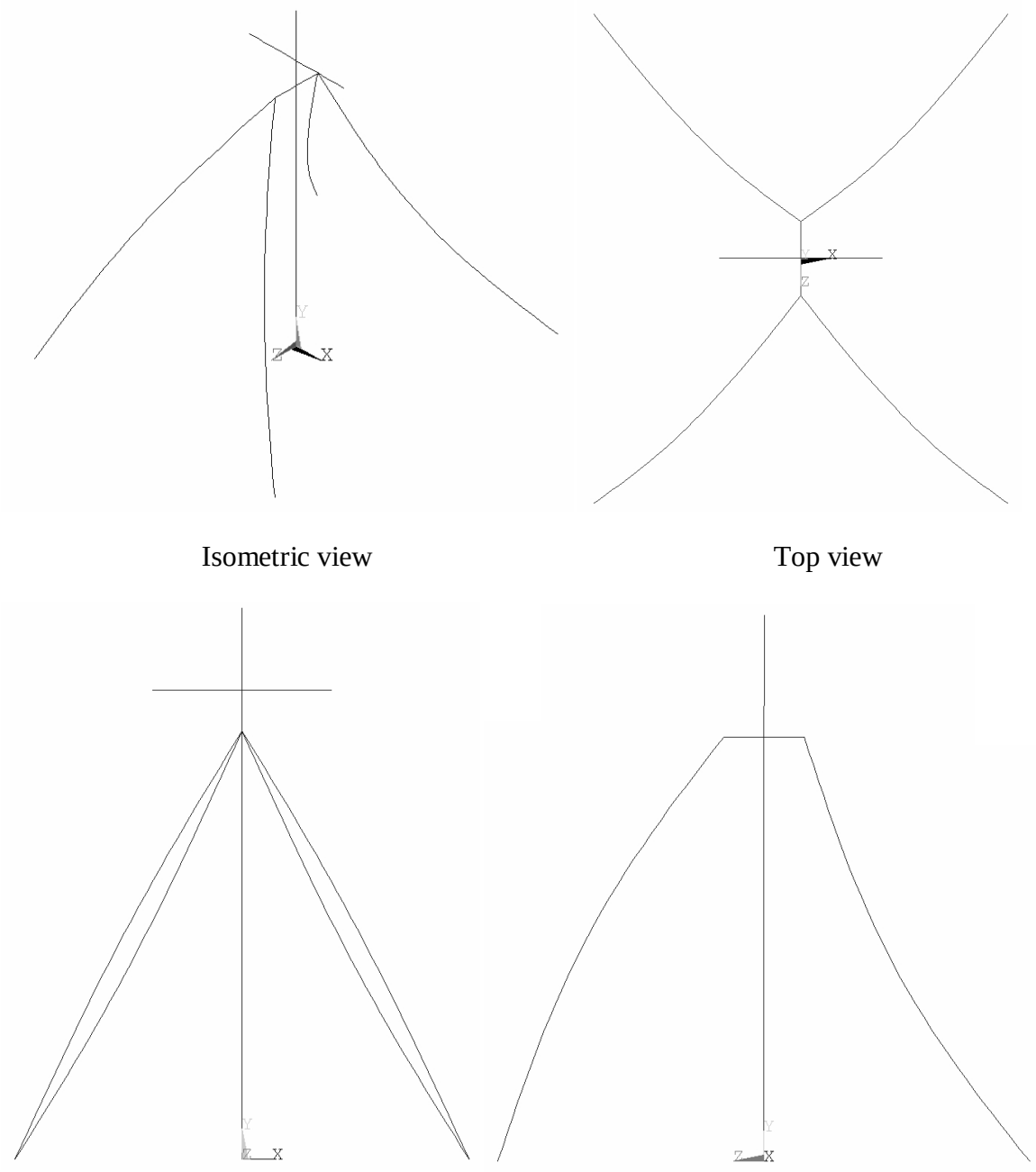

Figure A.10: 5th mode shape of the simplified tower (Frequency = 1.51 Hz)

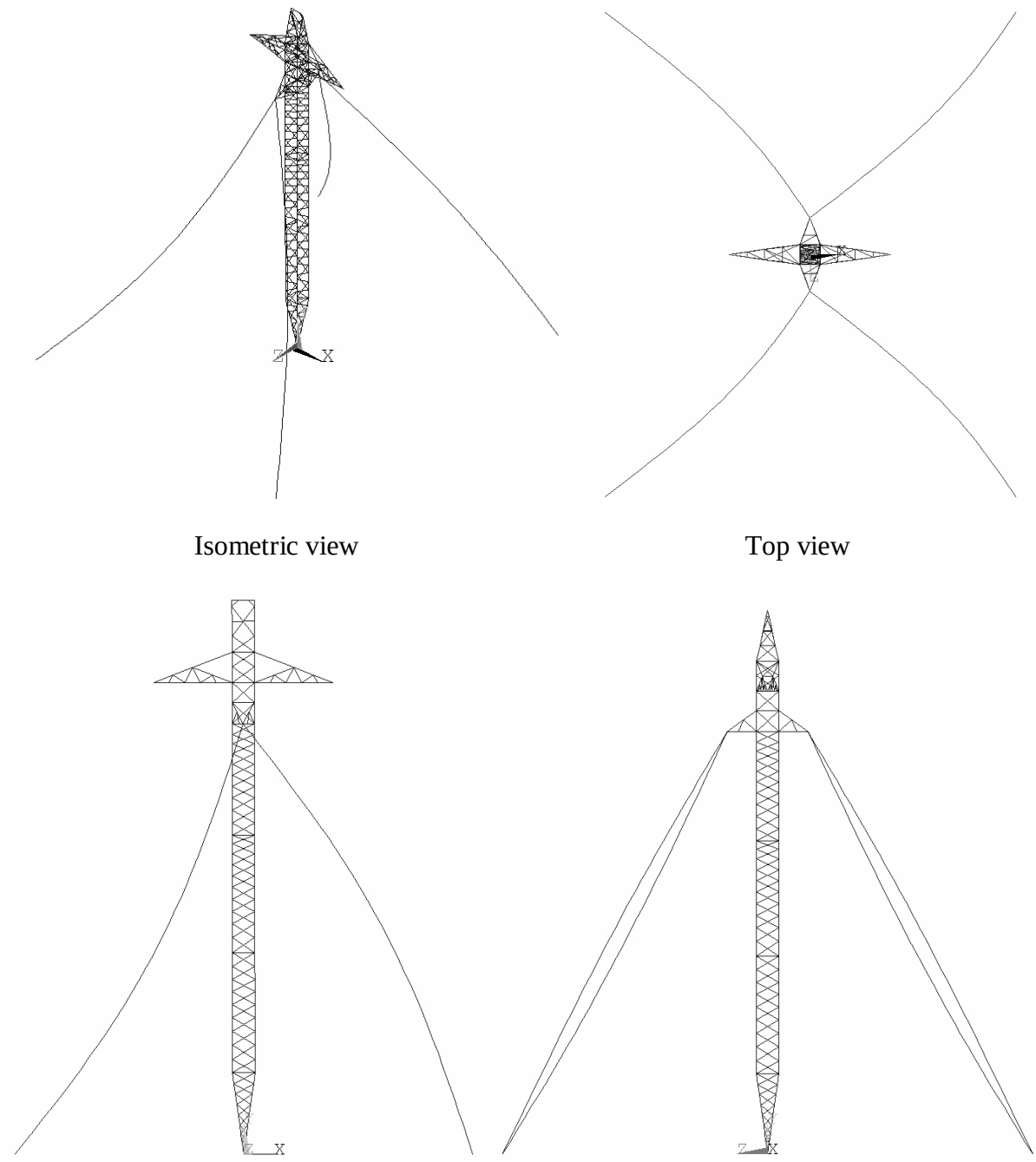

Figure A.11: 6th mode shape of the detailed tower (Frequency = 1.51 Hz)

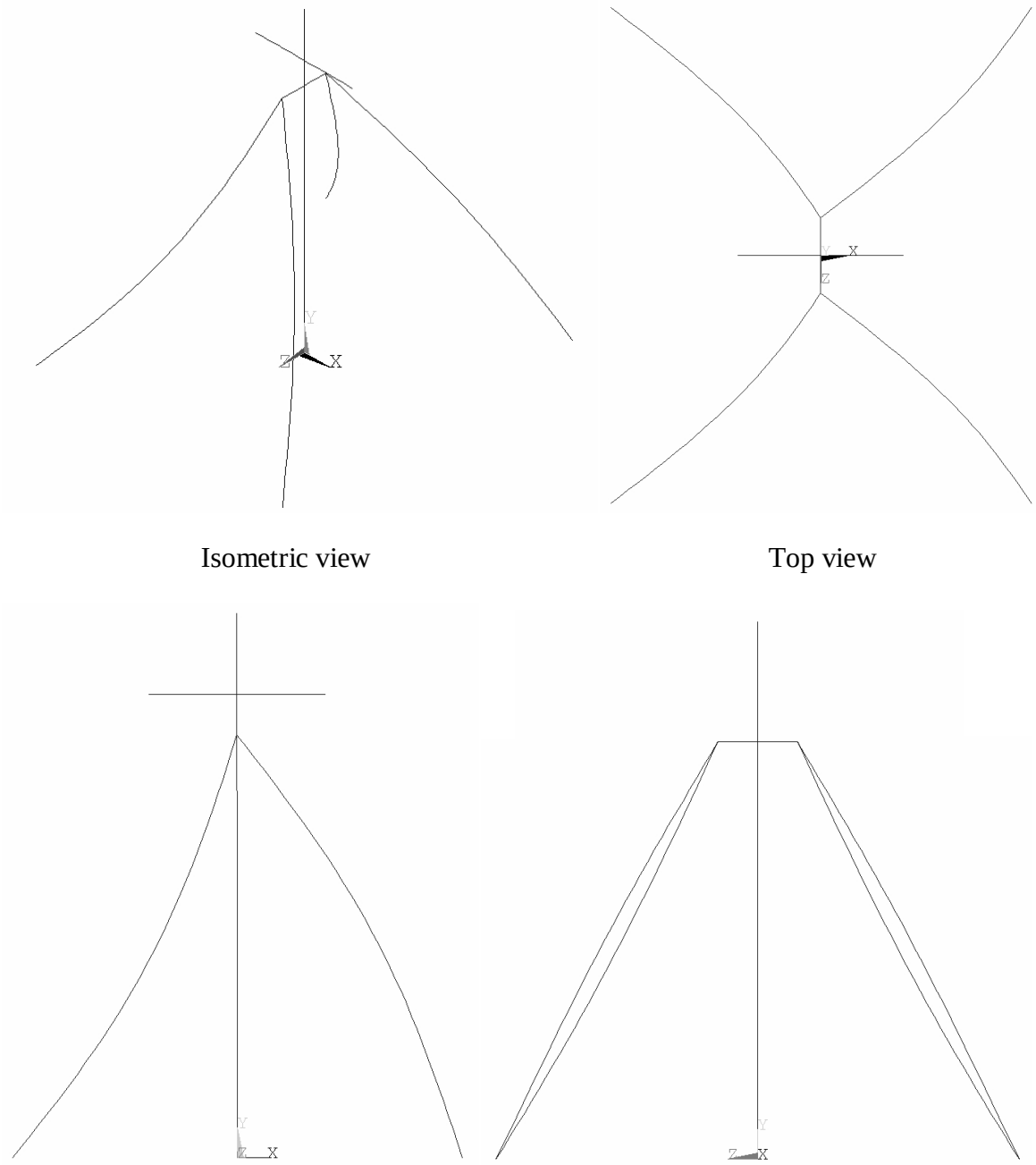

Figure A.12: 6th mode shape of the simplified tower (Frequency = 1.51 Hz)

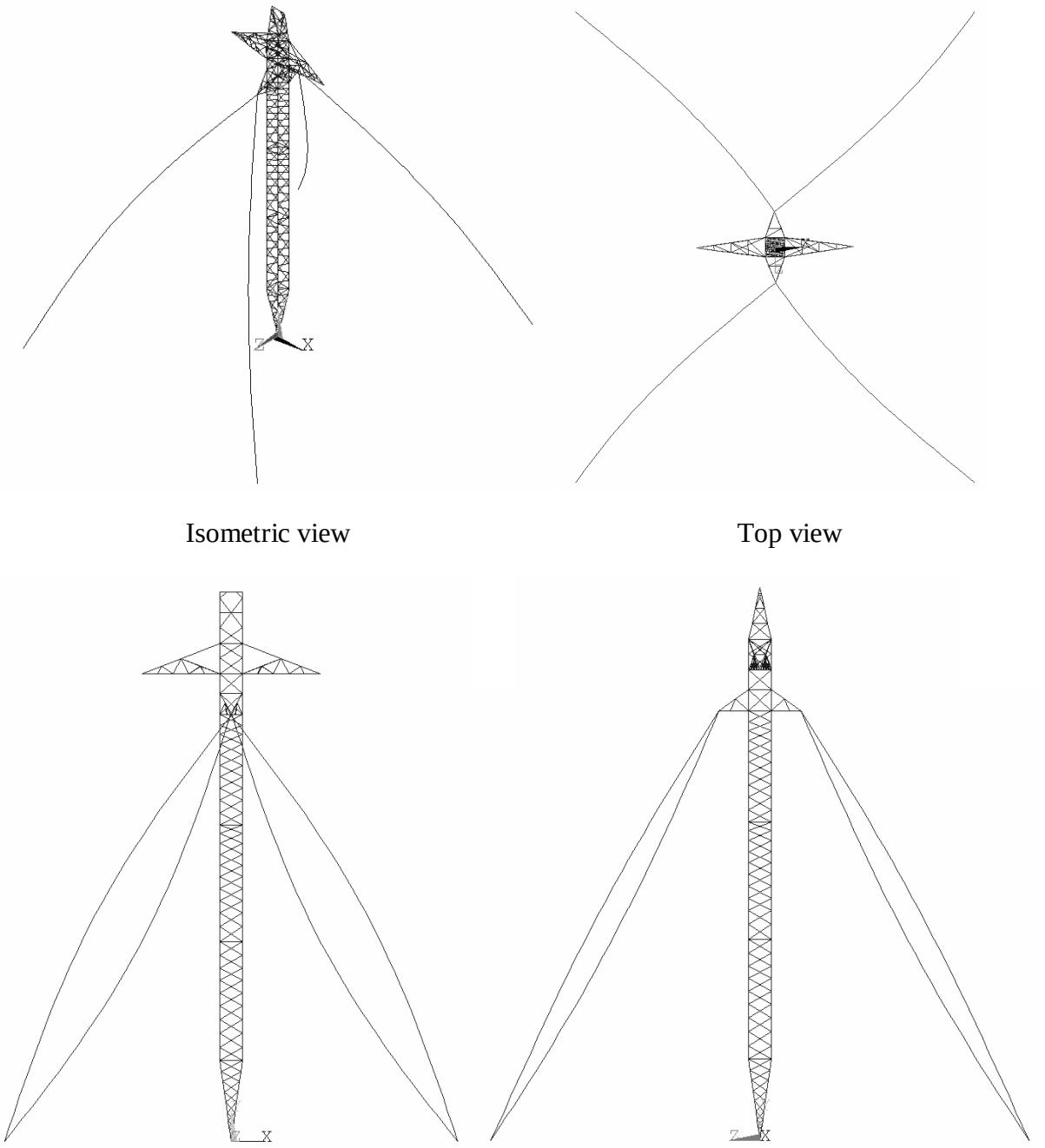

Figure A.13: 7th mode shape of the detailed tower (Frequency = 1.52 Hz)

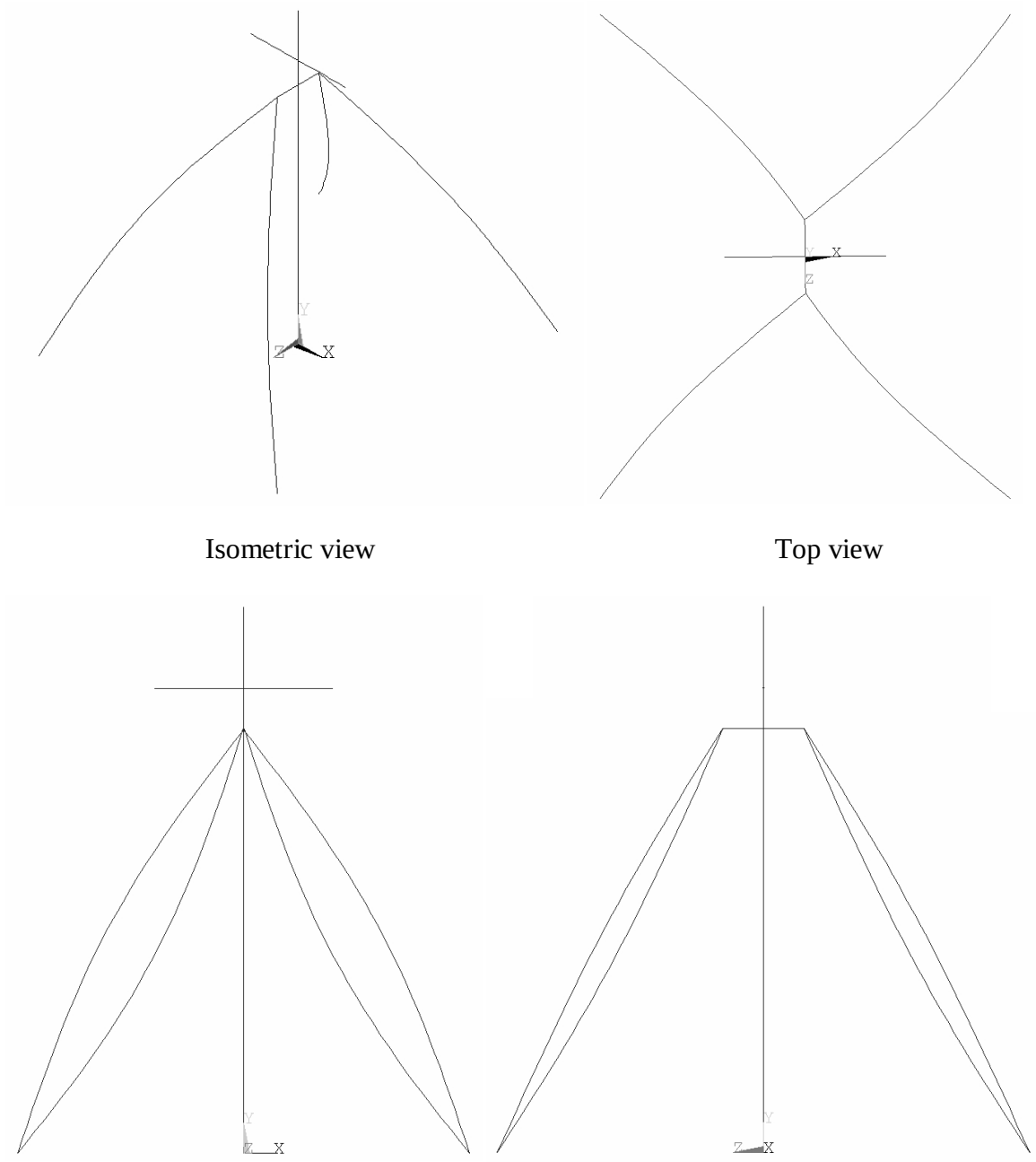

Figure A.14: 7th mode shape of the simplified tower (Frequency = 1.52 Hz)

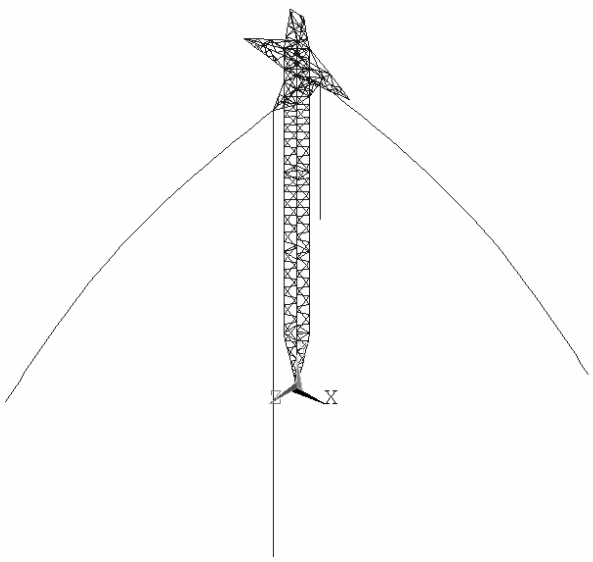

Isometric view

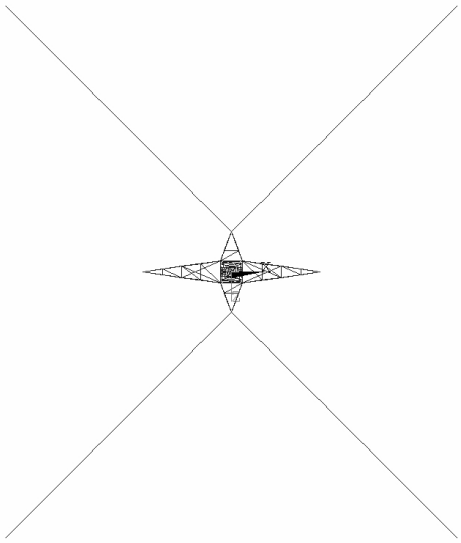

Top view

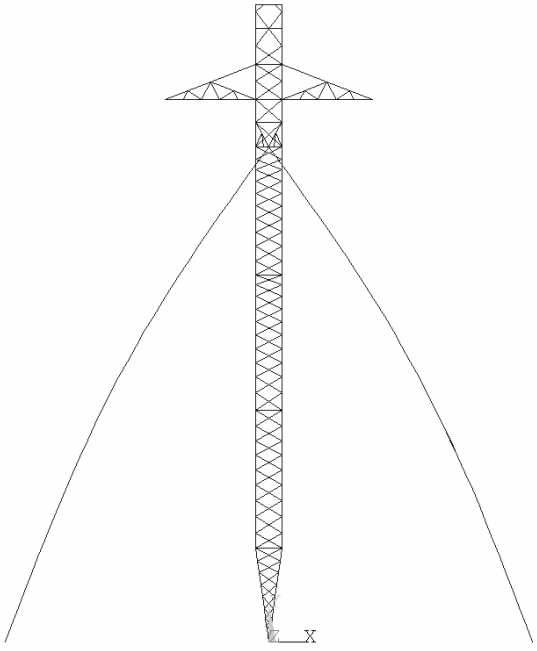

Longitudinal view

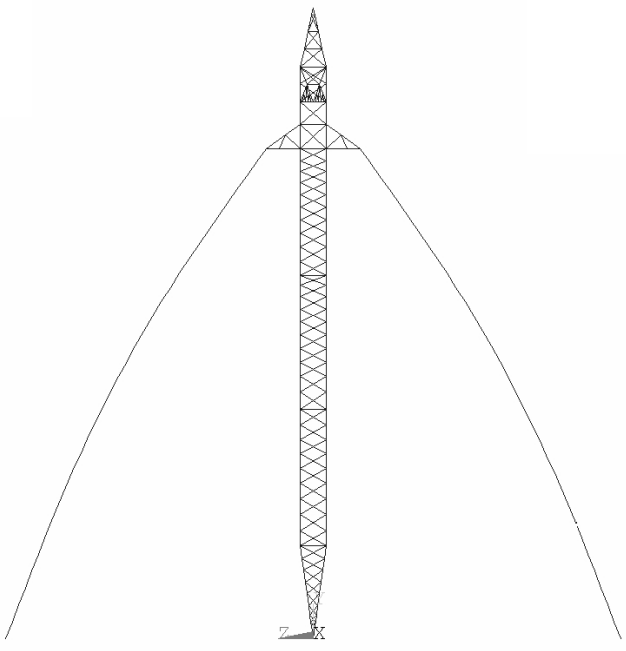

Transverse view

Figure A.15: 8th mode shape of the detailed tower (Frequency = 1.53 Hz)

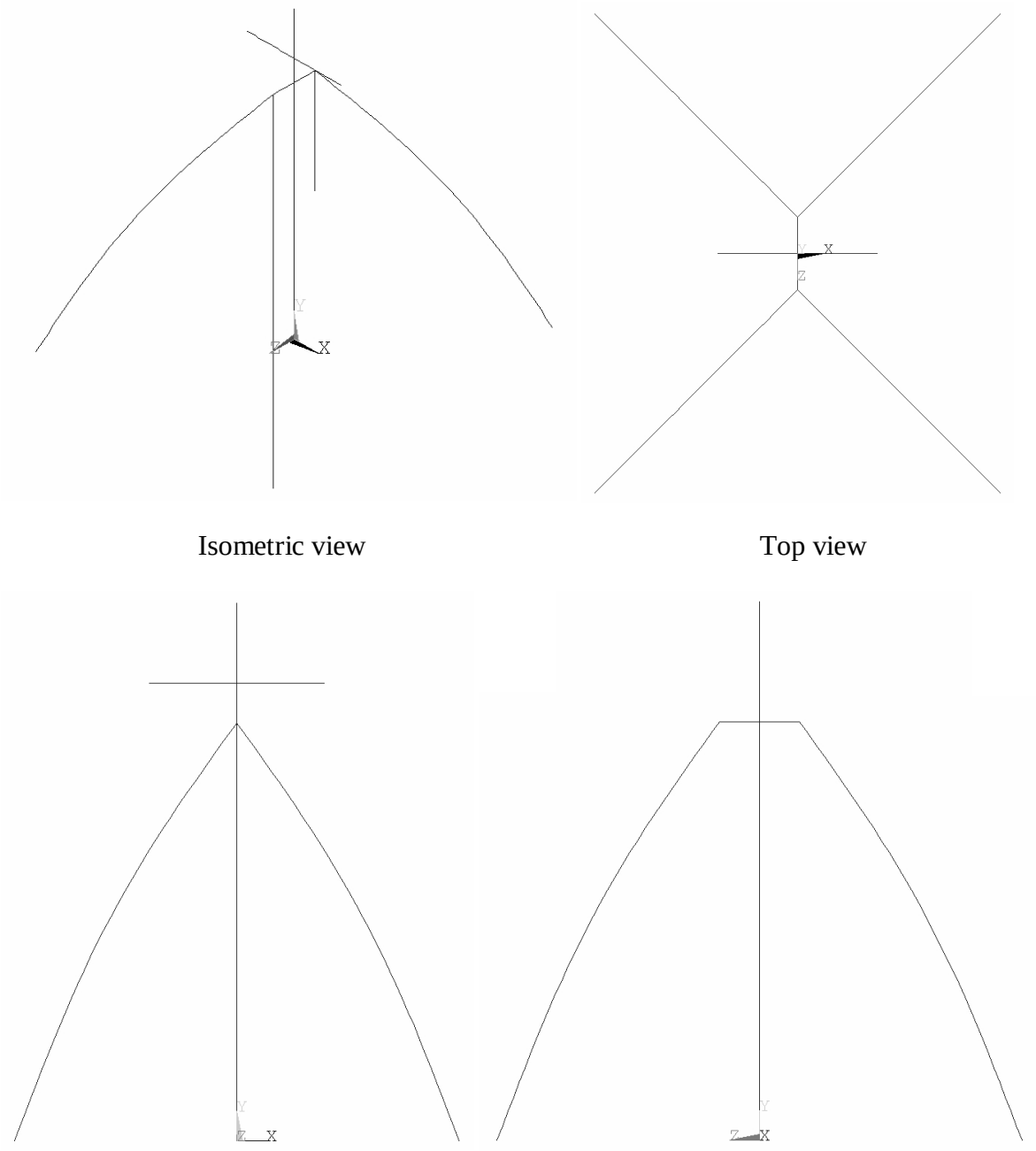

Figure A.16: 8th mode shape of the simplified tower (Frequency = 1.52 Hz)

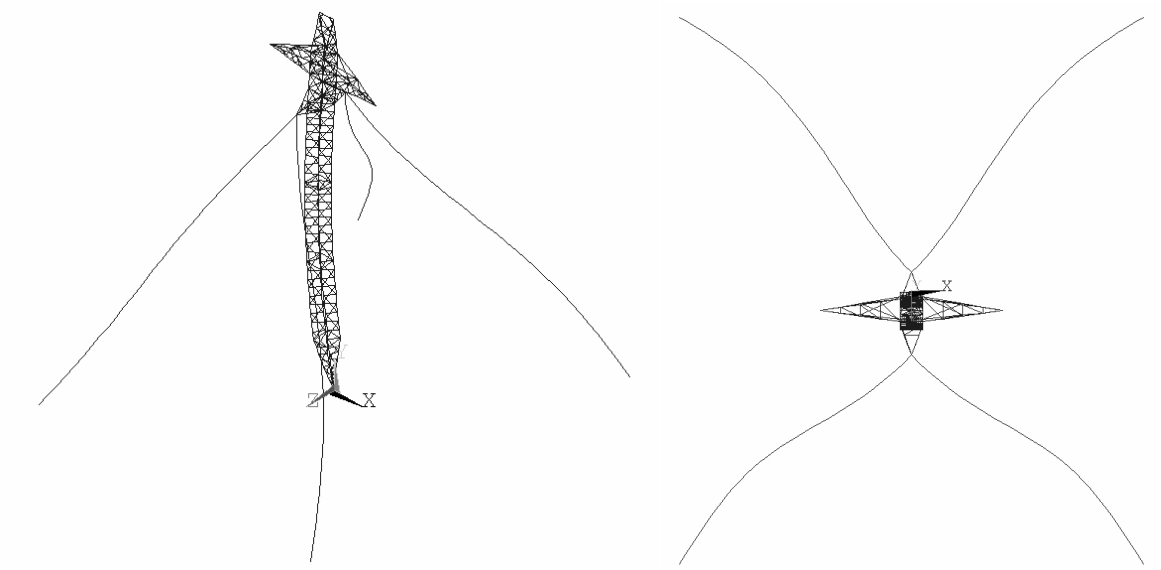

Isometric view

Top view

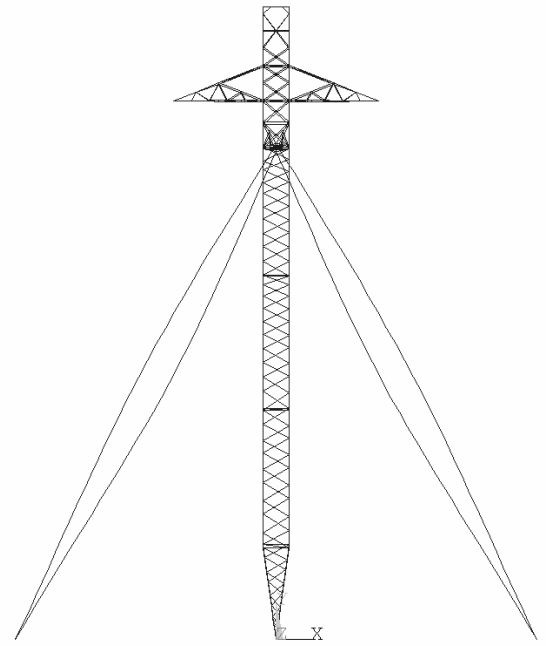

Longitudinal view

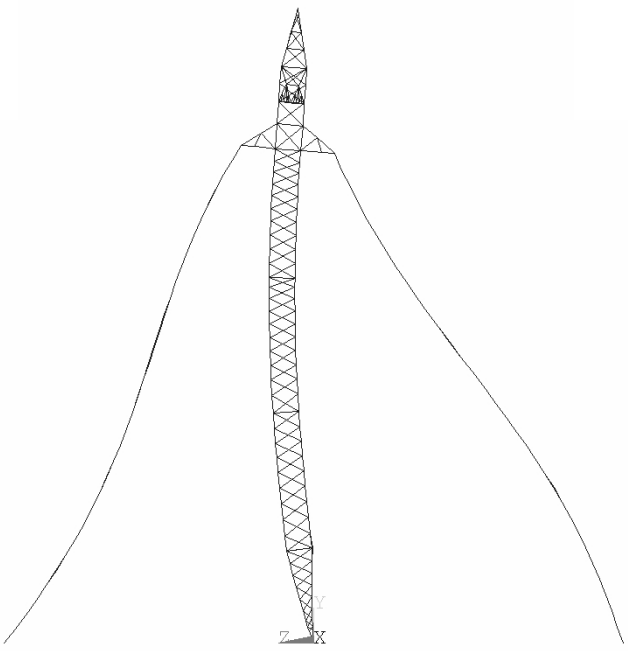

Transverse view

Figure A.17: 9th mode shape of the detailed tower (Frequency = 2.30 Hz)

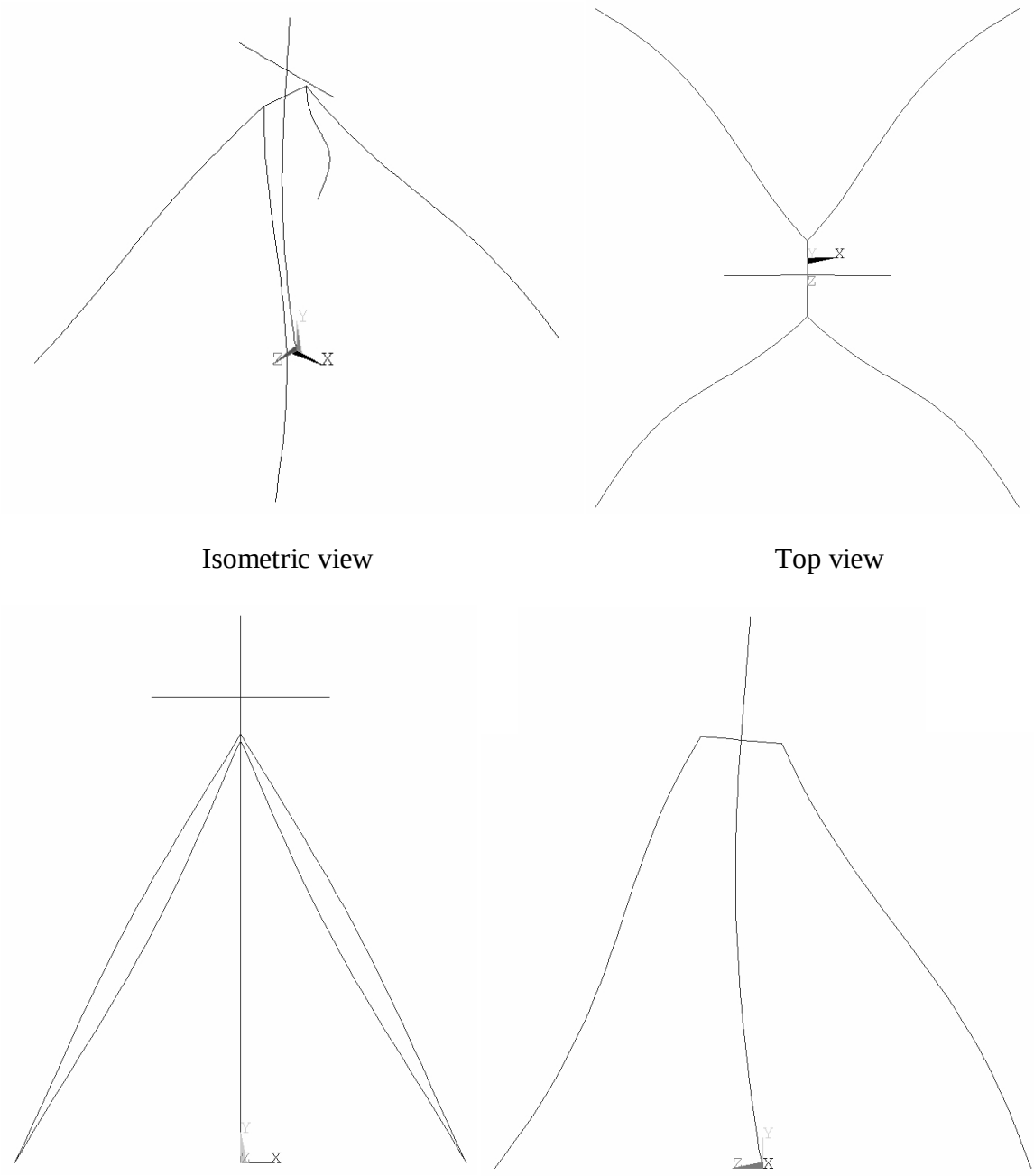

Figure A.18: 9th mode shape of the simplified tower (Frequency = 2.27 Hz)

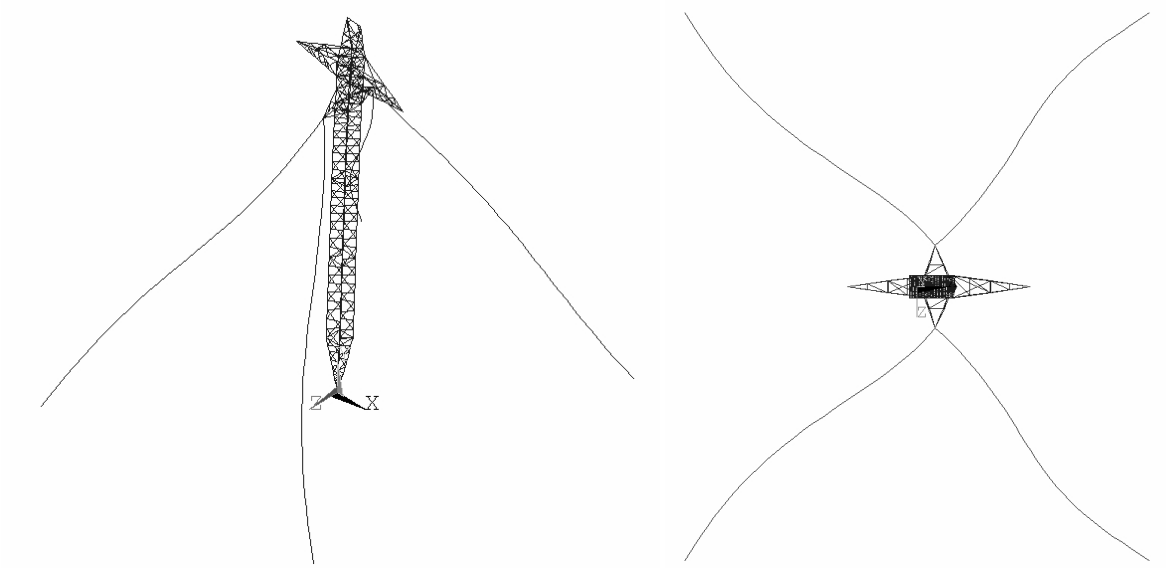

Isometric view

Top view

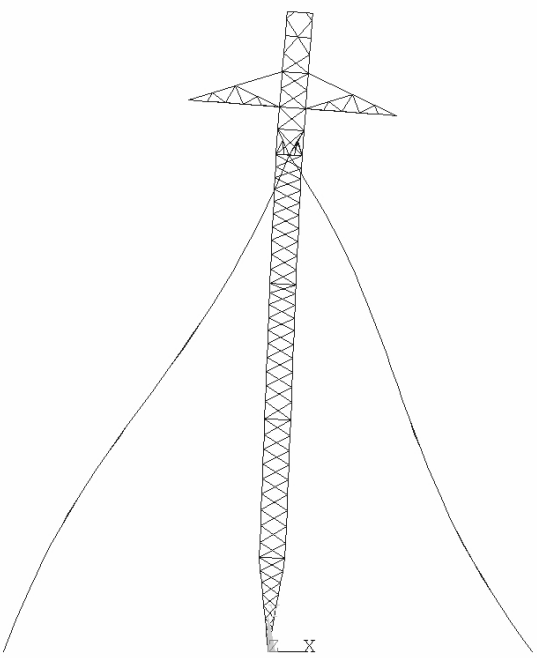

Longitudinal view

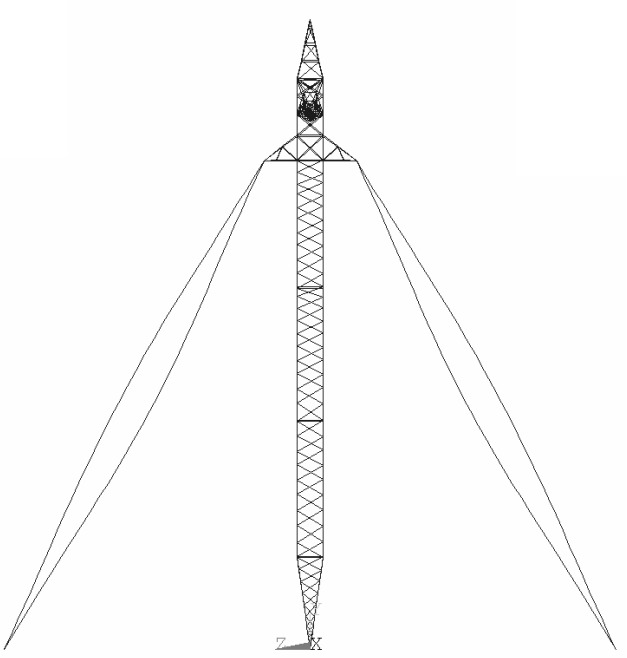

Transverse view

Figure A.19: 10th mode shape of the detailed tower (Frequency = 2.41 Hz)

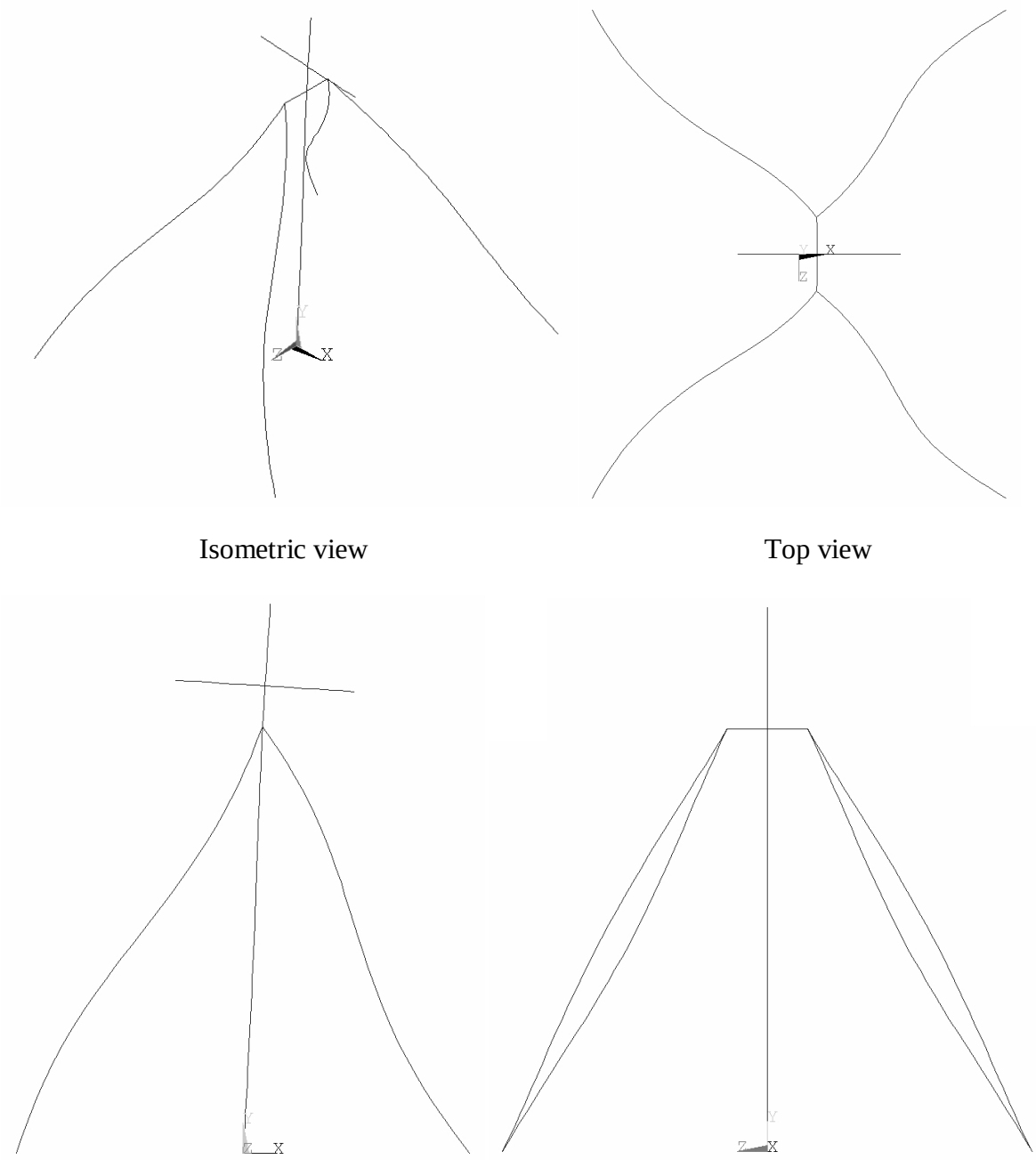

Figure A.20: 10^{th} mode shape of the simplified tower (Frequency = 2.48 Hz)

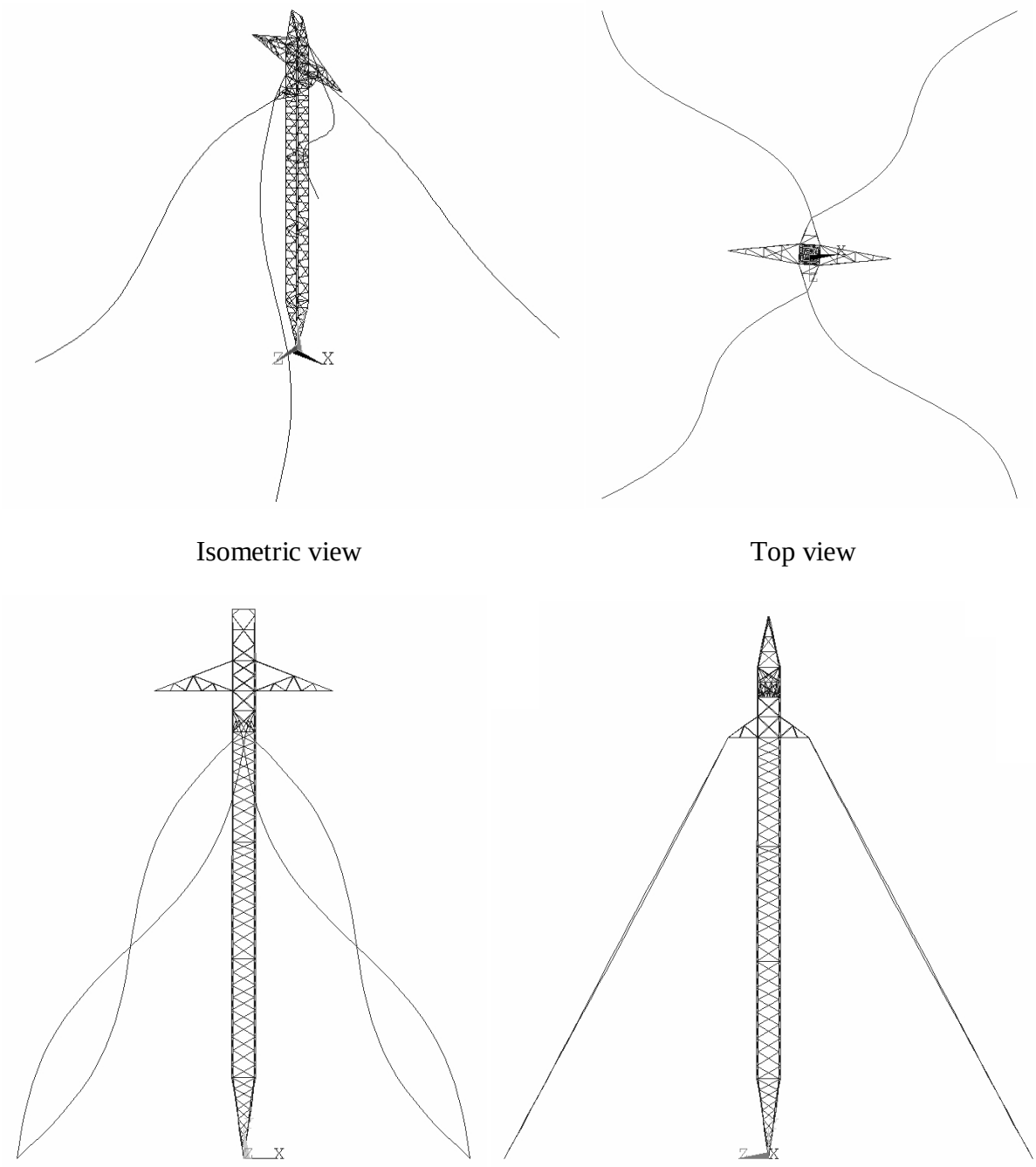

Figure A.21: 11th mode shape of the detailed tower (Frequency = 2.97 Hz)

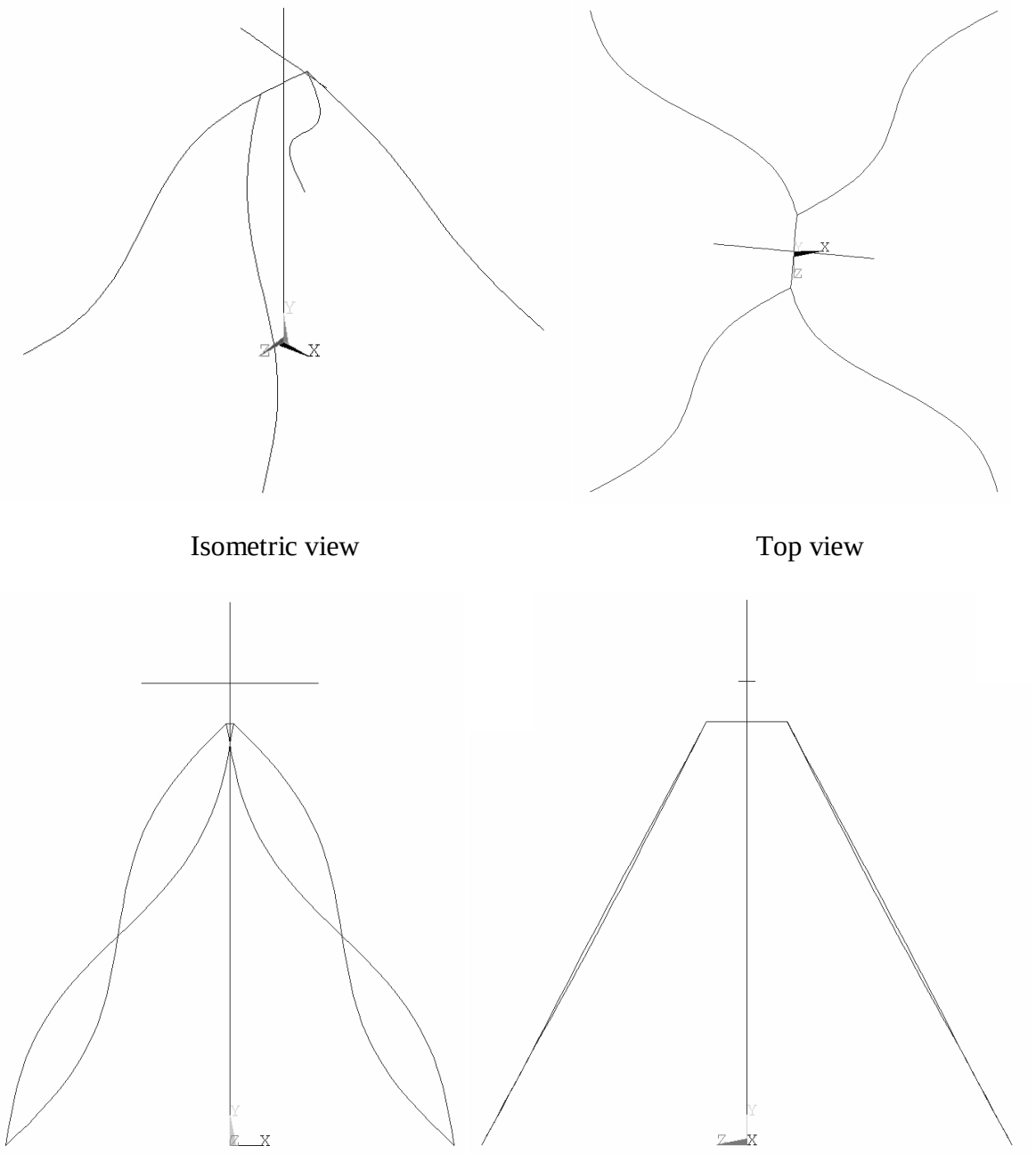

Figure A.22: 11th mode shape of the simplified tower (Frequency = 2.95 Hz)

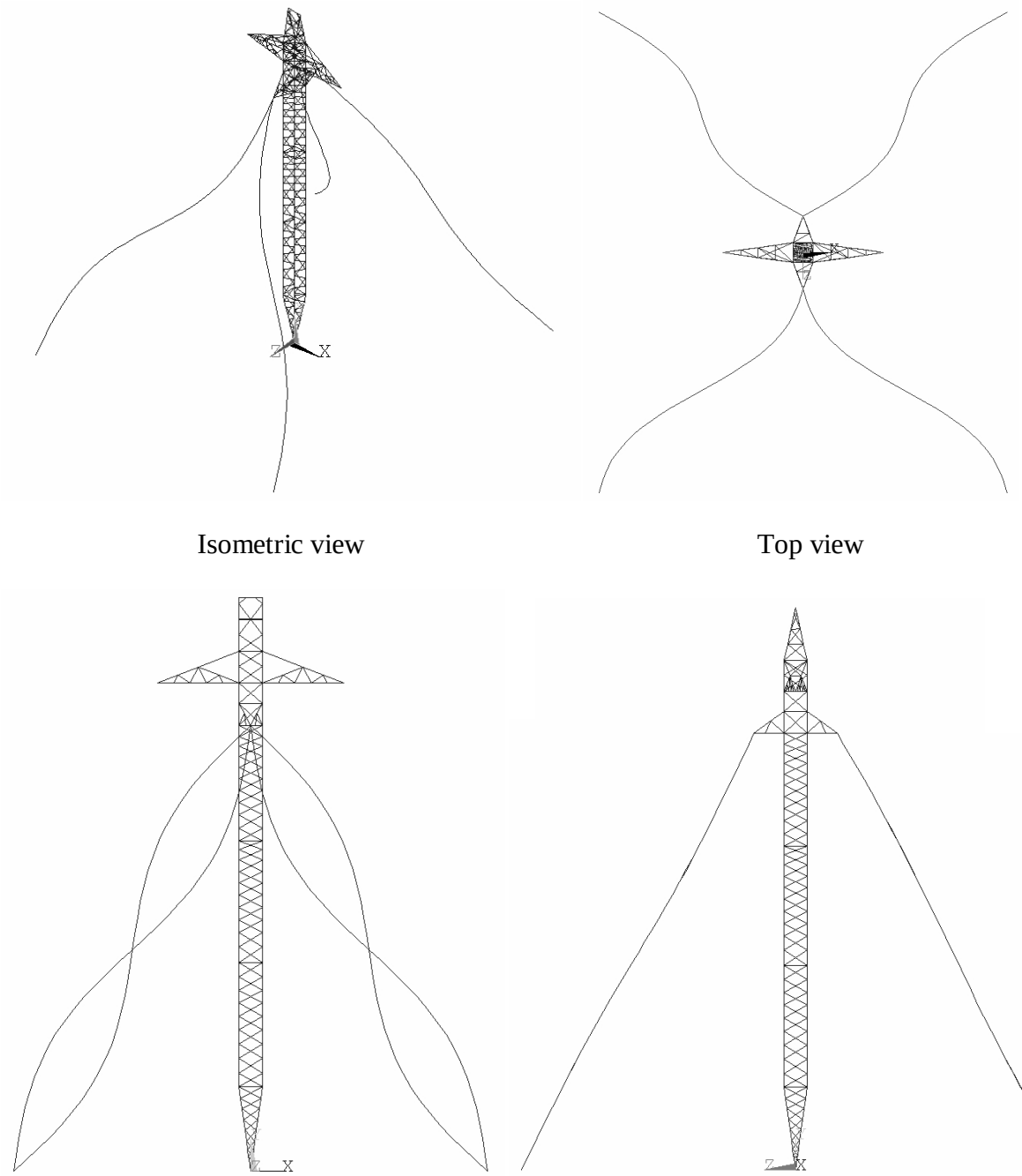

Figure A.23: 12th mode shape of the detailed tower (Frequency = 3.00 Hz)

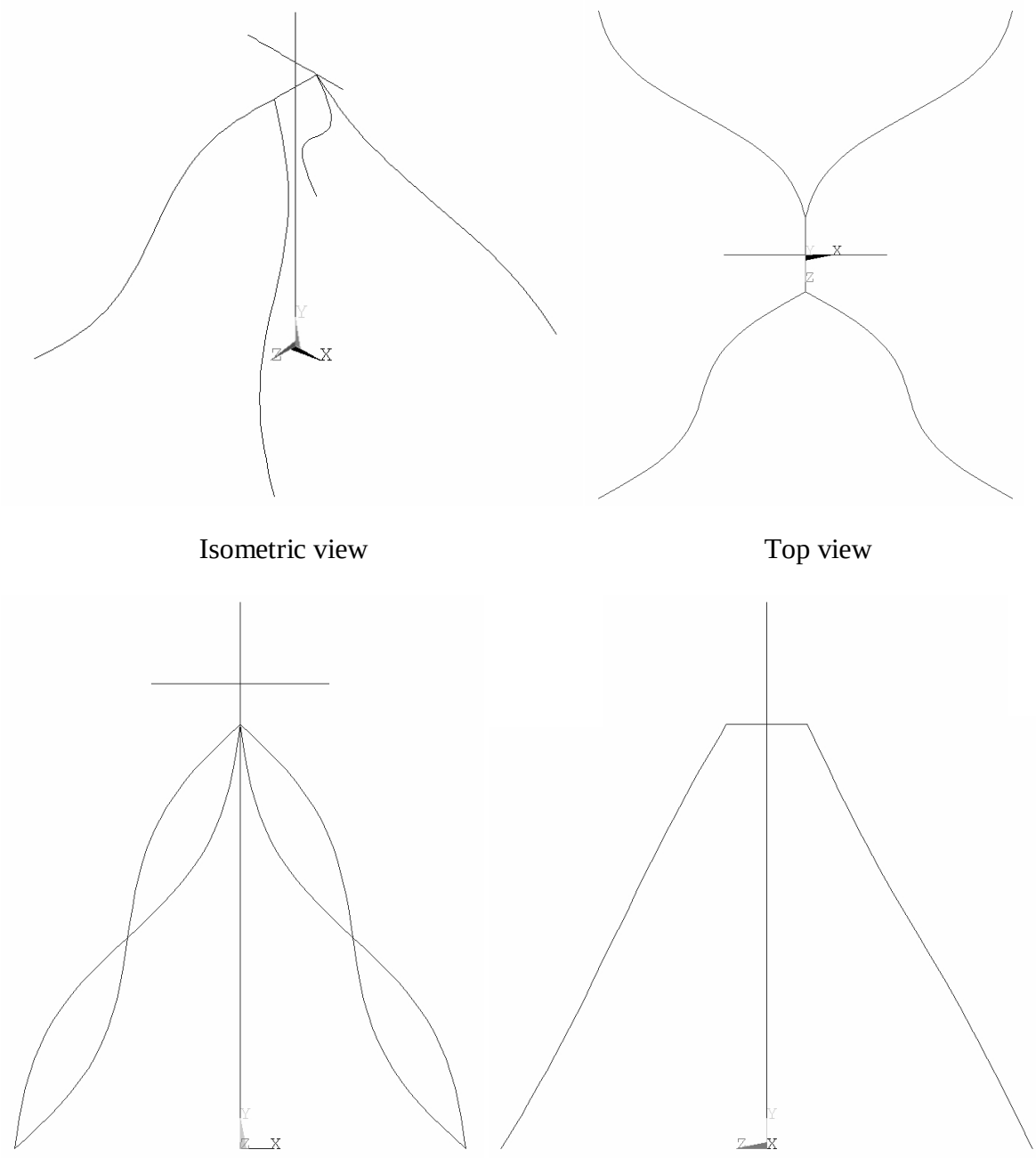

Figure A.24: 12th mode shape of the simplified tower (Frequency = 3.00 Hz)

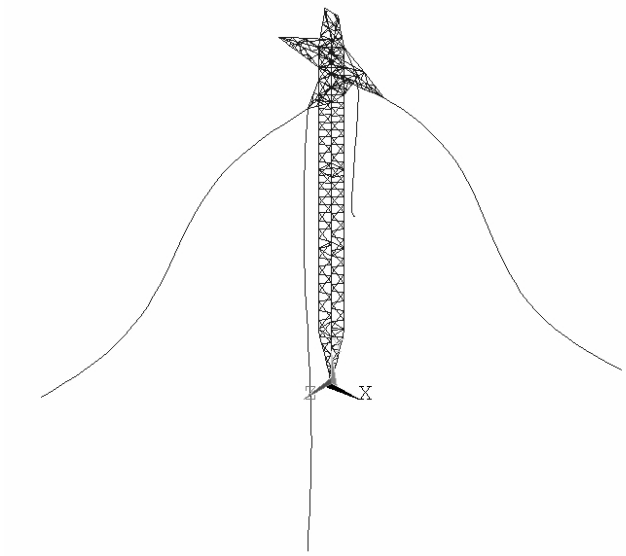

Isometric view

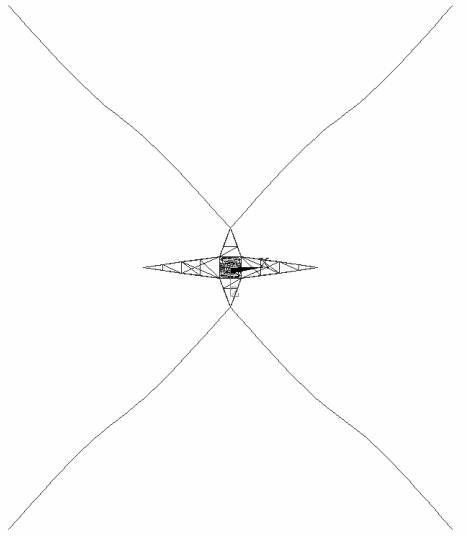

Top view

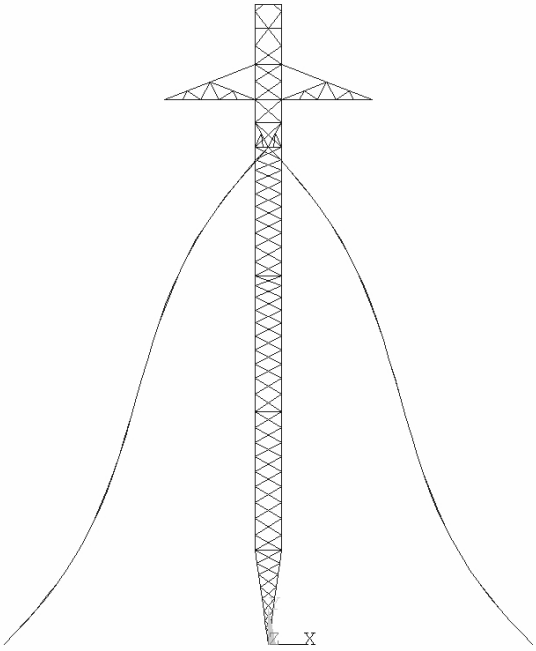

Longitudinal view

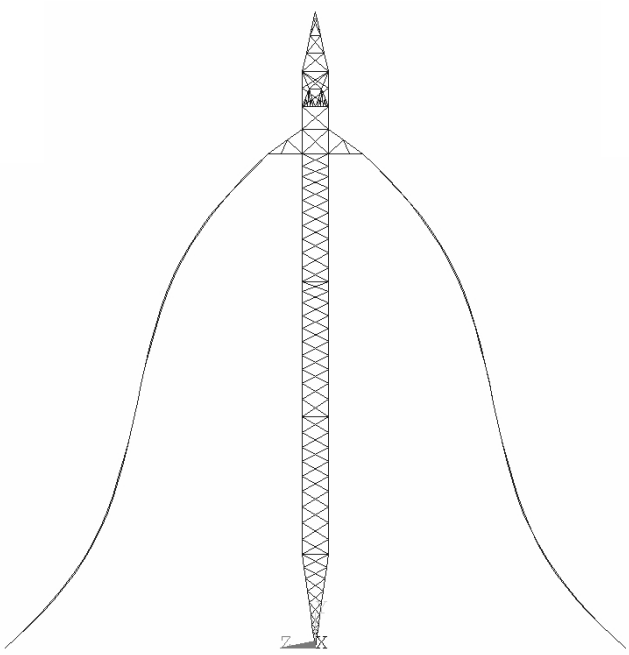

Transverse view

Figure A.25: 13th mode shape of the detailed tower (Frequency = 3.00 Hz)

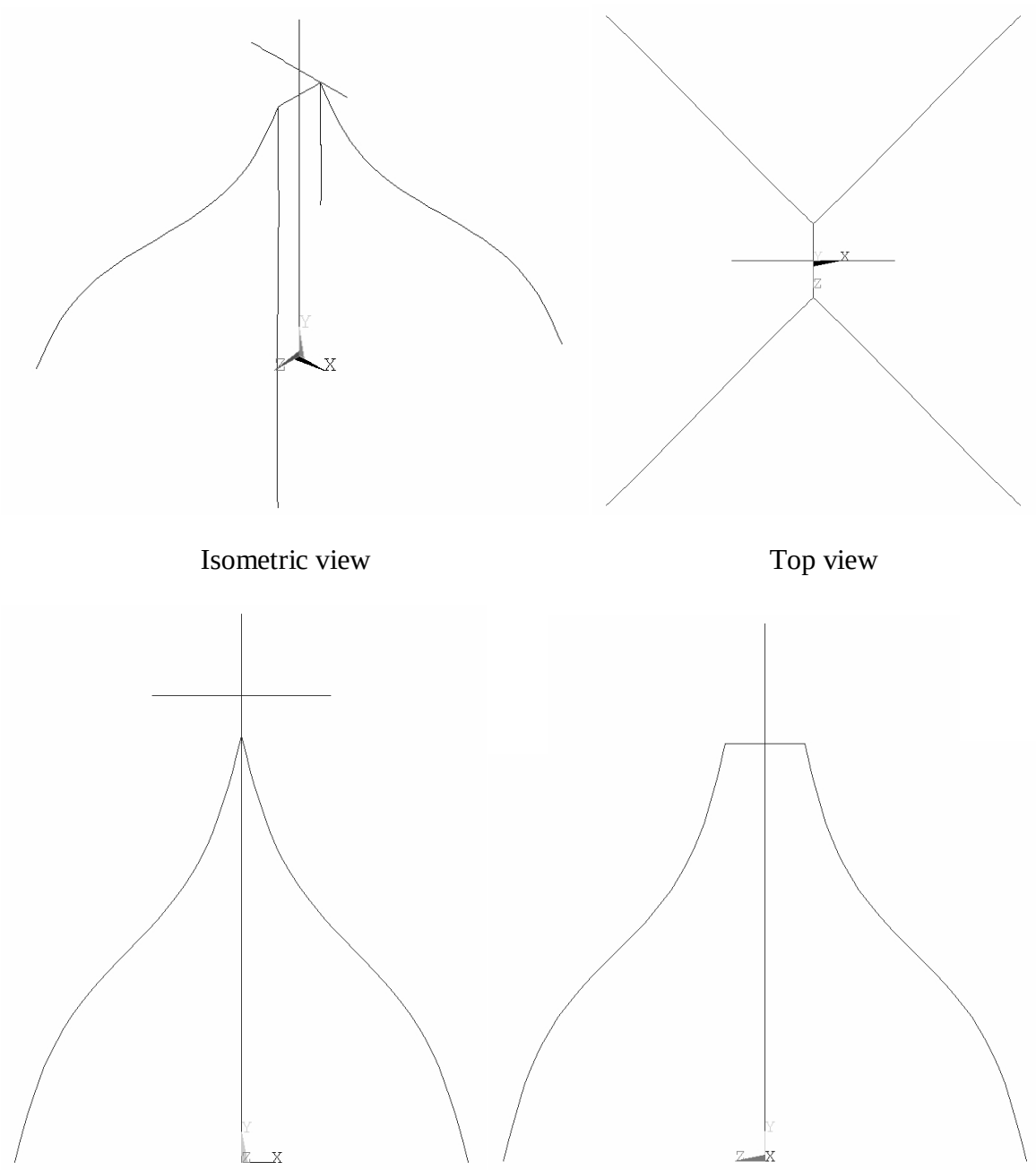

Figure A.26: 13th mode shape of the simplified tower (Frequency = 3.00 Hz)

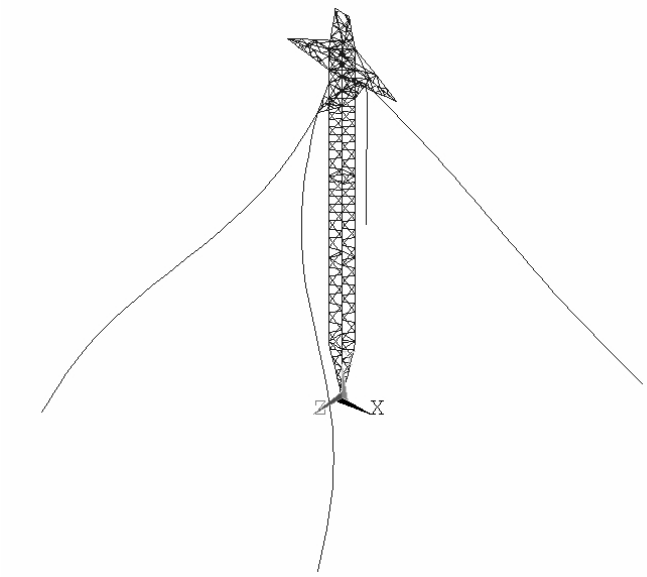

Isometric view

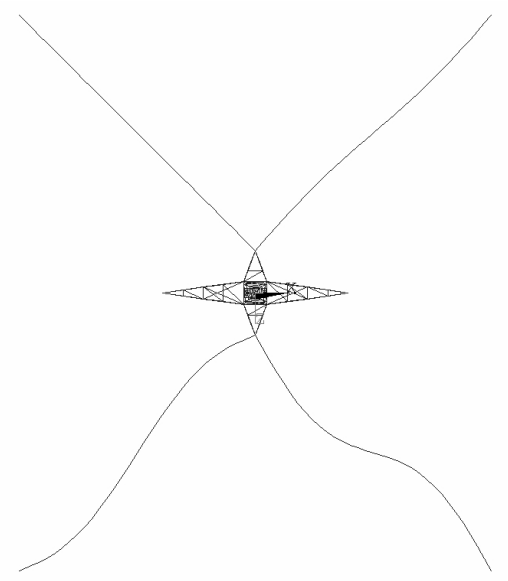

Top view

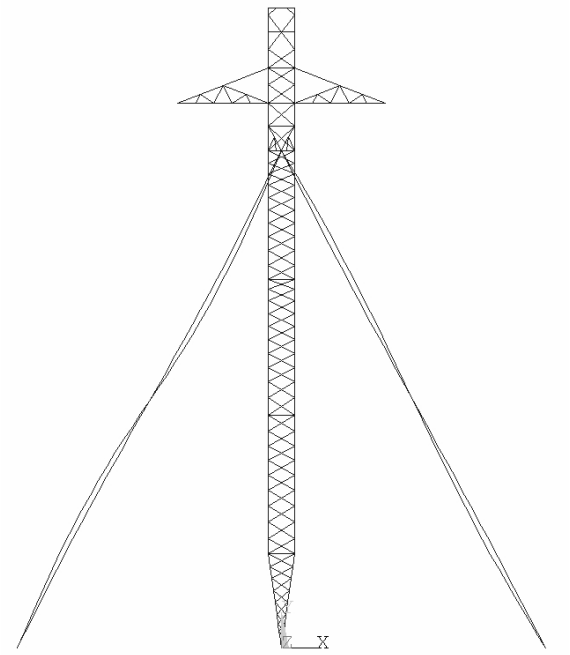

Longitudinal view

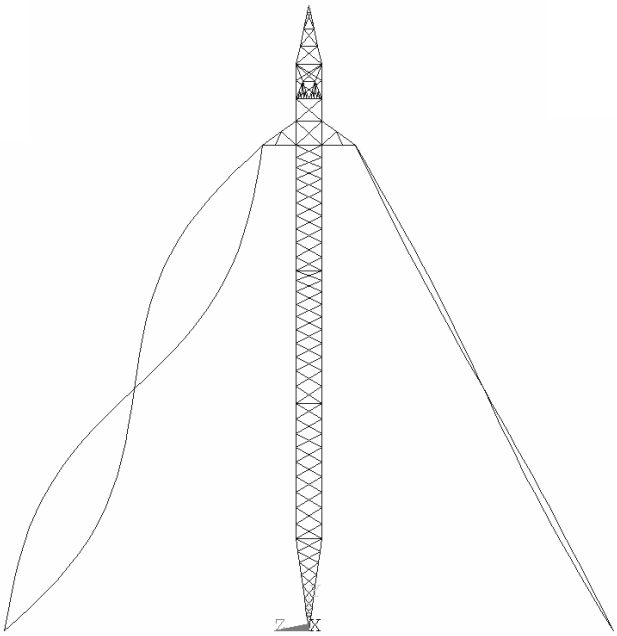

Transverse view

Figure A.27: 14th mode shape of the detailed tower (Frequency = 3.00 Hz)

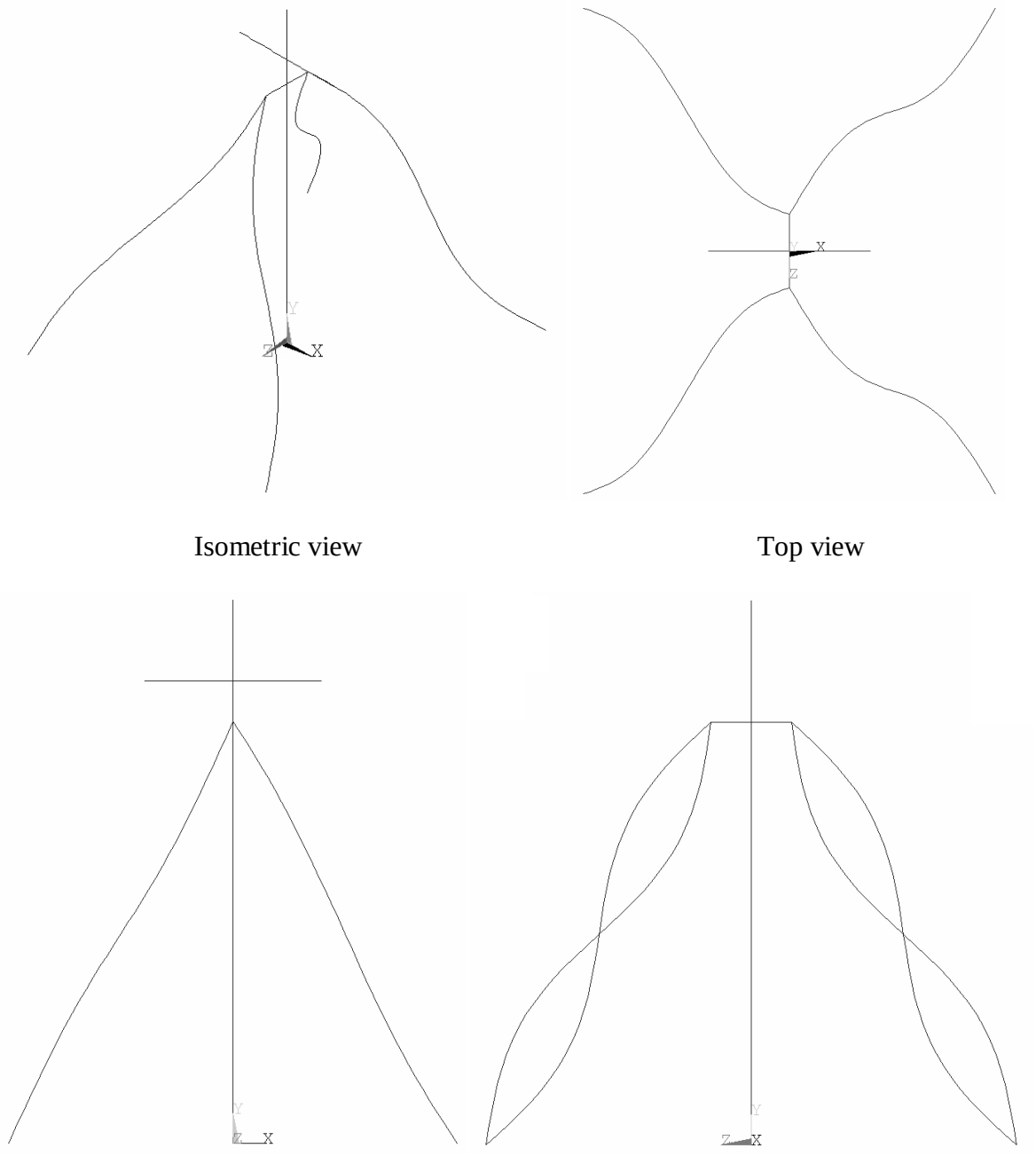

Figure A.28: 14th mode shape of the simplified tower (Frequency = 3.00 Hz)

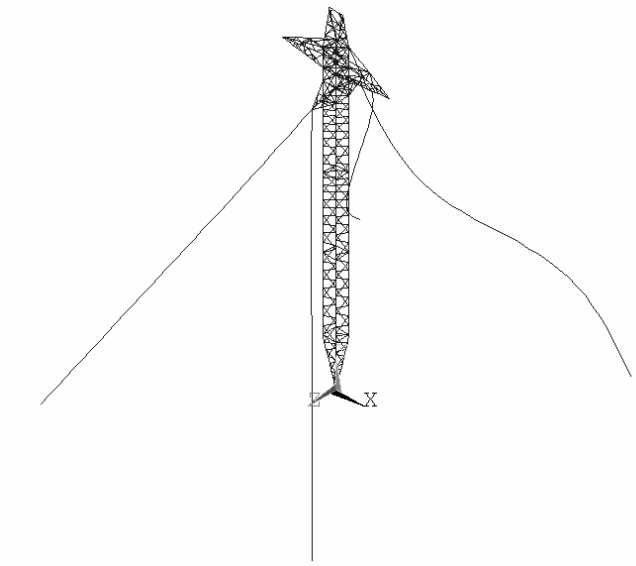

Isometric view

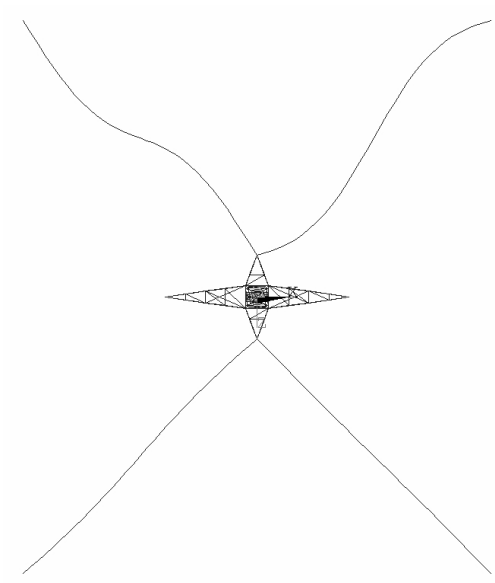

Top view

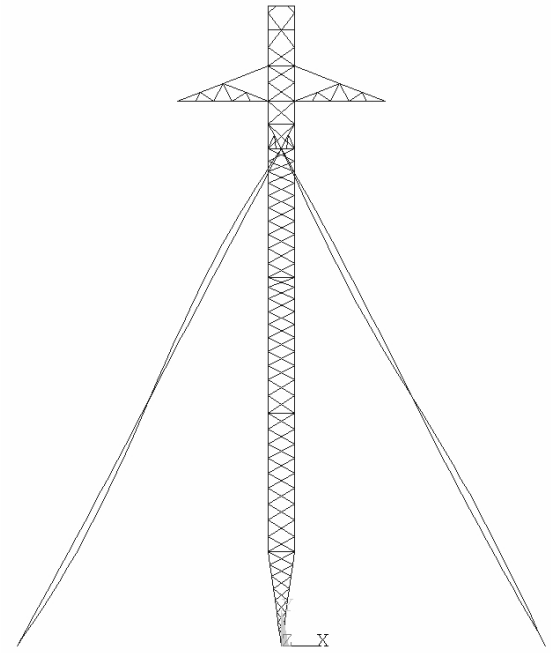

Longitudinal view

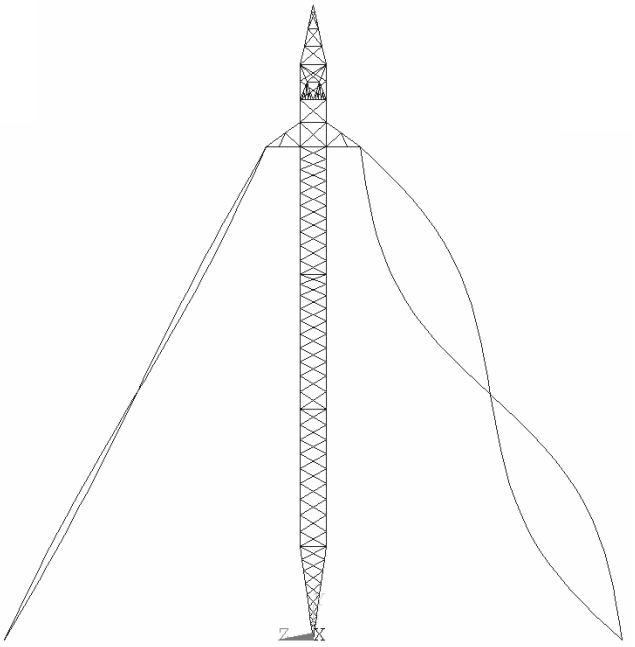

Transverse view

Figure A.29: 15th mode shape of the detailed tower (Frequency = 3.00 Hz)

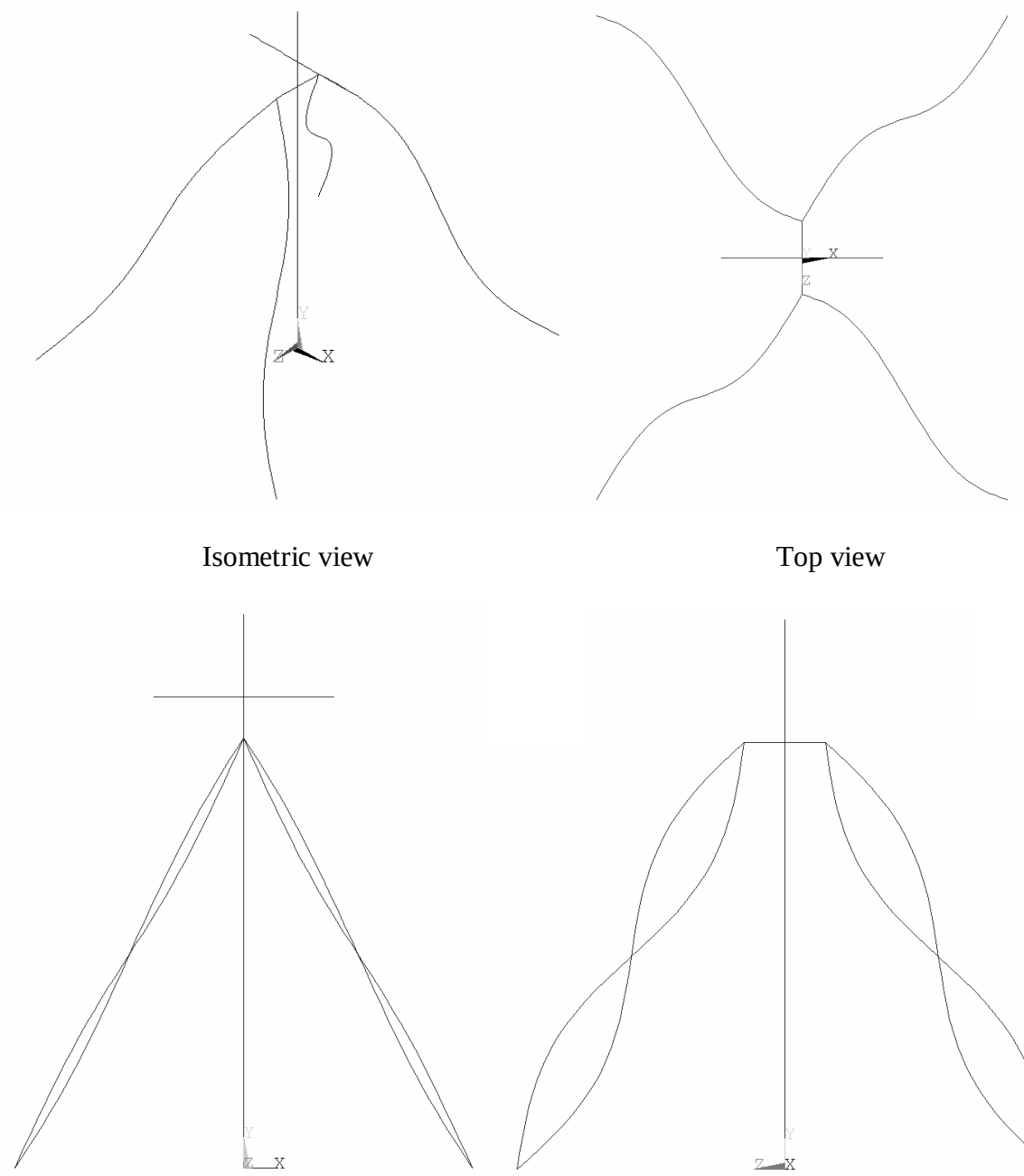

Figure A.30: 15th mode shape of the simplified tower (Frequency = 3.00 Hz)

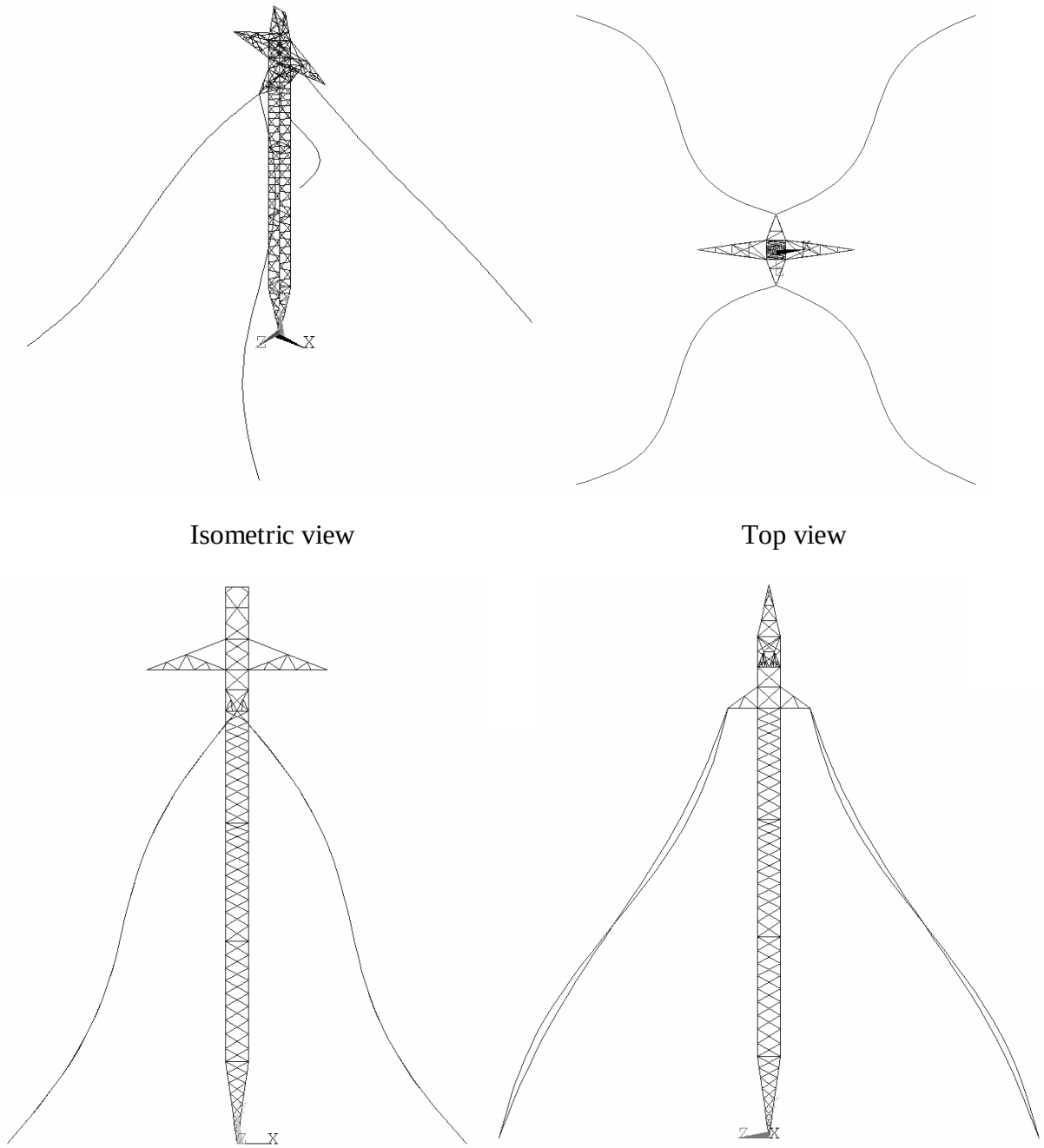

Figure A.31: 16th mode shape of the detailed tower (Frequency = 3.00 Hz)

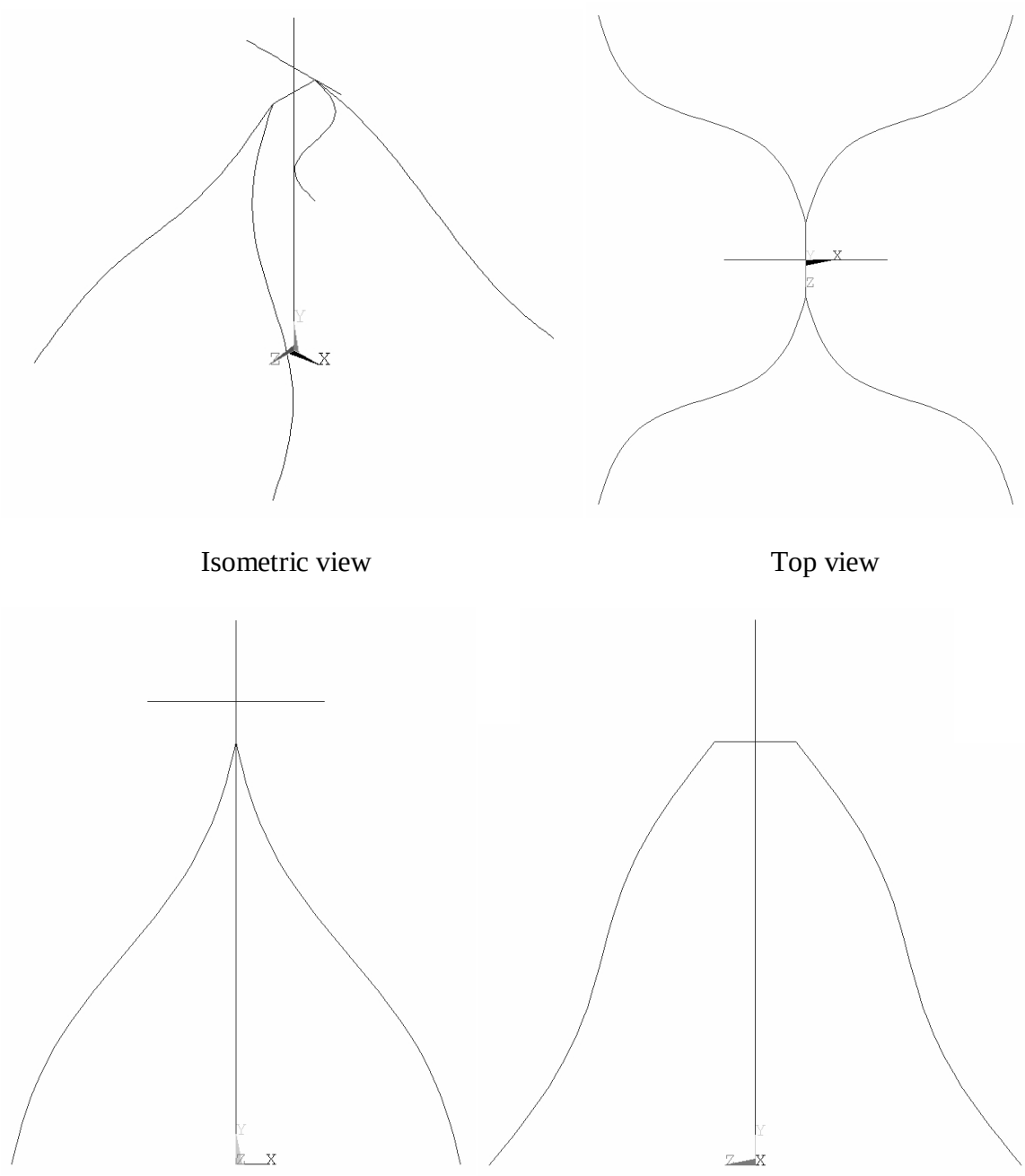

Figure A.32: 16th mode shape of the simplified tower (Frequency = 3.00 Hz)

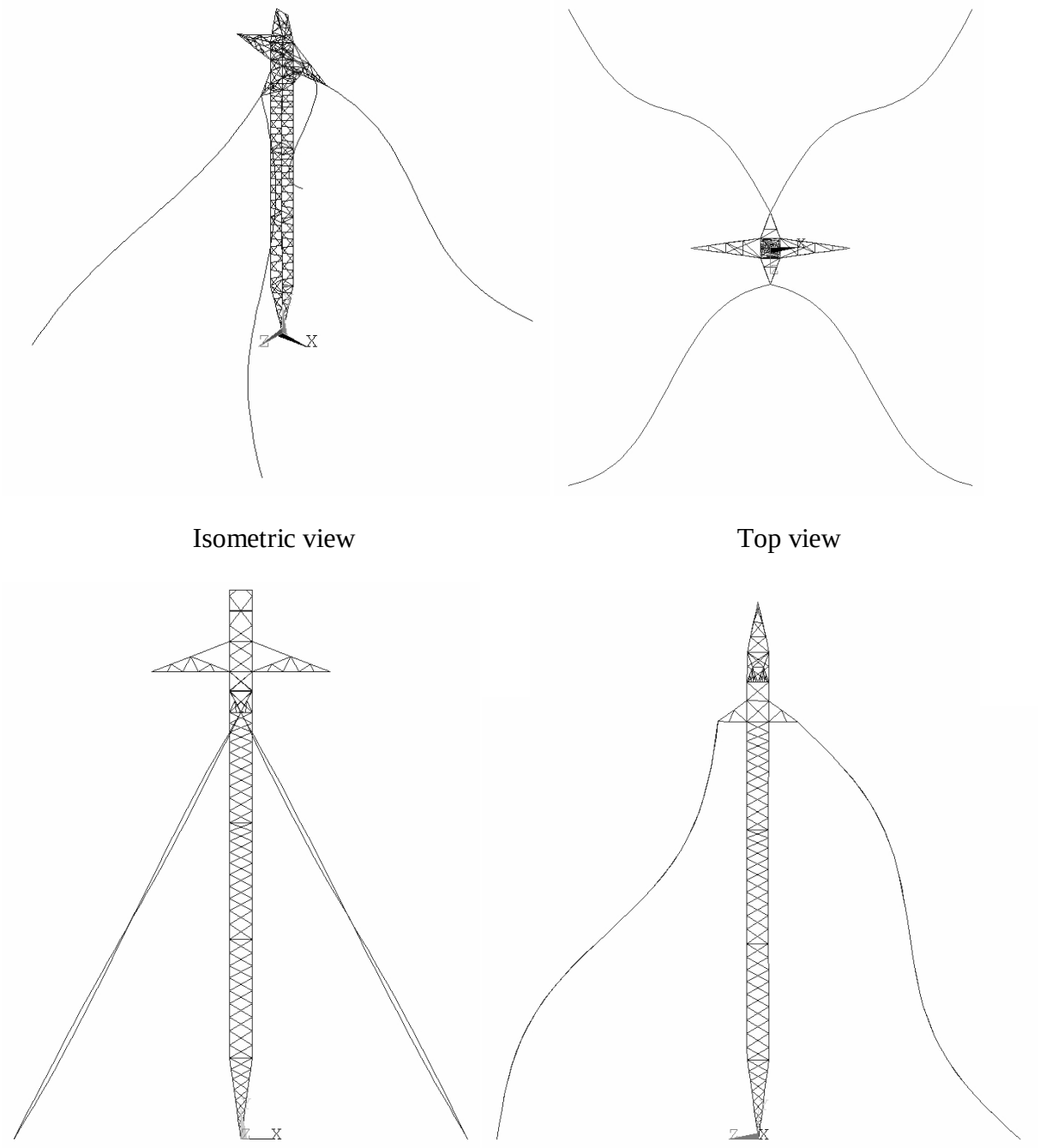

Figure A.33: 17th mode shape of the detailed tower (Frequency = 3.02 Hz)

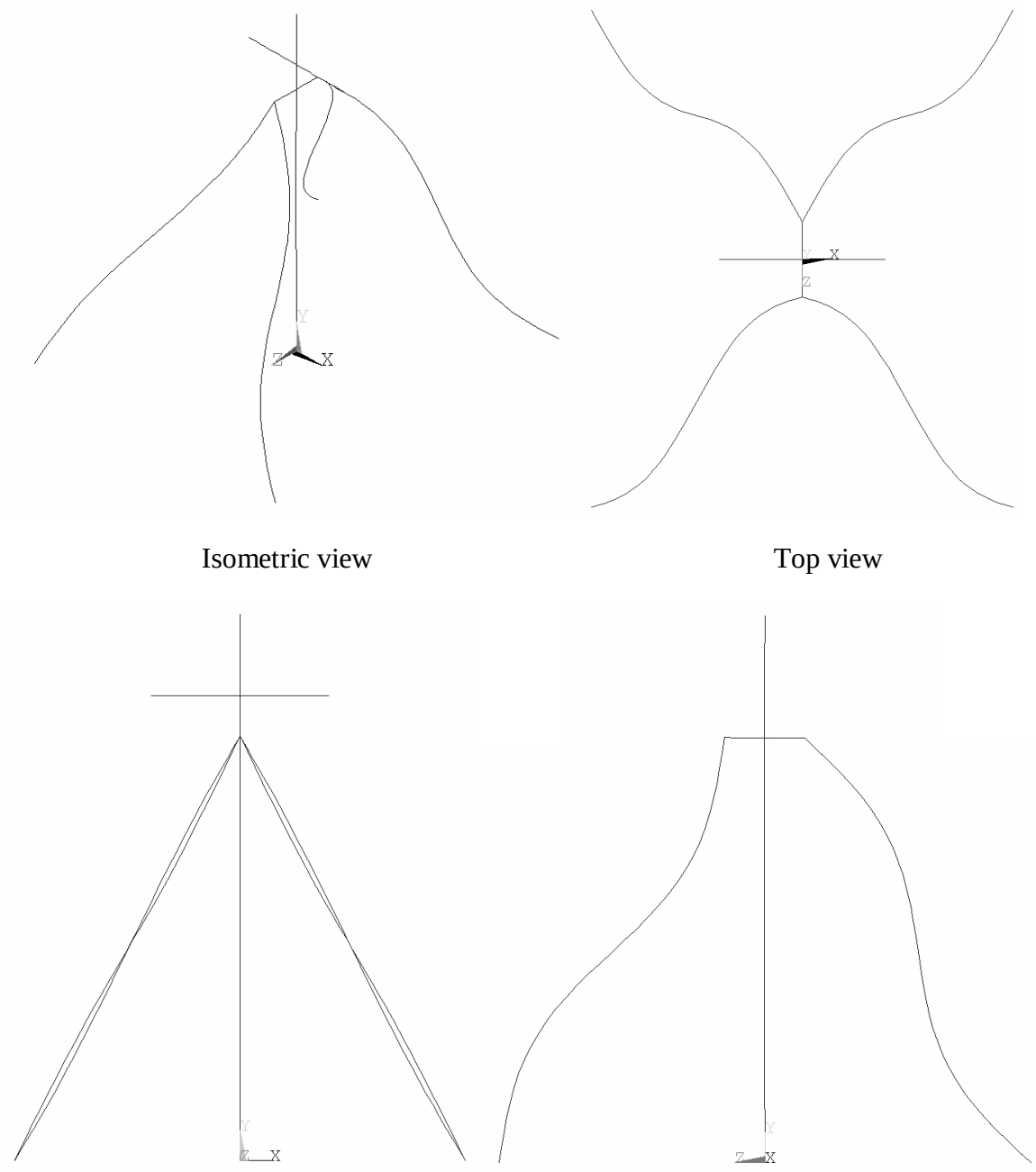

Figure A.34: 17th mode shape of the simplified tower (Frequency = 3.02 Hz)

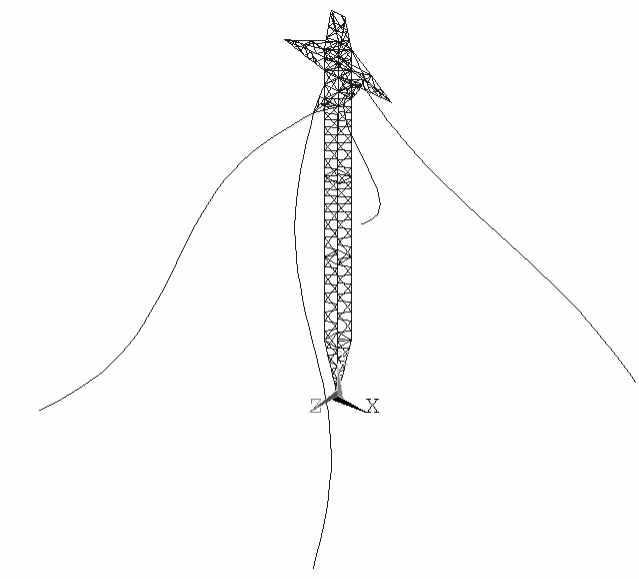

Isometric view

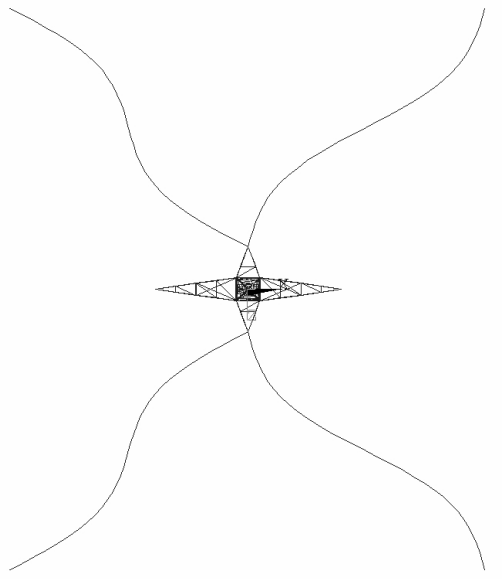

Top view

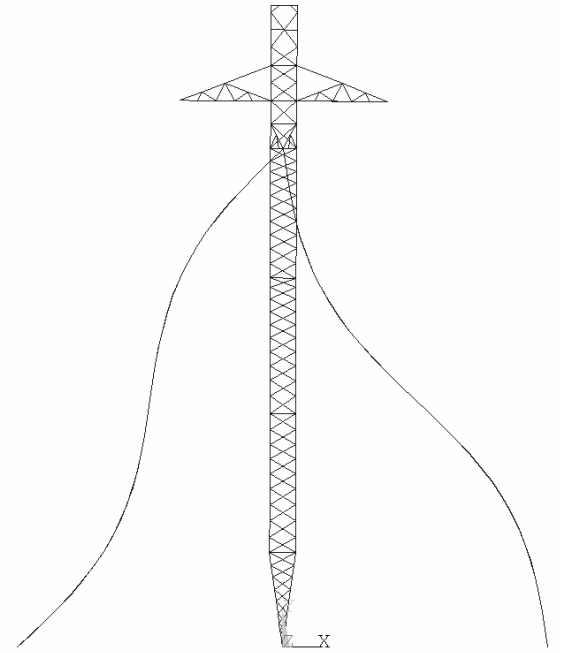

Longitudinal view

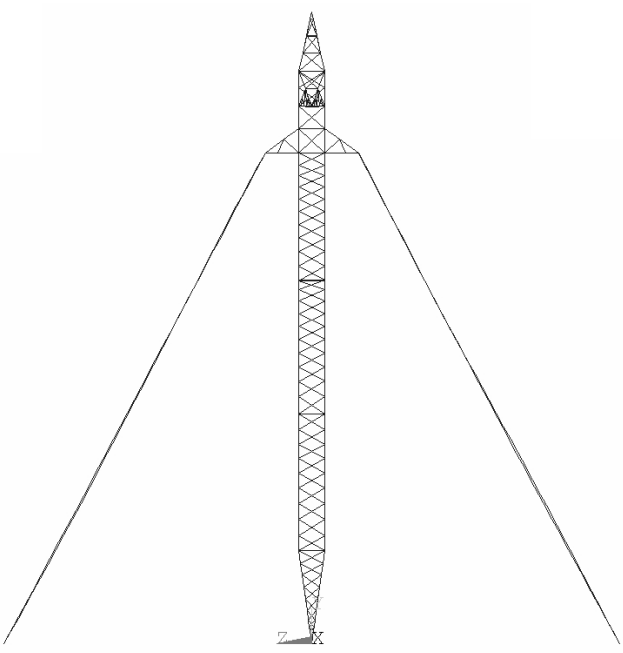

Transverse view

Figure A.35: 18th mode shape of the detailed tower (Frequency = 3.02 Hz)

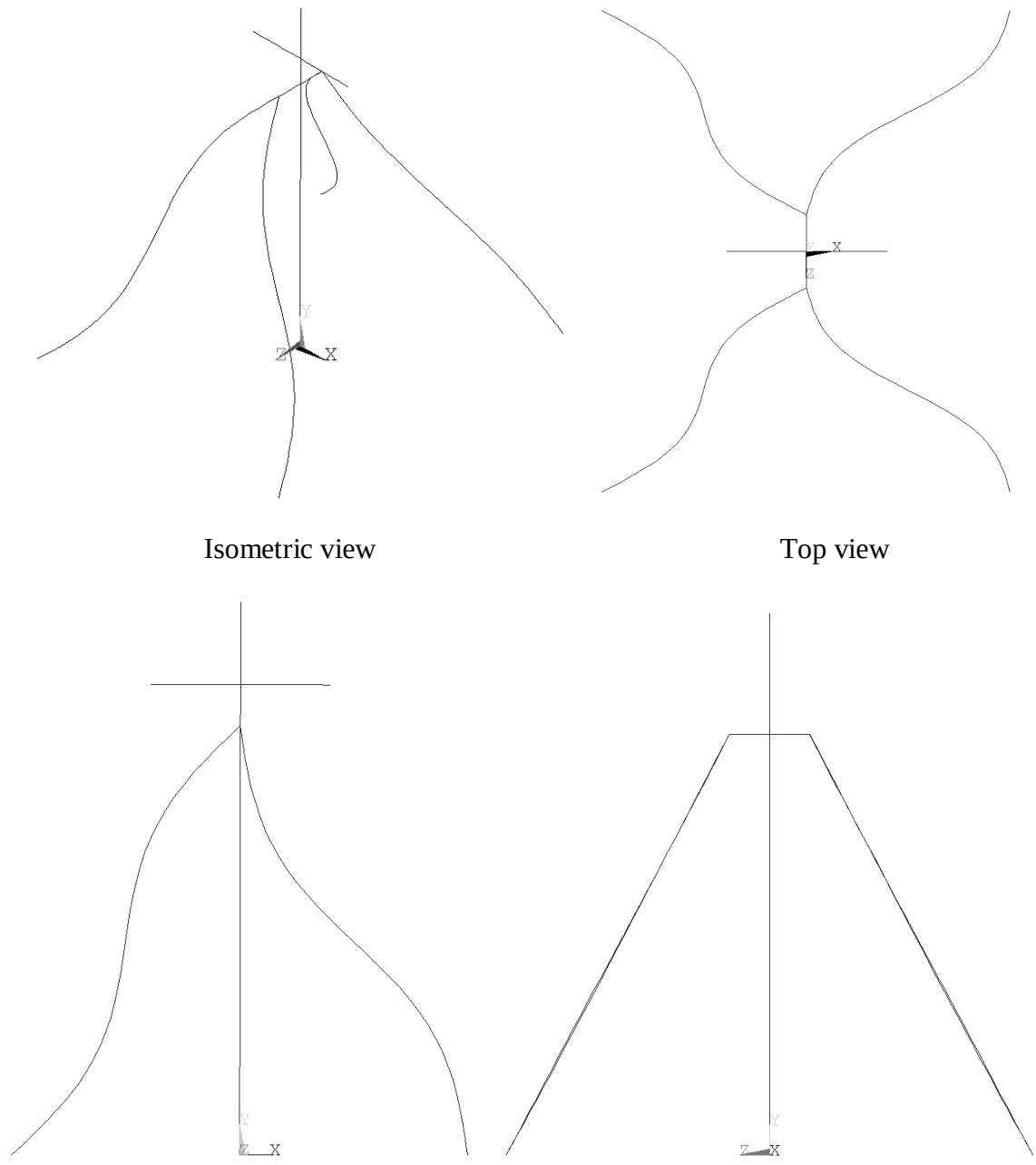

Figure A.36: 18th mode shape of the simplified tower (Frequency = 3.02 Hz)

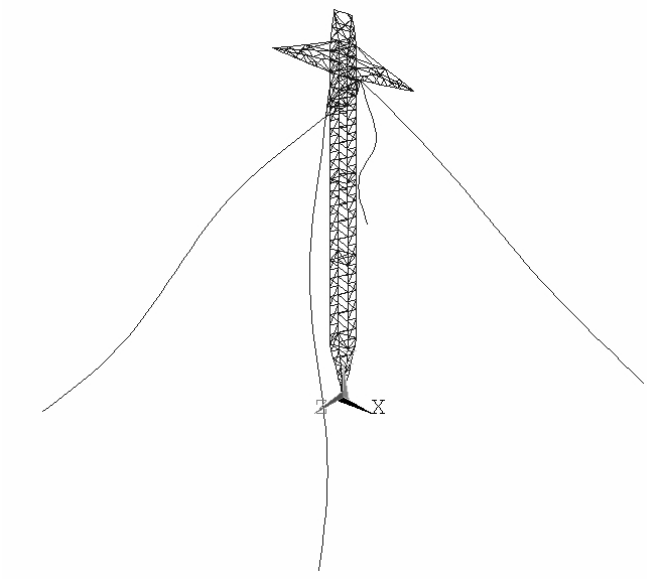

Isometric view

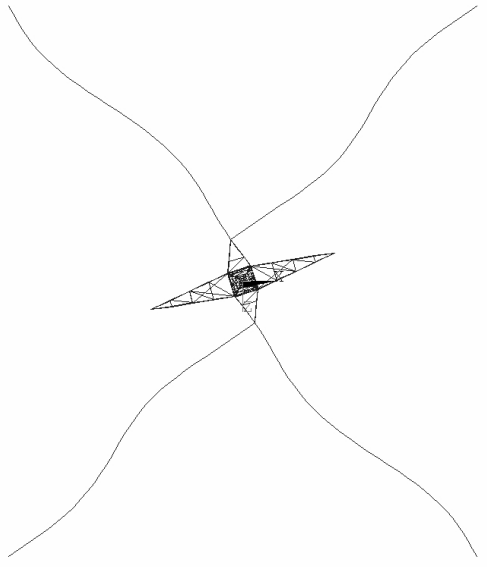

Top view

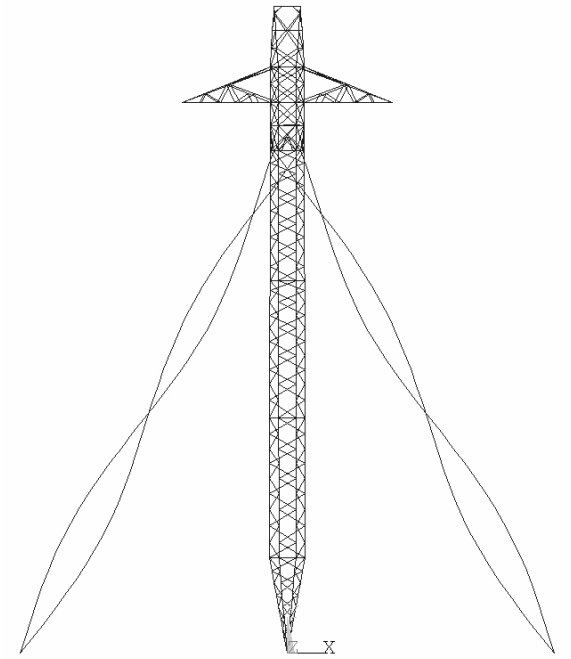

Longitudinal view

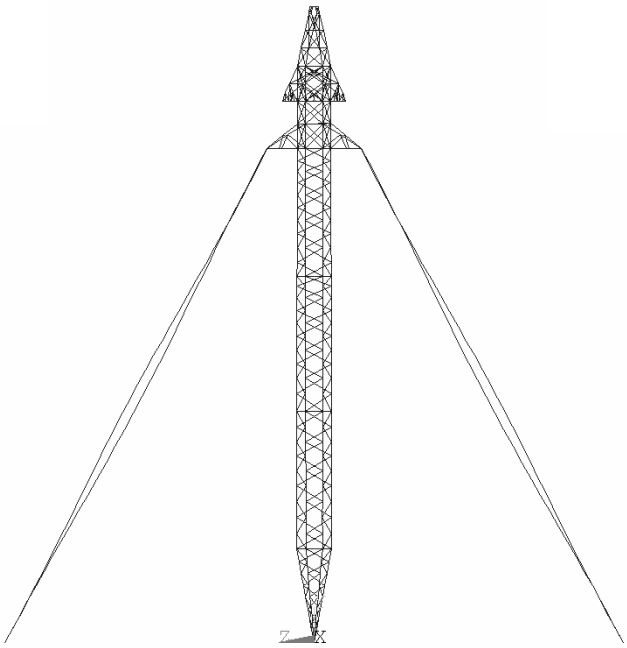

Transverse view

Figure A.37: 19th mode shape of the detailed tower (Frequency = 3.44 Hz)

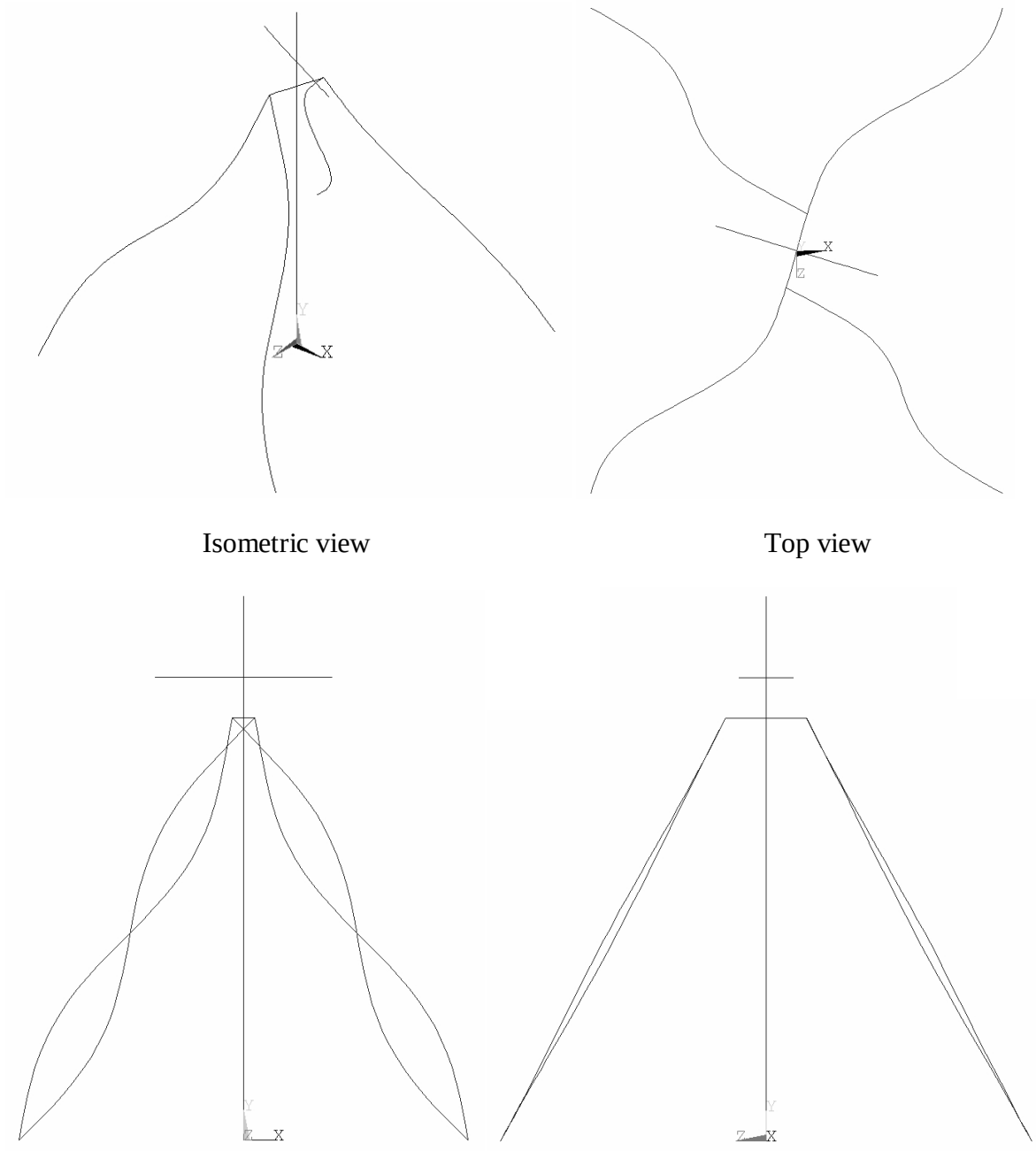

Figure A.39: 19th mode shape of the simplified tower (Frequency = 3.23 Hz)

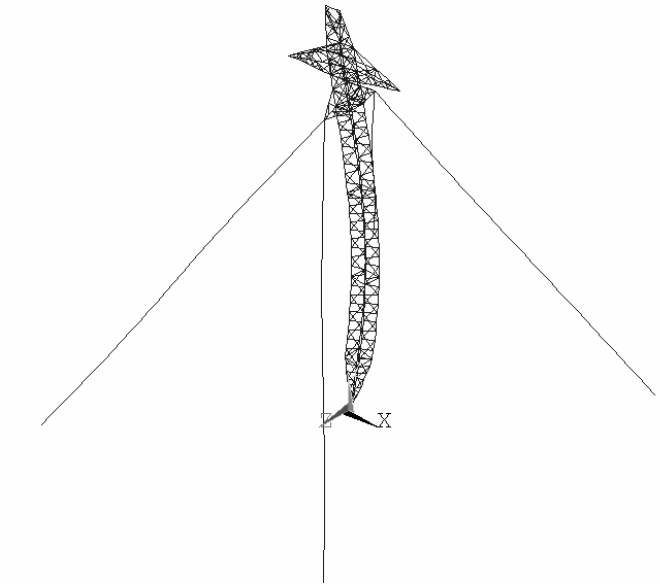

Isometric view

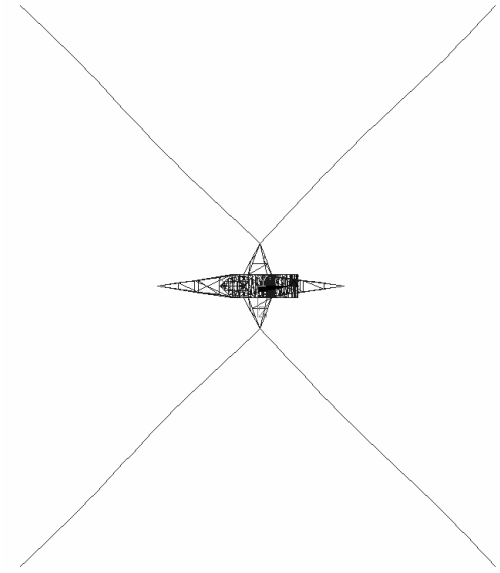

Top view

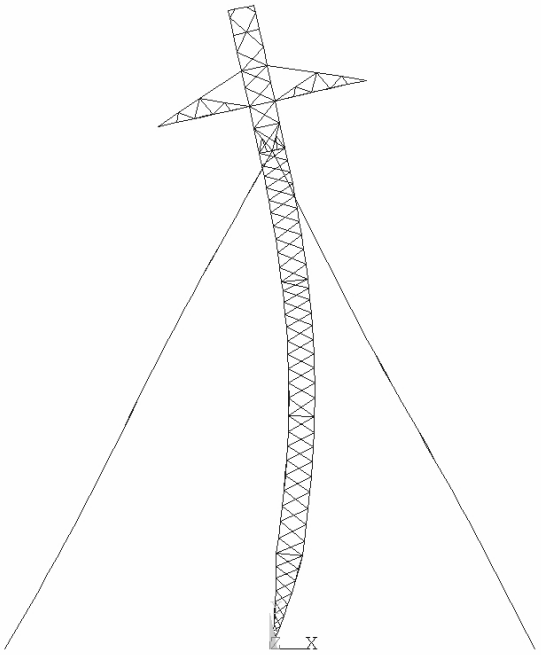

Longitudinal view

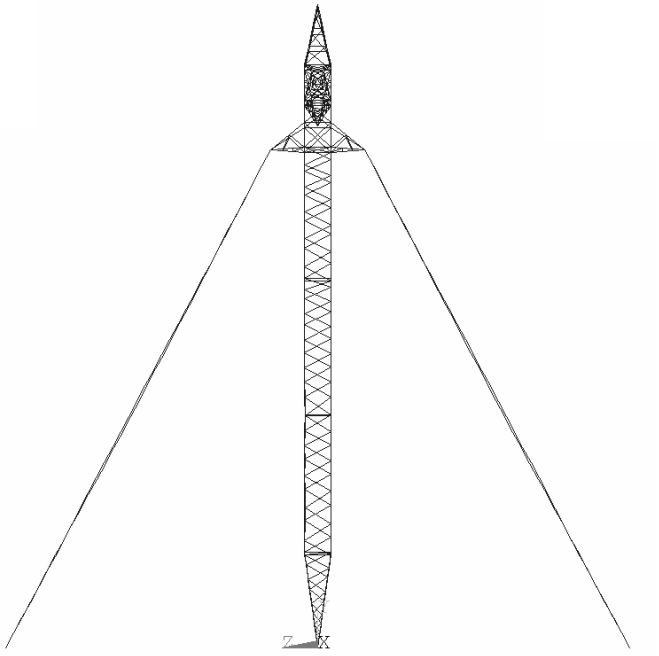

Transverse view

Figure A.39: 20th mode shape of the detailed tower (Frequency = 3.54 Hz)

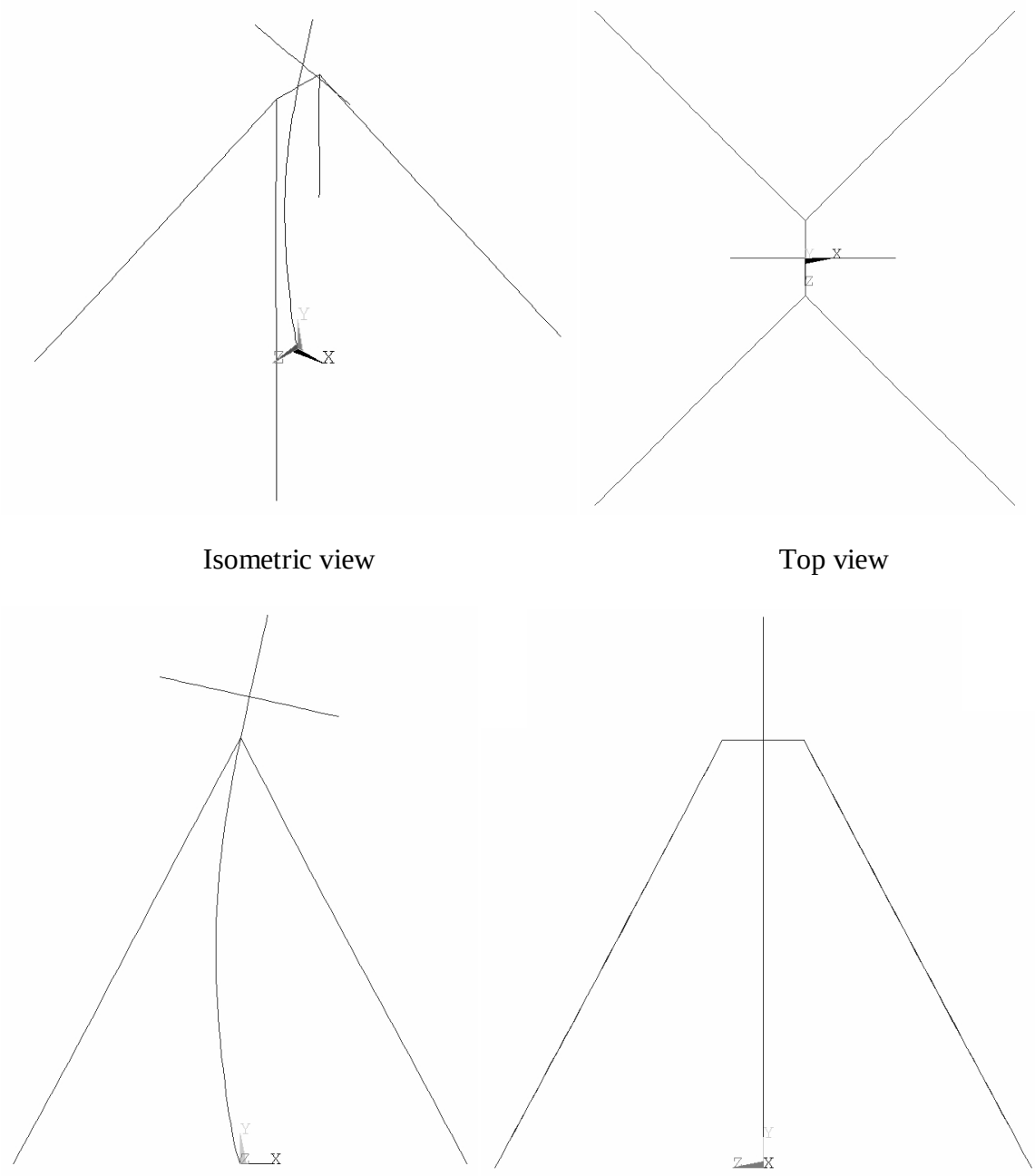

Figure A.40: 20th mode shape of the simplified tower (Frequency = 3.45 Hz)